DISSIPATION IN THE SUPERFLUID HELIUM FILM

Christopher J. Adie

A Thesis Submitted for the Degree of PhD
at the
University of St Andrews

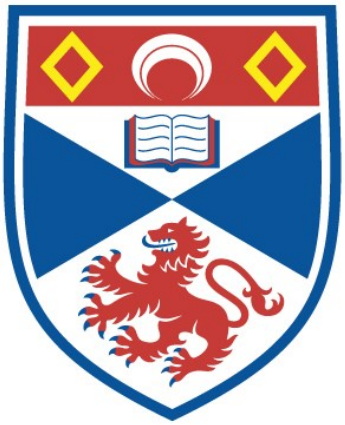

1984

DISSIPATION IN THE SUPERFLUID HELIUM FILM

Christopher J Adie

Thesis submitted for the degree of Ph.D.

at the University of St Andrews, 1983

ProQuest LLC.
789 East Eisenhower Parkway
P.O. Box 1346
Ann Arbor, MI 48106 – 1346

I declare that this thesis has been composed by myself, and that (except where explicitly stated otherwise) it is a record of work done by myself since my admission as a research student at the University of St Andrews in October 1977. It has not been submitted in any previous application for a higher degree.

Access to the thesis in the University library shall be governed by any regulations approved by the Library committee.

PERSONAL PREFACE

After four years as an undergraduate at the University of Aberdeen, I graduated in 1977 with a First Class Honours Bachelor of Science degree in Physics.

From October 1977 to September 1980 I held a University Research Scholarship at the University of St Andrews under the joint supervision of Professor J F Allen and Mr J G M Armitage. In October 1977 I enrolled under resolution of the University Court, 1967, No 1, as a candidate for a PhD.

CERTIFICATE

We certify that Christopher J Adie, BSc, has spent nine terms at research work in the School of Physical Sciences in the University of St Andrews under our direction, that he has fulfilled the conditions of the Resolution of the University Court, 1967, No 1, and that he is qualified to submit the accompanying thesis in application for the Degree of Doctor of Philosophy.

Joint Research Supervisors

ACKNOWLEGEMENTS

My main debt of gratitude is to J G M Armitage, without whose advice and encouragement this thesis would never have come into being. His combination of experimental innovation and theoretical expertise has been an invaluable source of inspiration. I am also very grateful to Professor J F Allen, whose practical advice and and suggestions have been most useful. Thanks are due to the technical staff of the Department of Physics, particularly to those who provided the supplies of liquid helium and nitrogen. I would also like to thank H M Brash and A L Muir of the Department of Medicine, Edinburgh University, who provided computing and word-processing facilities, and "time off" to complete this thesis. Finally, I wish to thank my wife for her encouragement and support.

ABSTRACT

Experimental apparatus to study dissipation in the saturated superfluid helium film has been developed. The low temperature parts comprise a sealed cell containing liquid helium, to which are affixed two parallel plate capacitors, functioning both as liquid reservoirs and as a way of measuring the liquid level. A small hole in a thin plastic film located in the flow path between the two capacitors forms the flow-limiting constriction. This arrangement introduces large velocity gradients in the vicinity of the hole. Film flow is initiated and sustained by an electric field in one capacitor, generated by a purpose-built Film Drive Unit (FDU) and a high-voltage amplifier.

Detailed study of the helium film under steady flow conditions was not possible, but those results which were obtained indicate that the transfer rate is about 30% higher than was anticipated. By applying positive feedback to the film through the FDU, the inertial oscillations can be studied over many cycles. This new method has revealed some unexpected results, and a variety of types of oscillation behaviour have been observed.

A theoretical model of dissipation has been developed, based on the premise that vortices in the film are oriented perpendicular to the film plane and are free to move and cross streamlines. According to this model, the large steady film transfer rates are due to the separation of the region of dissipation and the region of maximum velocity, an effect caused by the radial-flow geometry. Numerical simulation of the

inertial oscillations using the model reproduces some of the behaviour observed experimentally, provided that the rate of vortex creation is taken to be a step function of the velocity.

The shape of the liquid helium surface tension meniscus has been calculated numerically. The calculation is valid for the moving and static film in the absence of dissipation.

CONTENTS

CHAPTER 1

AN INTRODUCTION TO THE HELIUM FILM

1.1 Properties of the Helium Film

Any surface in thermal equilibrium with helium vapour at a sufficiently low temperature will have adsorbed upon it a thin film of helium atoms, held against the surface by van der Waals forces. The film thickness varies with temperature T and pressure P. If the system point (T,P) is on the vapour-pressure curve, the film is said to be "saturated", while if the system point is within the vapour region of the P-T plane, the film is said to be "unsaturated".

The thickness and density profile of the film have been determined both experimentally and theoretically. The first one or two atomic layers are solid, the remainder of the film being in the liquid phase[1,2]. The saturated film thickness varies with height above the level of bulk liquid in the system, and has been measured in a variety of experiments. Jackson and co-workers[3,4,5] found the film thickness d to be approximately 30nm at a height of h=1cm. The thickness decreased further up the film according to the relationship:

$$d \propto h^{-1/n} \qquad (1.1)$$

where n was between 2.3 and 2.6. Anderson et al.[6] found the same formula fitted their results, with n=3.

The saturated film profile (1.1) can be derived theoretically from the shape of the van der Waals potential. Schiff[7] and Frenkel[8] predict that the van der Waals potential energy per unit mass W(d), where d is the distance from the substrate, should be:

$$W(d) = -a/d^3 \qquad (1.2)$$

where a is called the van der Waals constant, and is substrate dependent. Since in equilibrium, the chemical potential $\mu = gh - a/d^3$ must be the same at the surface of the bulk liquid (where d is infinite) and at the surface of the film, we have that:

$$d = (gh/a)^{-1/3} \qquad (1.3)$$

which agrees with (1.1) if n=3.

The film thickness is related to the pressure of gas at the film surface. At a height h above the bulk liquid surface, the pressure is $P = P_0 \exp[-mgh/k_BT]$ where P_0 is the saturated vapour pressure and m is the mass of a helium atom. Since the vapour at height h must be in equilibrium with the film at the same height, we eliminate h from this equation using (1.3) and obtain:

$$-k_BT \ln(P/P_0) = a/md^3 \qquad (1.4)$$

This equation is known as the Frenkel-Halsey-Hill isotherm[9], and is valid[10,11,12] for both the saturated and unsaturated film (which is just the same as a saturated film at a very large height h).

Although the liquid helium forming the film is only about 100 atoms thick, it still behaves like bulk liquid helium in many ways. It undergoes a superfluid transition which in the saturated film occurs at the bulk lambda point T_λ. Because the film is so thin, the normal component is locked to the substrate due to its viscosity, while the superfluid is free to move.

In the saturated film (away from the substrate and far from T_λ), the superfluid fraction ρ_s/ρ is believed to be the same as that in the bulk. However, Ginzburg and Pitaevskii[13] demonstrated that it must fall to zero close to the substrate.

As in the case of bulk liquid helium, the flow of the film is governed by the two-fluid hydrodynamic equations[14], with the constraint that $v_n=0$. It is useful to quote the two most important equations here:

$$\partial\rho_s\underline{v}_s/\partial t + \nabla\cdot\rho_s\underline{v}_s = 0 \qquad (1.5)$$

$$D_s\underline{v}_s/Dt + \nabla\mu = 0 \qquad (1.6)$$

where $D_s/Dt = \partial/\partial t + \underline{v}_s\cdot\nabla$ is the co-moving derivative (derivative "moving with" the superfluid). Equation (1.5) is the law of mass conservation, while (1.6) expresses the fact that superfluid flow is driven by a chemical potential gradient. Since v_n is zero, there is no entropy transport through the film.

The terms contributing to the chemical potential are important, since they affect the superfluid velocity. Putterman[14] gives the following terms:

$$\mu = \Omega + P/\rho - (\underline{v}_n-\underline{v}_s)^2\rho_n/2\rho - sT \qquad (1.7)$$

where Ω represents all the potential fields experienced by the fluid, s is the specific entropy of the fluid, and P is the pressure. Ω comprises gravity (gh) and the van der Waals potential ($-a/d^3$) in the case of the helium film. Other terms which will contribute to the chemical potential at various points in this thesis are an electrostatic term (Chapters 3 and 4), and a surface tension term (Chapter 8).

1.2 Saturated Film Flow

When there is a chemical potential difference $\Delta\mu$ between two ends of a helium film, equation (1.6) states that the superfluid will accelerate towards the end with the lower chemical potential. Such a $\Delta\mu$ might arise from a difference in the

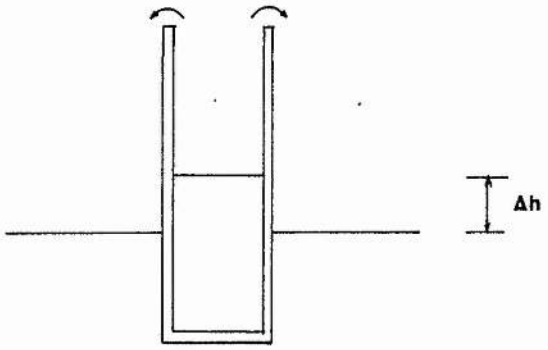

FIGURE 1.1 Beaker film flow

gravitational potential between the two ends. The typical situation in which this occurs is illustrated in figure 1.1 and is called "beaker film flow". This type of experiment, or a slight variant where two reservoirs of similar size are connected by a film, is the most common method of studying the flowing saturated helium film.

The first experiments specifically on beaker film flow were those by Daunt and Mendelssohn[15,16]. They observed that the volume rate of flow $\dot{V}$ ($cm^3 s^{-1}$) from one reservoir to the other (as deduced from the rate of change of liquid levels) was directly proportional to the minimum perimeter of the flow path between them, but was insensitive to the length of the path.

Since $\dot{V}$ is proportional to the minimum perimeter p_{min}, the ratio

$$\sigma = \dot{V}/p_{min} \qquad (1.8)$$

is usually used when quoting film flow results. It is called the film transfer rate, and is usually in the range 6 to 15 x 10^{-5} $cm^2 s^{-1}$. From the conservation of mass, one can infer the superfluid velocity in the film:

$$v_s = \sigma/\rho \, p_{min}/\rho_s dp \qquad (1.9)$$

where p and d are the perimeter and film thickness at the point where we wish to calculate v_s. If $p=p_{min}$ and d=30nm, the film velocity is in the range 20 to 50 cm s^{-1}.

The early experiments on film flow by Daunt and Mendelssohn[15,16], Mendelssohn and White[17], and Atkins[18] demonstrated two important effects. The first is that the film appears to flow at a constant "critical" velocity, independent of the driving chemical potential difference. However, Atkins[18] noted that the transfer rate fell when the liquid levels were

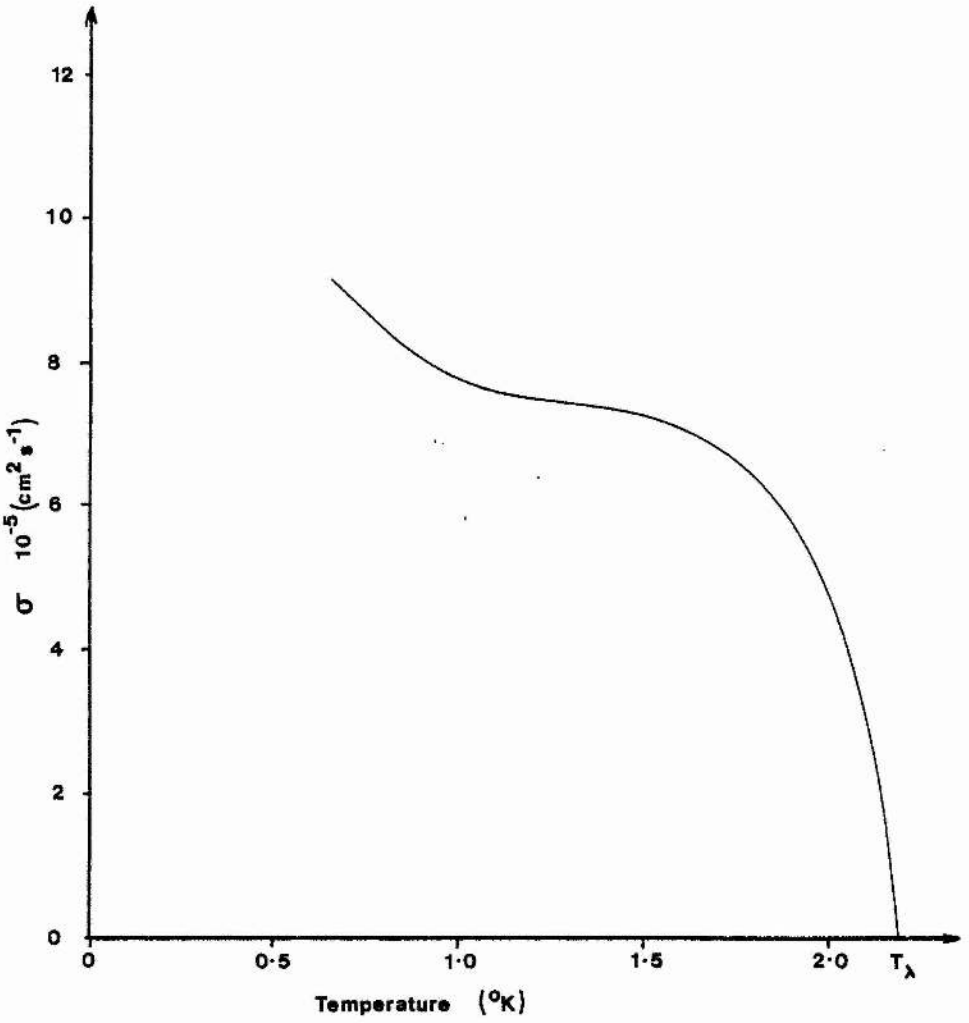

FIGURE 1.2 Transfer rate v Temperature
(based on data from ref. 1)

very close to each other. The second effect is that, as the liquid levels in the two reservoirs approach each other, they commence to oscillate about their eventual equilibrium position. The oscillations decay away, leaving the liquid levels stationary.

We first of all consider the critical velocity v_c, or rather the critical transfer rate σ_c (since the film thickness is not usually measured in such experiments). The transfer rate is limited by the critical velocity at the point in the flow path where the film has minimum cross-sectional area. In beaker flow experiments, this usually means the inside of the beaker rim. The approximate temperature dependence of σ_c is shown in figure 1.2.

Despite the reproducibility implied by figure 1.2, almost all investigators have found that the transfer rate varies from experiment to experiment, and from day to day and run to run in a given experiment, by anything up to a factor of two. It is found that σ_c depends on the height of the beaker rim above the liquid level[18,19], the presence of solid gas or other contaminants on the substrate[20], the substrate roughness[21], the method of filling the beaker[22,23], the thermal insulation between the two reservoirs[24], whether the flow was into or out of the beaker[23], the ^{3}He concentration[25], and the presence of vibration.

Some of these effects were explained on the basis of a constant critical velocity v_c, the variation in σ_c being caused by variations in the other parameters on the RHS of equation (1.9). Contamination of the substrate with solid air has been shown to increase the film thickness[26], and this resulted in the increased transfer rates observed by Bowers and Mendelssohn[20]. The difference between a polished and a rough substrate was

investigated by Smith and Boorse[21], who found that the increase of 20% in average transfer rate in the latter case could be accounted for by the increase in the microperimeter of the surface.

However, the critical velocity has been shown to depend explicitly on the film thickness d. Allen and Armitage[19] found that for flow out of a beaker, the dependence of transfer rate on the rim height h above the beaker level was:

$$\sigma_c \propto h^{-1/4}$$

Using equations (1.3) and (1.9), we obtain for the critical velocity at the beaker rim:

$$v_c \propto d^{-1/4}$$

This is in agreement with the work of van Alphen et al.[27] on film flow and bulk flow in narrow channels.

Atkins[18] and Selden et al.[28] have found that in contrast to the case of inflow, the transfer rate out of a beaker is dependent on the level difference and the history of the film, σ_c being much larger near the start of the flow. This effect remains unexplained.

Poor thermal contact between the two reservoirs will permit the existence of a temperature difference between them. This has two effects: there will be a fountain-pressure contribution to the chemical potential difference, and distillation of liquid from one reservoir to the other will alter the apparent film transfer rate. Selden and Dillinger[24] describe the latter effect, and some experimenters have used the former effect as the primary source of chemical potential difference[29,30].

Esel'son and Laserev[22] and Allen[23,31] found that a plunge-filled beaker emptied faster than if the beaker had been filled

by film flow. Allen suggested that plunge filling created turbulence in the beaker, affecting the transfer rate. Selden and Dillinger[24] found that mechanically induced turbulence in the source reservoir increased the transfer rate, while turbulence in the sink reservoir reduced the rate. This phenomenon may be connected with the common observation that vibration tends to increase the transfer rate.

Even when the most stringent precautions are taken to ensure good thermal contact between the reservoirs and to eliminate contamination, vibration and turbulence, it is still found that at a given temperature, level difference and rim height, there is significant variation in transfer rate. The common assumption that the transfer rate is a well-defined function of these parameters is thus not valid, as Harris-Lowe has pointed out[32].

Yet another transfer rate phenomenon which has been noted by a number of workers[19,28,33,34,35,36] is a spontaneous abrupt transition from one flow rate to another, usually lower, rate. Some workers[33,34] have reported that the jumps in flow rate are of uniform size (about 0.5×10^{-5} $cm^2 s^{-1}$), suggesting that σ is quantised in some way.

We now turn to consider the oscillations which occur as the liquid levels approach each other. The kinetic energy of the film causes the levels to overshoot their equilibrium position, initiating damped oscillations. They are referred to as inertial or U-tube oscillations, and their frequency may be calculated by taking the time derivative of the energy equation in the usual way. Details of the derivation are given in section 4.4; the result is:

$$\omega^2 = \rho_s g / \rho I A \qquad (1.10)$$

where A is the "reduced" area of the reservoirs and I is an integral along the flow path from one reservoir to the other:

$$I = \int dl/d(l)p(l)$$

The oscillation period can thus yield information on the film thickness, and Atkins[37] exploited this to obtain an estimate for the film thickness as a function of height.

The oscillation amplitude varies depending on the geometry of the apparatus. Unless the film flow path is exceptionally long and the reservoir areas small (as in the case of the Leiden experiments[38]), the amplitude is usually less than 1mm. As the oscillations progress, their amplitude falls off exponentially with time[39,40,41], indicating the presence of a damping force proportional to the velocity in the equation of motion of the film.

The source of this damping force has now been conclusively shown to be the entropy term sT in the chemical potential (1.7)[42,43,44,45]. Robinson[46] derived the value of the damping constant. As the superfluid flows from one reservoir to the other, the change in specific entropy results in a temperature difference between them. If the reservoirs are in thermal contact, there will be an irreversible heat flow between them, resulting in a net increase in the entropy of the system and therefore the temperature. This extra thermal energy is removed from the oscillations. The effect is called thermal or Robinson damping, and the oscillation decay rate is dependent on the thermal conduction between the reservoirs.

One other phenomenon in the helium film should also be mentioned. The thickness of the flowing film is predicted to be less than the static film thickness. This was pointed out by

Kontorovich[47], and it is usually referred to as the film-thinning or Kontorovich effect. Substituting (1.7) with $\underline{v}_n=0$ into the superfluid equation of motion (1.6), and using the relationship $\rho_n + \rho_s = \rho$, we obtain:

$$\partial \underline{v}_s/\partial t + \nabla\mu' = 0 \qquad (1.11)$$

where
$$\mu' = v_s^2\rho_s/2\rho + \Omega + P/\rho - sT \qquad (1.12)$$

μ' is often loosely referred to as the chemical potential. Using equations (1.2) and (1.3) we see that the flowing film will be thinner by approximately:

$$\Delta d = \sigma^2\rho/ghd\rho_s$$

The work of Graham and Vittoratos[48], of Flint and Hallock[51], and of Eckholm and Hallock[49,50] (on the unsaturated film), has shown that film thinning occurs and is of the predicted magnitude.

1.3 Vortices

The hydrodynamics of superfluid helium permits the existence of vortex lines, similar to the vortex lines of classical hydrodynamics. Onsager[52] and Feynman[53] independently suggested that the circulation of vortex lines in liquid helium would be quantised. This can be understood by considering the complex order parameter $\psi(\underline{r})$ introduced by Ginzburg and Pitaevskii[13], which is in a sense the "wave function" of the superfluid component. It can be written:

$$\psi(\underline{r}) = \eta(\underline{r}) \exp[i\phi(\underline{r})]$$
where
$$\rho_s = \eta(\underline{r})^2 \quad ; \quad \underline{v}_s = (h/m)\nabla\phi(\underline{r}) \qquad (1.13)$$

and where m is the mass of a helium atom. For a vortex, the lines of equal phase ϕ radiate outwards from the vortex core,

where ψ is zero. Integrating the above expression for $\underline{v}_s$ round the vortex line, we obtain for the circulation:

$$K = (\hbar/m)\Delta\phi$$

where $\Delta\phi$ is the change in phase on moving right round the vortex and back to the starting point. Since ψ is single-valued, $\Delta\phi$ must be an integral multiple (n) of 2π, and thus the circulation must be quantised in units of $\kappa = h/m = 9.97\times10^{-4}$ cm^2s^{-1}:

$$K = n\kappa = nh/m \qquad (1.14)$$

In a classic experiment, Vinen[54] measured the circulation round a thin wire in liquid helium, and found that it was either zero, or h/m. Similar experiments were performed by Whitmore and Zimmermann[55], who found the same value for κ, and observed a wider range of quantum numbers n. The vortex ring experiments of Rayfield and Reif[56] also support (1.14).

We now consider a mechanism known as Anderson phase slippage, through which vortex motion can give rise to a chemical potential gradient[57]. Let us consider two points 1 and 2 on a streamline of $\underline{v}_s$. If we substitute $\underline{v}_s = (h/m)\nabla\phi$ into the superfluid equation of motion (1.11) and integrate along the streamline from 1 to 2, we obtain:

$$(h/m)\, d(\phi_2-\phi_1)/dt = -(\mu_2-\mu_1) \qquad (1.15)$$

Thus, a chemical potential difference always involves a changing phase difference, or "phase slip". Such slippage can arise either from a non-zero $\partial\underline{v}_s/\partial t$, or from vortex motion, as we shall now show.

Suppose that a vortex line of unit circulation starts from far to one side of our streamline and moves so as to cross it

between 1 and 2, ending up far away on the other side of the streamline. The phase difference between 1 and 2 will change by $\pm 2\pi$, the sign of the change depending on the sense of the vortex circulation and the direction in which it crosses the streamline. If $\dot{n}$ vortices per second (all of the same sign) cross the streamline between 1 and 2, then the rate of phase change will be $-2\pi\dot{n}$, and equation (1.15) becomes:

$$\Delta\mu = \dot{n}\,\gamma\kappa \tag{1.16}$$

This equation is sometimes known as the Anderson relation[57]. If there is no other source of chemical potential difference, the vortex motion will cause $\underline{v}_s$ to increase or decrease, depending on the vortex sign and direction of movement.

One mechanism by which vortices can cross streamlines depends on the interaction of the normal fluid with the vortex core. When a vortex line moves relative to the normal fluid, the thermal excitations scatter off the vortex core, causing the line to experience a net force per unit length[58]. The component of this force parallel to the vortex line has been shown[59,60] to be very small. The magnitude of the force was deduced by Rayfield and Reif[56] from their experiments on the motion of charged vortex rings. By measuring the energy loss of the rings as they drifted relative to the normal fluid, they found that the force was directed antiparallel to $\underline{v}_L - \underline{v}_n$ (where $\underline{v}_L$ is the vortex line velocity) except near to T_λ, when there was a component perpendicular to both the vortex core and to $\underline{v}_L - \underline{v}_n$. We are concerned here only with the first-mentioned component.

If $\underline{v}_n = 0$ (as in a film or narrow channel), the normal fluid interaction will drag on the vortex, so that it moves more slowly than the superfluid. This induces a Magnus force on the vortex line[14], perpendicular to $\underline{v}_L - \underline{v}_s$. The net effect is that the

vortex moves forward at an angle to $\underline{v}_s$, the perpendicular component of its velocity causing it to cross streamlines. This subject is dealt with more fully in section 6.1.

We have thus seen that there exists a mechanism by which vortices can cross streamlines, producing a chemical potential difference. However, very little direct experimental evidence is available to support equation (1.16). Richards and Anderson[61] studied the flow of bulk helium through a small hole in a thin nickel foil, and observed step-like behaviour in the decay of the chemical potential difference across it. Their results, however, were not conclusive, and further work would be required to demonstrate the correctness of (1.16).

Despite the lack of direct experimental evidence, (1.16) is now generally accepted as a necessary condition to be met by any theory which attempts to explain critical behaviour in superfluid flow.

1.4 Dissipation

In a typical beaker film-flow experiment, the investigator creates a level difference between two reservoirs of liquid helium, thus imparting potential energy to the system. When the experiment is over and the levels are again at equilibrium, this energy will (presumably) have been dissipated as heat, causing a very small rise in the temperature of the system. The term "dissipation" in the context of superfluid flow is generally taken to mean the process by which the energy imparted to the system is converted to heat.

It is clear that the experimental observations of critical velocity behaviour are in serious conflict with equations (1.11) and (1.12), in that a constant velocity is observed when there is apparently a chemical potential gradient. If equation (1.15) is

taken as the basic physical law, rather than (1.11), then the crossing of streamlines by vortices can compensate for the experimentally observed chemical potential difference $\Delta\mu$. Note that when v_s is constant, the rate of energy loss is proportional to $v_s\Delta\mu$, and it is therefore usual to speak of $\Delta\mu$ as the dissipation. When the driving force is purely a level difference Δh, then $\Delta\mu = g\Delta h$, and one can speak interchangeably of the dissipation or the level difference.

Landau[62] was the first to attempt to explain the dissipation mechanism in superfluid flow. His argument, involving roton creation when the Landau critical velocity is exceeded, is well known. However, the Landau velocity is two to three orders of magnitude higher than the observed critical velocities.

Atkins[63] applied Landau's criterion to the generation of a vortex ring. He obtained a critical velocity of the form:

$$v_c = (h/mr)\ \ln(1.4r/a)$$

where r is the maximum radius at which vortex rings could be created in a given experiment, and a is the vortex core radius. Feynman[53] obtained a similar result. If r is of the order of the channel diameter in bulk flow experiments, then approximate agreement with experiment is obtained[1]. However, the equation does not explain the observed temperature dependence of the transfer rate, nor is it clear how vortex rings of the required macroscopic size can suddenly appear in the liquid.

Glaberson and Donnelly[64] suggested a mechanism which overcame this problem. They showed that a vortex line with both ends pinned on the walls of the channel could act as a "vortex mill", generating macroscopic vortex rings. The predicted critical velocity was essentially the same as the Atkins/Feynman

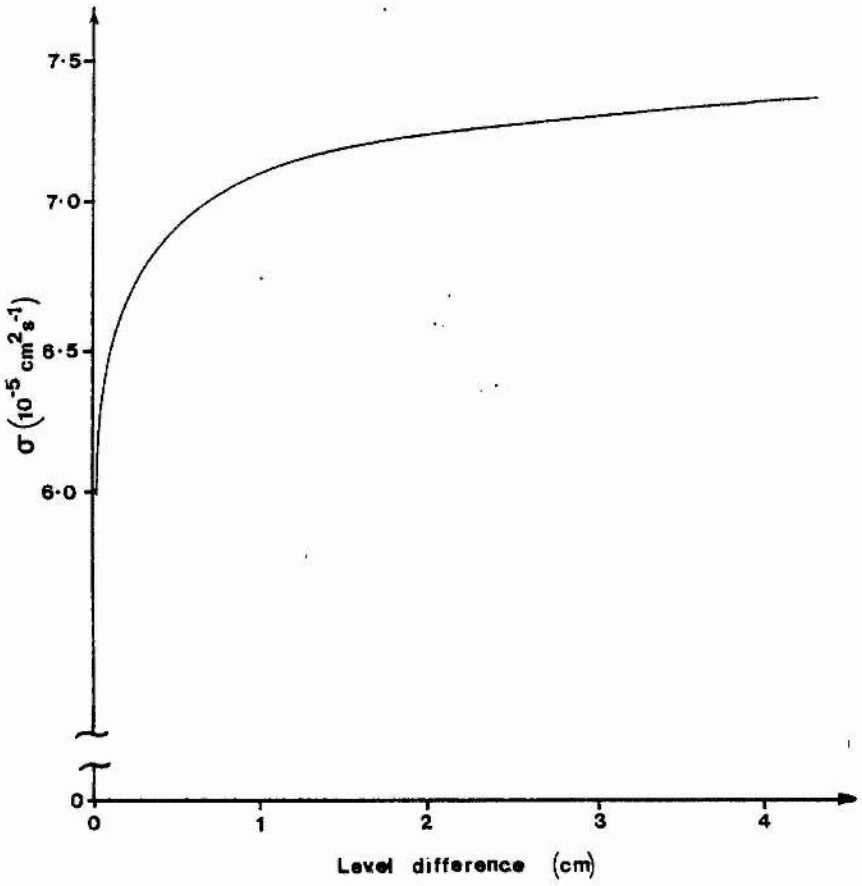

FIGURE 1.3 Transfer rate v level difference

value. Donnelly and Roberts[65] suggested that the vortex mill would be temperature dependent.

Up to about 1968, all the models of dissipation removed energy from the flow in order to create vortex lines or rings. Campbell[66] showed that (based on his definition of the momentum of a vortex ring) there is insufficient energy in the flow to simultaneously create vortices, and satisfy the Anderson condition. He pointed out that the energy lost to the normal fluid due to vortex line/normal fluid interaction could completely account for the dissipation. Theories which did not explicitly show how the Anderson relation (1.16) was satisfied were unacceptable.

However, the critical velocity is not the whole story of dissipation in superfluid film flow. Atkins' observation[18] that the transfer rate was reduced when Δh was very small has subsequently been observed by many workers[67,68,69], and has led to the classification of film flow into two regimes: critical and sub-critical. In the sub-critical regime (which usually pertains for Δh less than about 50μm) the velocity rises rapidly with increasing level difference. In the critical regime, there is little or no increase in velocity with increasing level difference.

It is often useful to plot transfer rate against level difference. Figure 1.3 is an example of this kind of graph. However, there is no agreement on the exact shape and size of the curve at a given temperature, reflecting the observed multiplicity of transfer rates. The sub-critical portion of the curve is appropriate to the inertial oscillations, and can be probed if Robinson damping is allowed for or is absent[36,68].

The region in the film where dissipation occurs is of interest. Workers at Los Alamos[70,71] developed a technique to

probe the chemical potential at different parts of the film in a beaker film flow experiment. For outflow, they found that usually, all the chemical potential drop occurred at the inside rim of the beaker, but that it could redistribute itself down the inside wall of the beaker during a run, causing the transfer rate to jump to a lower value in the manner reported by (eg) Allen and Armitage[19]. For inflow, the dissipation region extended down the inside wall of the beaker.

We briefly mention one more recent theory due to Harris-Lowe[32]. He imagines a vortex line with one end pinned to the substrate, which trails downstream at an angle to $\underline{v}_s$. The theory yields a prediction for the rate at which dissipation increases above the critical velocity, and this is supported by the experimental work of Turkington and Harris-Lowe[72]. The theory also offers a possible explanation of the observed abrupt transfer rate changes.

Dissipation in film flow and channel flow is a complex phenomenon, and none of the theories mentioned so far describe it adequately. In the following chapter, we describe an important theory which succeeds in explaining some of the results in channel flow, but is less good in the saturated film. We also describe a relatively new theory which successfully explains superfluid onset and dissipation in the unsaturated film, and which has relevance to the theoretical work in Chapters 6 and 7.

CHAPTER 2

TWO THEORIES OF SUPERFLUID FLOW

2.1 The Thermal Fluctuation Theory

In the late 1960's and early 1970's, a theory of dissipation in flowing superfluid helium was developed, based on the generation of vortices as thermal fluctuations. This model predicted a particular form for dissipation as a function of superfluid velocity, and some experimental evidence appeared to support the theory. In recent years however, the theory has lost some of its popularity.

The standard review paper on the thermal fluctuation theory (which has come to be referred to as the Iordansky-Langer-Fisher or ILF theory) was published in 1970 by Langer and Reppy[73]. Other important papers are those by Iordansky[74], Langer and Fisher[75], and Langer[76]. The following summary relies mainly on these papers.

In the ILF theory, superflow is regarded as a non-equilibrium phenomenon. A flowing superfluid is in a metastable state, and may make an irreversible transition to a state of lower energy and superfluid velocity. The mechanism by which this transition takes place is assumed to be intrinsic to the superfluid itself, independent of the nature of the flow path or the walls of the container. Dissipation which has this property is called <u>intrinsic</u> dissipation. This assumption means of course that the theory (in its most general form) may be applied to bulk flow of superfluid, superfluid flow in superleaks, and film flow.

An appropriate intrinsic transition mechanism to a state of smaller v_s involves the thermal nucleation of some suitable excitation in the fluid. A similar situation obtains in the condensation of a supersaturated vapour, where the nucleation of

a sufficiently large liquid droplet will cause condensation to occur. In either of these cases, the probability of a suitable fluctuation occurring is just given by the Boltzmann factor, $\exp(-E_a/k_BT)$, where E_a is the energy of the fluctuation relative to the background fluid.

The dissipative fluctuation is highly likely to involve some form of vorticity, and the simplest localised flow pattern containing vorticity is a vortex ring. A ring of circulation κ, oriented in a plane perpendicular to the externally imposed superflow v_s and moving against it with a velocity v_0, has energy:

$$E = E_0 - p_0 v_s \qquad (2.1)$$

where the energy E_0, velocity v_0 and impulse p_0 of the ring measured in the frame of reference of the superfluid are given by:

$$\begin{aligned} v_0 &= (\eta - 1/4)\,\kappa/4\pi R \\ E_0 &= (\eta - 7/4)\,\rho_s \kappa^2 R/2\pi \\ p_0 &= \pi \rho_s \kappa R^2 \end{aligned} \qquad (2.2)$$

where $\eta = \ln(8R/a)$, R = radius of vortex ring, and a = vortex core radius. The total energy $E(R,v_s)$ is a minimum at some critical ring radius $R_c(v_s)$. Below this radius, the ring will tend to collapse. Above R_c, it is energetically favourable for the ring to expand, crossing streamlines and causing dissipation. We can therefore identify the activation energy as:

$$E_a = E(R_c) = (\eta - 1/4)(\eta - 11/4)\,\rho_s \kappa^3/16\pi v_s \qquad (2.3)$$

In this equation, $\eta = \eta(R_c)$, which can be shown to be approximately temperature independent. This mechanism avoids

Campbell's[66] objection, since the energy required to create the vortex ring at the critical radius comes from the thermal energy of the fluid.

The rate of generation of fluctuations will be $\exp(-E_a/k_BT)$ multiplied by some (unknown) attempt frequency per unit volume $\mathcal{V}(T)$, times the system volume AL, where A is the area perpendicular to the flow and L is the length of the flow path. Each fluctuation will cross all the streamlines in the flow once before it annihilates at the perimeter of the flow path. For each fluctuation, the decrease in the flow velocity will be, from equations (1.6) and (1.16),

$$\Delta v_s = -\kappa/L$$

The rate of decrease of the superfluid velocity will therefore be:

$$dv_s/dt = -\kappa A\, \mathcal{V}(T)\, \exp[-E_a(v_s)/k_BT] \qquad (2.4)$$

Using (2.3), we obtain the dissipation equation of the ILF theory:

$$dv_s/dt = -\kappa A\, \mathcal{V}(T)\, \exp[-v_B/v_s] \qquad (2.5)$$

where $v_B(T)$ is a "barrier" velocity having the temperature dependence of ρ_s/T. For $v_s \ll v_B$, this function increases extremely rapidly with increasing v_s. $\mathcal{V}(T)$ is expected to be only weakly temperature dependent.

There are two interesting consequences of this equation. In the first place, (2.5) does not predict a unique critical velocity. The interpretation of the observed critical velocities is that they correspond to a value of dv_s/dt which is lower than can be detected in that particular experiment. Secondly, (2.5) exhibits "saturation of dissipation", in that for sufficiently

large v_s ($>>v_B$), the dissipation becomes velocity independent.

We shall now discuss some of the experiments which test the ILF theory. Reppy and co-workers[73,77,78,79,80,81] performed experiments on the persistent flow of bulk superfluid helium, using a "superfluid gyroscope". An annular container was filled with superleak material, immobilising the normal fluid. The gyroscope was spun up to a known angular velocity at $T>T_\lambda$, and then cooled through the lambda point before being brought to rest. The superfluid continued to rotate, and its angular momentum and superfluid density could be measured. They were thus able to determine the average superfluid velocity and its decay rate (2.4) as a function of time.

The persistent currents were found to decay logarithmically with time:

$$v_s = v_0 - \alpha^{-1}\ln(t/t_0) \qquad (2.6)$$

where t_0 and α are constants and $v_s=v_0$ at $t=t_0$. α^{-1} was found to be small (about 5% per decade of time).

Langer and Reppy[73] showed that this behaviour was predicted by the theory. Using the experimental value of α, they were able to deduce the magnitude of $E_a(v_s,T)$, which they found to be smaller by nearly a factor of 10 than their theoretical prediction based on the experimental sensitivity. Their critical velocities were also approximately ten times smaller than their theoretical estimate.

A number of other experiments have tested the ILF prediction (2.5) in bulk superflow. Notarys[82] measured the pressure/velocity relationship for bulk helium transport through a porus mica plate. His results agreed with (2.5), and yielded a temperature-independent attempt frequency ν. The temperature

dependence of v_B was found to be correct, but as with the persistent current experiment, E_a was found to be too small, by a factor of approximately 20.

Hess[83] studied superflow through 10μm diameter "orifices". (Such "orifices" are strictly speaking narrow channels, since their length is typically several tens of μm.) He too found the appropriate temperature dependence of v_B. Banton[84] observed various flow regimes through 2.5μm and 5μm diameter "orifices". Some of his data corresponded to (2.5), and he obtained values of E_a in agreement with those of Notarys.

It appears that in many circumstances, the thermal nucleation of vortex rings may be responsible for dissipation in the flow of bulk liquid helium through small apertures. It was at first assumed that the saturated helium film was similar to the narrow channels in which bulk flow was studied. However, the film thickness is a factor of 10^3 smaller than the above channel diameters, and it is not clear that the hydrodynamic analysis of Langer and Reppy[73] can be applied. Nevertheless, a number of workers have analysed their results in terms of (2.5).

Liebenberg[29] studied film flow driven by a temperature gradient, and his results agreed closely with the orifice experiments. Keller and Hammel[85] at Los Alamos obtained agreement with (2.5) at T=1.6K, but did not study other temperatures. Hoffer et al.[41], also at Los Alamos, studied the damping of the inertial oscillations between two reservoirs, and found (in addition to the Robinson damping) dissipation which could be explained in terms of (2.5). They found that both ν and v_B were very strong functions of temperature. Between 1K and the lambda point, $v_B T/\rho_s$ (which is predicted to be a constant) decreased by a factor of 30, while the supposedly nearly temperature independent parameter ν fell by 20 orders of

magnitude! The Los Alamos group subsequently studied the "run in" and inertial oscillations of the film (Campbell et al.[44]). They compared four different dissipation functions, and found that (2.5) was a slightly better fit to their results than the other three. Their results for the parameters $\mathcal{L}$ and v_B again showed large unexplained temperature variations.

In an experiment on thermally driven film flow, Campbell and Liebenberg[30] found that at sufficiently large v_s, the dissipation reached a plateau, as predicted by (2.5). However, a second plateau was found at even higher dissipation and velocity. The second plateau height corresponded more nearly to the value predicted by (2.5) with $\mathcal{L}$ and v_B derived from the oscillation experiments, and they inferred that the thermal fluctuation model was essentially correct.

Notwithstanding the general agreement with the ILF theory found by the Los Alamos workers, there is a large body of experimental evidence which does not support the theory. Martin and Mendelssohn[67] using a glass beaker, obtained a variety of different dissipation/velocity relationships at temperatures between 0.3K and the lambda point. Very few of these show the characteristic sharp variation implied by (2.5). Crum, Edwards and Sarwinski[25] used a stainless steel beaker to study the effect of ^{3}He impurity on the film profile and critical velocity. They stated that their results (for pure ^{4}He) did not agree with the thermal fluctuation theory. Using the same beaker, Armitage et al.[68,36] found that at low dissipation values, the ILF formula was not obeyed. Blair and Matheson[69] also found basic inconsistencies between their results and the ILF theory. The theory does not account for the jumps in transfer rate observed by Allen and Armitage[19] and by Harris-Lowe and Turkington[35], nor

does it explain the "quantised" transfer rates of Turkington and Edwards[34].

Taking all these experimental data into consideration (particularly the large temperature variation of the supposed constants of the theory), it is at least rather questionable that thermal nucleation of vortex rings is an important source of dissipation in the helium film. We shall now see that there are basic theoretical doubts about equation (2.5) as applied to the helium film.

The most obvious impediment to applying the vortex ring model of dissipation to the helium film is that it does not fit the symmetry of the situation. As it expands, the top and bottom of the ring will encounter the film surface and the substrate before the sides reach the limits of the flow path. (This is unlike the situation in superleaks and small channels, where the flow path dimensions are of the same order in all directions perpendicular to v_s.) The vortex ring will tend to break up into a vortex pair - two vortices of opposite circulation perpendicular to the film.

In fact, Langer and Reppy[73] suggested that a vortex pair would be the critical fluctuation appropriate to the ILF theory in the helium film. Based on this assumption, they inferred the activation energy to be:

$$E_a = [\ln(\kappa/2\pi v_s a)-1]\, d\, \rho_s \kappa^2/2\pi$$

where d is the film thickness. Substituting this into (2.4), we obtain that dv_s/dt is proportional to v_s^{λ}, where λ is given by (2.11). This is exactly the relationship derived by McCauley[86,87] for the unsaturated film, based on the Kosterlitz-Thouless picture of superfluid onset (see section 2.2). However, in the same paper, Langer and Reppy[73] present a dimensional

argument to show that in the unsaturated film, E_a should be velocity-independent. It is obvious that the appropriate form for the activation energy is in considerable doubt.

The ILF prediction (2.4) assumes that dissipation is a process limited by the rate at which vortices can be created; every vortex is assumed to cross all streamlines in the flow and be annihilated at the boundaries. In the case of vortex rings in narrow channels or superleaks, this is not unreasonable. However, for vortex pairs in the helium film, it is not at all obvious that this is the case. In film flow experiments, there is usually no boundary parallel to the flow direction against which vortices can annihilate. Other effects such as the vortex dynamics and vortex-vortex annihilation must be taken into consideration, and the problem at once becomes more complex (see references 87, 88, 89 and Chapter 7).

Further objections to the ILF theory have been highlighted by Harris-Lowe[32], who points out that at high superfluid velocities the theory should break down, and the predicted saturation of dissipation is irrelevant. He also identifies a possible error in the analysis of Campbell and Liebenberg's[30] experiment which observed saturation.

We have thus seen that the application of equation (2.5) to helium film flow experiments is questionable. Since it is certainly the case that the dissipation increases sharply with increasing v_s, it is to be expected that a sharp function such as (2.5) can be fitted to a given set of experimental data. The observed rapid temperature dependence of the fitting parameters just reflects the fact that (2.5) is the wrong shape to fit all the data. The equation is a (rather poor) yardstick against which film flow results are compared.

In conclusion, it can be said that the application of the theory to bulk flow of liquid helium in superleaks and narrow channels seems to be justified. However, it is doubtful that the thermal nucleation rate of vortices in the helium film is primarily responsible for limiting the superfluid velocity. Thermal nucleation may indeed occur, but it appears that other factors control the rate of dissipation.

2.2 The Kosterlitz-Thouless Theory

In 1972, Kosterlitz and Thouless[90,91] (referred to as KT) published a theory of ordering and phase transitions in two-dimensional systems. They pointed out that for dislocations in a two-dimensional solid (or vortices in a two-dimensional superfluid), the energy E and the entropy S both increase logarithmically with the size of the system. At low temperatures, the free energy $F = E - ST$ will be dominated by the energy term E, but as the temperature rises, the entropy term ST will eventually take over. The temperature T_c at which the free energy changes sign was taken by them to be the critical temperature of a phase transition. Below the transition, bound pairs of dislocations (or vortices) exist as thermal excitations. Above the transition, the pairs dissociate, destroying the topological order (or superflow). The theory provides an unambiguous prediction of the critical temperature; for the case of a two-dimensional superfluid it is:

$$T_c = \pi \hbar^2 \rho / 2mk_B \qquad (2.7)$$

where ρ is the density of particles per unit area and m is the effective mass of one particle.

Kosterlitz[92] investigated the critical properties of this theory, with particular reference to the "X-Y model" of spins

confined to a plane, but his results are also applicable to the case of the two-dimensional superfluid. Nelson and Kosterlitz[93] reinforced the result that ρ_s/T_c was a universal constant, and derived (numerically) an expression for the superfluid density for $T<T_c$ (see equation 2.9).

The theory was extended by Ambegaokar, Halperin, Nelson and Siggia[94] (AHNS) and simultaneously by Huberman, Myerson and Doniach[95] (HMD) to the moving superfluid film. Both these calculations showed that a large increase in dissipation was to be expected near the transition temperature.

The situation considered by AHNS is a thin superfluid film on an oscillating substrate. This was prompted by the experimental work of Berthold, Bishop and Reppy[96] (see below). AHNS introduced a diffusion constant D, representing the vortex diffusion perpendicular to $(\underline{v}_s-\underline{v}_n)$. They assumed that all interactions between the vortices and thermal excitations and the substrate may be incorporated into D. Pointing out an analogy between the vortices in the film and a plasma confined between capacitor plates, subject to an oscillating electric field, they obtained expressions for the superfluid density and dissipation as a function of frequency and temperature.

HMD independently obtained the same results as AHNS in the low-frequency limit below T_c. They emphasised that the physical reason for the increased dissipation near T_c is that the energy needed to separate a vortex pair is reduced due to screening by the other (polarised) vortex pairs. Myerson[97] in a separate paper extended the work of HMD, and obtained explicit expressions for the superfluid density and the dissipation in terms of the temperature and the superfluid velocity. His results are applicable up to higher velocities than those of AHNS.

At this point, it is useful to summarise the predictions of the theory. For the static film, the superfluid density jumps discontinuously to zero as T_c is exceeded. From equation (2.7), the size of the jump is:

$$\rho_s(T_c^-) = 8\pi k_B T_c/\kappa^2 \qquad (2.8)$$

where κ is the quantum of vortex circulation. The superfluid density below T_c is also predicted by the static theory:

$$\rho_s(T) = \rho_s(T_c^-)\ (1+b(1-T/T_c)^{1/2}) \qquad (2.9)$$

where b is a (substrate dependent) constant.

For the dynamic film, the step in ρ_s is rounded; its shape is predicted by AHNS and by Myerson, as is the shape of the dissipation peak near T_c.

The first indication that the theory might be the correct description of the superfluid transition in the real unsaturated helium film came from Rudnick[98]. He presented a variety of third-sound measurements made near the transition temperature at his laboratory, from which he calculated ρ_s. The results showed that ρ_s/T_c was very nearly constant between T_c = 0.75K and 1.85K, at coverages between 2.1 and 5.6 atomic layers. The average value of ρ_s/T_c was in close agreement with equation (2.8).

Bishop and Reppy[99] measured ρ_s for the unsaturated film using an Andronikashvili torsional pendulum, with Mylar as the adsorbing substrate. As the pendulum was cooled down below T_c, the superfluid component decoupled from the substrate, and the effective moment of inertia of the bob fell, causing the frequency to increase. The change in period allowed the superfluid mass to be determined. The Q of the oscillator was used to measure the dissipation.

The data obtained by Bishop and Reppy showed excellent agreement with the dynamic theory of AHNS, both in the superfluid density variation, and in the dissipation. The value of $\rho_s(T_c^-)$ was found to be very close to equation (2.8) for all film thicknesses that were studied. Bishop and Reppy also pointed out that some earlier experiments (such as that of Chester and Yang[12]) had implied a jump in ρ_s at the transition temperature.

Further confirmation of the theory came in 1980, when Roth, Jelatis and Maynard[100] published the results of an experiment on Grafoil (a type of graphite foam). They measured the third-sound velocity near onset, and determined the adsorbtion isotherm on Grafoil. Their result for ρ_s/T_c was within 11% of the predicted value (equation 2.8).

All experimental data do not, however, support the KT theory. An earlier (1977) experiment by Berthold, Bishop and Reppy[96] used an Andronikashvili torsional pendulum to measure ρ_s on Vycor glass. This porus material has a very large specific surface area, due to the large number of interior channels, which form a highly connected three-dimensional network. The Vycor glass used in the experiment had a mean pore diameter of approximately 8nm. Berthold, Bishop and Reppy found no discontinuity in the superfluid density near the transition; their results showed a dependence of ρ_s on T of the form:

$$\rho_s = A(1-T/T_c)^{0.635} \qquad (2.10)$$

with A dependent on the film thickness. This is similar to the behaviour of bulk helium, and is incompatible with the KT theory. The explanation put forward was that the highly three-dimensionally connected system of pores destroyed the two-dimensional nature of the film, making the KT theory

inapplicable. However, the Grafoil substrate used by Roth, Jelatis and Maynard[100] was also highly connected, and it seems strange that third-sound measurements should indicate the applicability of the KT theory to such a system, while the torsional pendulum experiment should not.

A further (theoretical) doubt has been cast on the applicability of the KT theory to the real helium film. Dash[101] has pointed out that "phase condensation" should occur in the film. He argued that below a certain temperature, the normal-to-superfluid transition will be a percolation transition from patches of unconnected superfluid to a continuous connected superfluid sheet as the density is increased. This transition should happen at a constant density, independent of temperature. No KT type transition should be observed between the percolation transition onset temperature and T=0.

Dash interpreted the absence of this critical temperature gap as showing that either the heterogeneous nature of real substrates has a major effect on the interpretation of the theory, or that two-dimensional superfluidity can be a two-phase phenomenon, involving both the superfluid patches and the surrounding two-dimensional vapour. The controversy between Dash and his supporters and believers in the KT theory continues.

Despite this unresolved problem, research on the KT model has continued. Berker and Nelson[102] have extended the theory to ^3He - ^4He mixtures, and have calculated the contribution of the vortices to the specific heat. McCauley[86,87] derived expressions for the vortex dissociation and recombination rates at temperatures far below T_c. He assumed that the vortex distribution is principally due to Brownian motion of the vortices in the gas of thermal excitations. He demonstrated the importance of the "vortex-vortex coupling constant":

$$\lambda = \rho_s \kappa^2 / 2\pi k_B T \qquad (2.11)$$

$\lambda < 4$ above T_c

$\lambda = 4$ at T_c

$\lambda > 4$ below T_c

This is analogous to the Reynolds number for the two-dimensional film.

Another experiment which has been interpreted in terms of the KT theory is that of Eckholm and Hallock[103]. They created a persistent current over a toroidal path in the unsaturated film, and monitored the velocity by measuring the Doppler shift of third sound. Their results showed that for films thicker than approximately d = 8 atomic layers, the velocity decayed following a logarithmic law (equation 2.7). For thinner films, (d < 8 layers), the decay was slower at late times; the velocity was found to be given by:

$$v(t) = A(1+Bt)^{-n} \qquad (2.12)$$

where n varied between approximatly 0.3 and 1. The problem arose because although the KT theory could be used to derive the empirical formula (2.12), the value of λ was required to change rapidly with thickness, and indeed for the thinnest films, $\lambda<4$, violating the KT condition for superfluidity.

Various attempts were made to explain this discrepancy; all of them relied on "vortex density relaxation" (allowing the vortex density to vary explicitly with time during the flow). McCauley[104] suggested that the thicker (d>8) films started with less vorticity than the thinner films, but was unable to obtain satisfactory fits to the data. Yu[88] incorporated vortex creation and annihilation at the film edges as well as in the bulk, and

studied the effects of vortex pinning. He obtained reasonable fits to the persistent current data with three adjustable parameters, and obtained values of λ which were in reasonable agreement with the third sound experiments of Rudnick. However, to explain the thin film ($d<8$) data, he relied on film-edge effects. It is very difficult to see where these edges could arise in the geometry of the experiment. Browne and Doniach[89] also considered vortex density relaxation and vortex pinning effects, and obtained good fits to the data, but at the expense of using five adjustable parameters.

The ideas presented in Chapter 7 are similar to some of those used by Yu and by Browne and Doniach. The importance of vortex-density relaxation has now been recognised in the unsaturated film; the work presented in Chapters 6 and 7 demonstrates its importance in the saturated film.

CHAPTER 3

THE EXPERIMENTAL APPARATUS

3.1 General Design

We have seen that the situation regarding dissipation in the saturated film is far from clear. Further experimental and theoretical effort is required to clarify the position, and therefore the work presented here was undertaken.

There are a number of factors to be taken into consideration in the design of a film flow experiment. In many cases, it is largely a question of eliminating unwanted effects, and we now describe how such requirements affect the experimental geometry.

The asymmetry of beaker film flow experiments results in a difference between inflows and outflows, as we have noted. To eliminate this effect, a "twin-reservoir" design was adopted, comprising two similar reservoirs connected by the film.

The experiments of the Los Alamos group[70,71] have shown that changes in the region where dissipation occurs affect the transfer rate. To avoid this variation, it is necessary to confine the dissipation to a known part of the flow path. A possible way of doing this is to ensure that the region of maximum velocity is well localised, which is achieved in our experimental apparatus by constraining the film to flow through a small hole in a plastic film. The maximum velocity occurs in the hole, and there are large velocity gradients on either side of it. It is of course necessary that the substrate should be clean and smooth in the dissipation region.

The experimental cell was designed as a small, self-contained chamber, to be filled with helium gas at room temperature and then sealed off. Provided the design allows sufficient 'dead volume' so that the pressure of gas need not be too high, such a scheme has several advantages compared with

other commonly used methods.

Many previous studies have used the technique of filling the cell at low temperature down a stainless steel capillary from a room temperature gas supply. However, such an approach would involve additional plumbing, and be a source of leaks. In addition, a capillary leading into the cell adds complicating effects such as film refluxing up and down the capillary, and the possibility of bulk liquid helium moving between the experimental region and the capillary due to fountain pressure.

An alternative scheme utilised in early experiments was filling the experimental cell from the main bath through a needle valve. In the present case, the intention was to use ^{4}He with as little ^{3}He impurity as possible, to eliminate any transfer rate variation from this source[25]. The liquid helium in the main bath was insufficiently pure to use for the experimental cell. This scheme was therefore also rejected in favour of the sealed cell system.

The technique chosen for monitoring the liquid level in the reservoirs was by measuring the change in capacitance of a parallel plate capacitor as the amount of helium between the plates varied. This method is now used almost universally, the only alternative being visual observation using a cathetometer, which among other disadvantages is very slow. To reduce the dead space necessary for the gas at room temperature, the minimum amount of liquid helium possible was to be used. The most efficient utilisation of the liquid helium is when it is all between the capacitor plates, contributing to the level measurement. The capacitors were therefore designed such that the space between the plates formed the reservoirs.

To maximise the sensitivity of the capacitors to change in

(vertical) liquid level, the capacitor-reservoirs were inclined at a small angle to the horizontal. A given change in vertical liquid level would then correspond to a greater change of liquid volume between the plates than if the capacitor were vertical.

The film was driven by applying a DC voltage to one of the capacitor reservoirs. The resulting decrease in the chemical potential of the liquid in that reservoir resulted in a chemical potential gradient over the length of the film, initiating flow between the reservoirs through the film. The DC voltage source was programmable, to allow extremely flexible drive/time profiles to be used.

This electrostatic drive method was chosen in preference to the main alternative, which involved liquid displacement using a moving bellows. One disadvantage of the latter technique is the necessity of transmitting a smoothly changing mechanical displacement down to the low temperature parts of the apparatus. The mechanical method is also less flexible, since the chemical potential cannot be changed as quickly or as easily as in the electrostatic case.

The chemical potential of liquid helium in an electric field is given by

$$\mu = -\chi \varepsilon_0 E^2/2\rho \qquad (3.1)$$

The chemical potential change due to the electric field thus varies as the square of the applied voltage. The programmable voltage source used to drive the film was therefore preceeded by a square-root stage. The input to this stage was thus directly proportional to the electrostatic chemical potential difference.

In order to control the input (V_0) to the square-root stage, a 'Film Drive Unit' (FDU) was constructed. It consisted of several signal sources, each of which could be individually

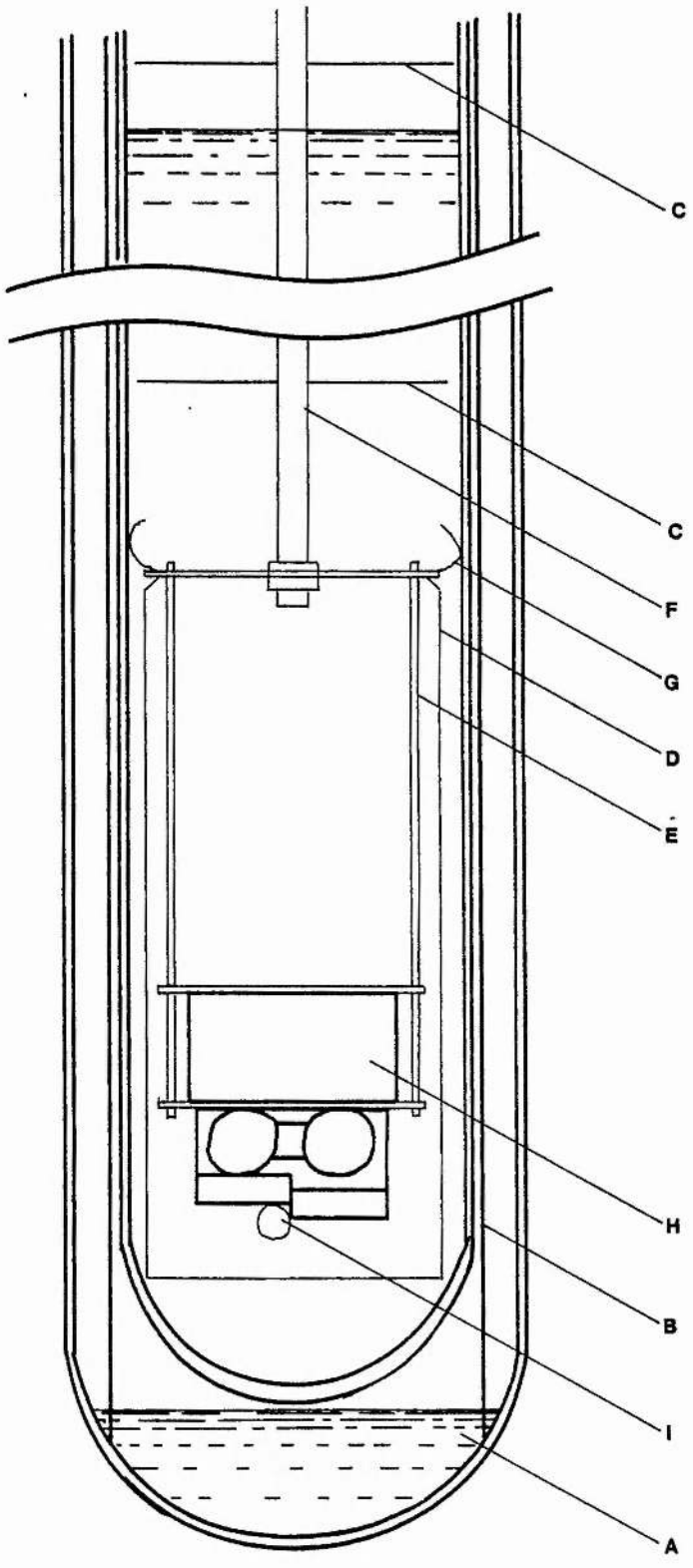

FIGURE 3.1 The cryostat (not to scale)

disabled, feeding into a summing amplifier, the output of which was connected to the square root stage. Provision was made for a signal proportional to the liquid level in the measurement capacitor to be (optionally differentiated and) added to the other signals. A feedback loop was thus established, comprising the drive capacitor, the helium film, the measurement capacitor and its associated electronics, the FDU and the programmable voltage source. By inverting and differentiating the liquid level signal, inertial oscillations in the helium film could be built up and maintained essentially indefinitely.

3.2 The Cryostat

The experimental cell was originally designed to be used in a very low temperature adiabatic demagnetisation cryostat. However, circumstances dictated that a silvered glass cryostat be used, which was capable of reaching only 1.10°K. All experiments were carried out at or near this temperature.

Figure 3.1 shows the low temperature parts of the apparatus. An outer dewar contained liquid nitrogen (A), both to precool the the inner helium dewar before liquid helium was transferred into it, and as a thermal shield. During the course of the experiment, the level of nitrogen in the outer dewar was kept below the bottom of the inner dewar in order to eliminate vibration of the latter due to boiling of the liquid nitrogen. To maintain the effectiveness of the nitrogen as a thermal shield, a cylindrical copper radiation shield (B) was situated between the two dewars, with its lower end in the nitrogen. The maximum time for which data could be taken was limited by the time for which the bottom of the radiation shield remained in the liquid nitrogen. As soon as the shield emerged it started to warm up, causing a temperature change in the helium bath.

The liquid helium filled inner dewar was pumped on through a 2" diameter flexible pipe connected to a rigid 4" diameter pumping line and thence to a large rotary pump, two rooms away from the experiment. No vibration was detectable at the experimental apparatus due to this (or any other) source.

Two circular radiation shields (C) were situated in the helium space above the experimental cell in order to reduce the thermal radiation falling on the cell from the top of the cryostat. Another cylindrical copper radiation shield (D) was situated in the liquid helium surrounding the cell.

The experimental cell (H) was supported in a brass frame (E) connected to a stainless steel tube (F) suspended from the cryostat top plate. Small german silver tongues (G) were mounted on the frame to effect mechanical contact with the cryostat walls. Electrical connections were made through glass-to-metal seals at the cryostat top.

A mercury manometer was connected to the cryostat top, and the pressure was read off with a cathetometer. By reference to a table of the liquid helium vapour pressure, the temperature was determined.

A 220Ωcarbon resistance thermometer (I) was mounted on the experimental cell, and its resistance was measured with an Oxford Instruments resistance thermometer bridge. The off-balance signal from the bridge was rectified and connected to a heater in the liquid helium, thus forming a feedback loop to control the temperature in the cryostat. The rectifier was included so that a rise in temperature beyond the bridge null point could not supply power to the heater. The off-balance signal was recorded on a chart recorder. Using this control system, the temperature remained constant to within 3mK so long as the 77K radiation

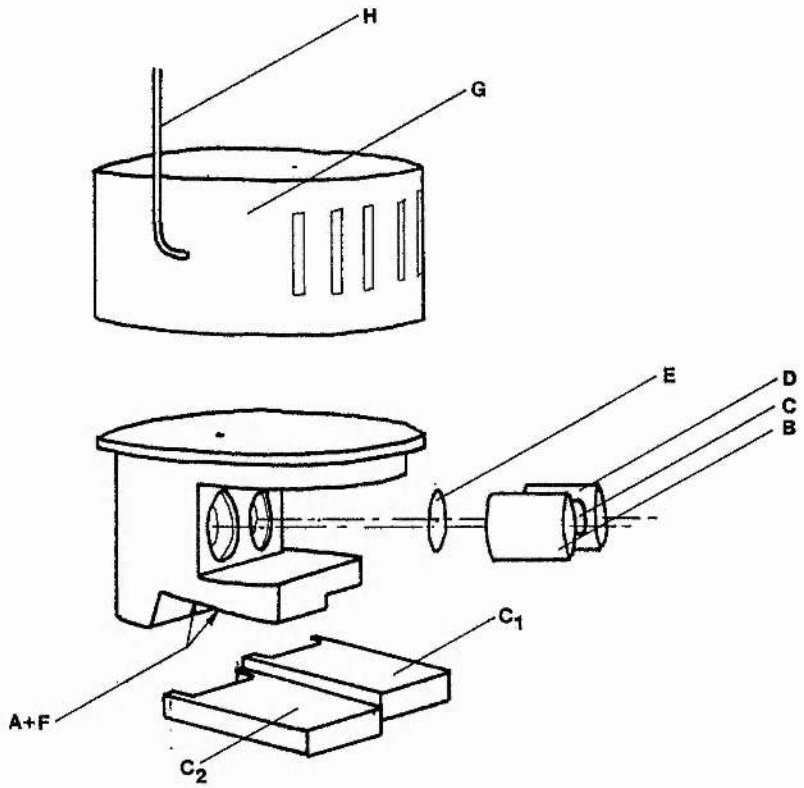

FIGURE 3.2 The experimental cell

shield remained in the liquid nitrogen.

3.3 The Experimental Cell

The experimental cell (figure 3.2) was made mainly from Stycast 1266, a cold-setting two part transparent epoxy resin, much used for the construction of low-temperature apparatus. Among the advantages of this material is the ease with which complex-shaped parts may be moulded or machined and the variety of constructional techniques which may be used.

The two reservoirs of liquid helium between which flow took place were formed by two capacitors, separated vertically by 4mm. To maximise the sensitivity of the capacitors, they were inclined at an angle of approximately 12^{o} to the horizontal. The upper capacitor (the drive capacitor C_1) was connected to a programmable high voltage supply, and the lower capacitor (the measuring capacitor C_2) was connected in one arm of a ratio arm transformer bridge.

With no voltage applied to C_1, the lower capacitor C_2 contained its maximum volume of liquid helium. As the voltage to C_1 was increased, helium flowed from C_2 through the film joining the two capacitors to C_1.

The path taken by the film was: from capacitor C_2 up through a slot (A) onto the walls of a cylindrical chamber (B); thence through a tube (C) into a second cylindrical chamber (D), where a constriction (E) in the form of a Melinex disk with a central hole was encountered. The film then entered C_1 through another slot (F).

The flow-constricting hole was formed using a red-hot needle point to melt the film. The plastic drew back from the needle point, leaving a nearly perfect circular hole edged by a bead of smooth plastic. Care was taken to keep the film as clean as

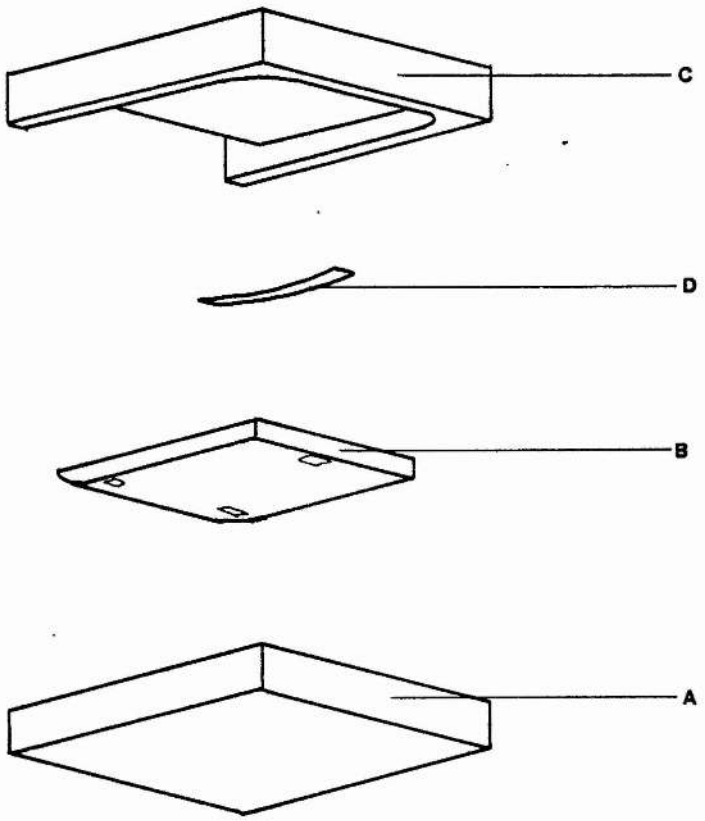

FIGURE 3.3 Capacitor construction

possible to reduce the possibility of enhanced transfer rates due to contamination.

There was a dead volume (G) above the rest of the cell, connected by a small hole to (A). This was to provide space for the helium to expand into as the cell was warmed. On the exterior of this dead space were glued eight copper strips, to act as terminals for the connections to the cell capacitors and the resistance thermometer.

The cell was filled through a German silver capillary (H) embedded in the wall of the dead space. After filling with pure helium gas (containing less than one part in 10^9 of ^3He) to the required pressure, the tube was pinched off and the end soft soldered.

3.4 The Capacitors

The measurement and drive capacitors C_1 and C_2 were constructed identically and differed only in their electrical connections. Figure 3.3 shows the method of construction.

The capacitor plates were made of perspex. It was found that perspex sheet 'as rolled' was sufficiently flat (typically to a few wavelengths of light) for this purpose. The lower plate, (A) in the figure, was cut from 5mm perspex sheet, while the upper plate (B) was of 1mm perspex. Plate (B) (1.1cm x 1.7cm) was chamfered on its upper edge in order to allow electrical contact to be made to its surface. Both plates were thoroughly cleaned and degreased in an ultrasonic bath before being gold plated on one side in a vacuum deposition chamber to a thickness of approximately 300nm. The lower plate (2.3cm x 2.0cm) was masked round the edge in order to prevent gold from reaching the areas which had to be glued.

The distance between the capacitor plates was defined and

maintained by three 1.5mm squares of 100μm thick Melinex sheet. Two squares were located at the top end of the capacitor plates, one on either side, and the third was positioned at the bottom end in the centre, as shown in the figure. Due to the 'rag' on the edges of the squares, their effective thickness was measured to be 120μm. (Details of this measurement are to be found in section 4.1).

A top member (C) was glued onto the lower plate around the edges, using quick setting cyano-acrylate adhesive. The join was made leak free with an exterior coating of Stycast 1266. The upper plate with the Melinex spacers resting on it was inserted into the upside-down assembly, which was then inverted. To retain the upper plate in position, a small leaf spring (D) was inserted between it and the top of the capacitor 'box'.

Electrical connection was made to the gold-coated surfaces through two 42 SWG copper wires which were affixed to the plates at their upper ends using Dag silver paint.

The small gap between the capacitor plates ensured that any bulk liquid helium in the cell was held by surface tension within the capacitors. A volume of 0.018cm^3 was calculated as being sufficient for the experiment. However, it was found that 0.05cm^3 had to be introduced into the cell in order to provide a satisfactory liquid level in the capacitors. This may be explained by the existence of cracks within the cell, of smaller width than the capacitor plate separation. These cracks would be the first to fill with liquid helium due to surface tension.

The total internal volume of the cell (approximately 35cm^3) was such that one atmosphere of helium gas at room temperature provided approximately 0.05cm^3 of liquid helium.

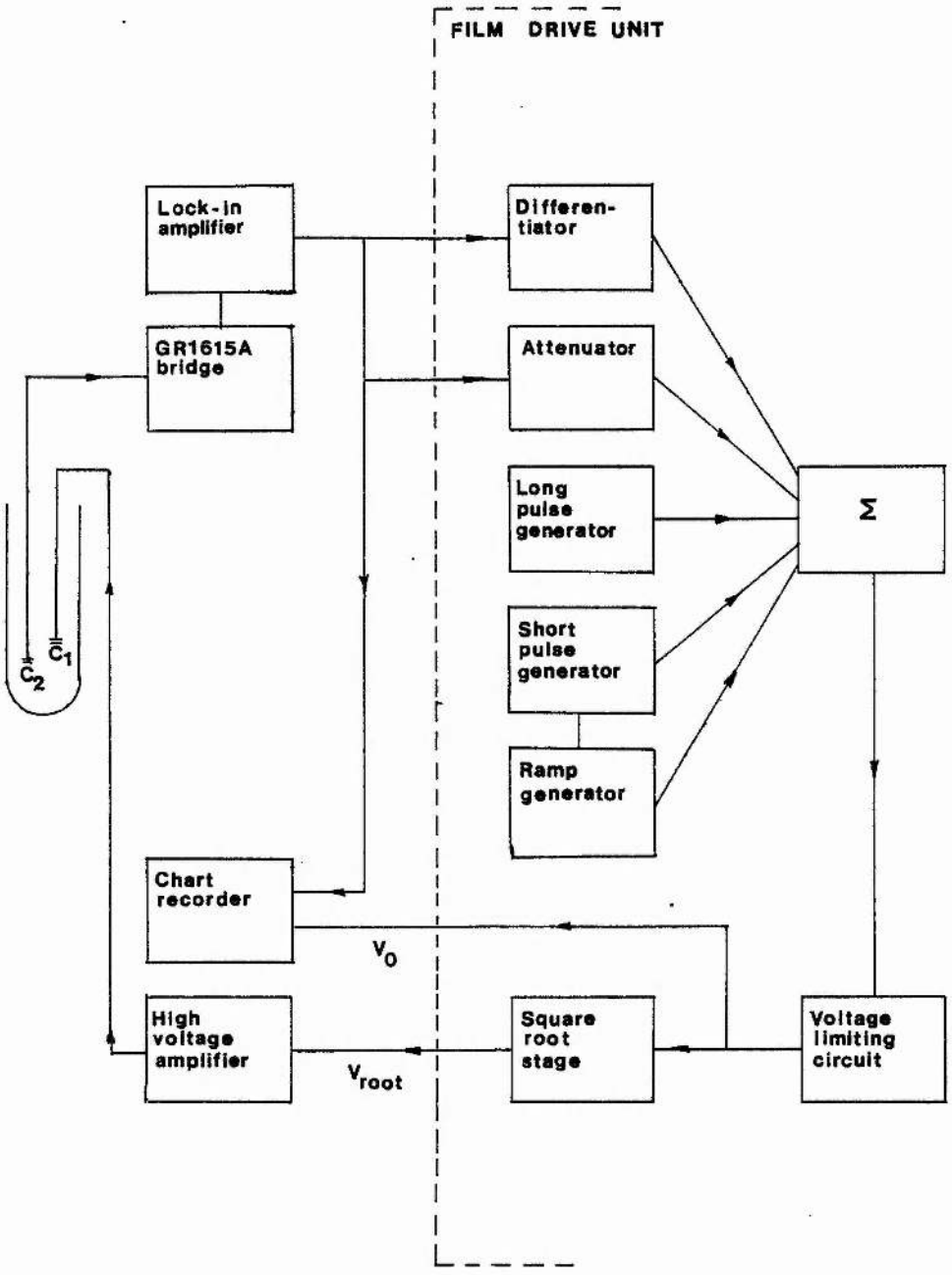

FIGURE 3.4 Block diagram of the electronics

3.5 The Measurement and Feedback System

A block diagram of the measurement and feedback electronics is shown in figure 3.4. The lower capacitor C_2 was incorporated in the measurement arm of a ratio-arm transformer bridge (type GR1615A). Its capacitance was measured using the three terminal technique, which eliminated the effect of lead capacitance. The transformer could be used to measure the capacitance to 6 digit accuracy, or alternatively could be set at a particular capacitance value. In the latter mode, the signal seen by the null detector of the bridge was proportional to the difference between the value dialled on the bridge and the actual value of C_2. This proportionality was measured to be accurate to 0.01% over the range used. However, the proportionality constant (ie the out-of balance sensitivity) was found to be slightly dependent on the bridge setting.

The null-detector used was a Brookdeal 9503 lock-in amplifier, containing an integral oscillator which provided excitation for the bridge and a reference signal for the phase-sensitive detector. Excitation at 5kHz at 5Vp-p was used. The output of the lock-in amplifier was a -10V to +10V DC level representing either the in-phase or the quadrature component of the output of the bridge. Which phase it represented was switch selectable. The quadrature component could be balanced out by introducing compensating resistive loss into the reference arm of the bridge. The in-phase off-balance signal was then proportional to the value of C_2 and thus proportional to the level of liquid helium between its plates.

The lock-in amplifier output was smoothed by an internal integrator. For optimum noise reduction, a time constant of 1s was chosen for this stage. The output was recorded on a two pen

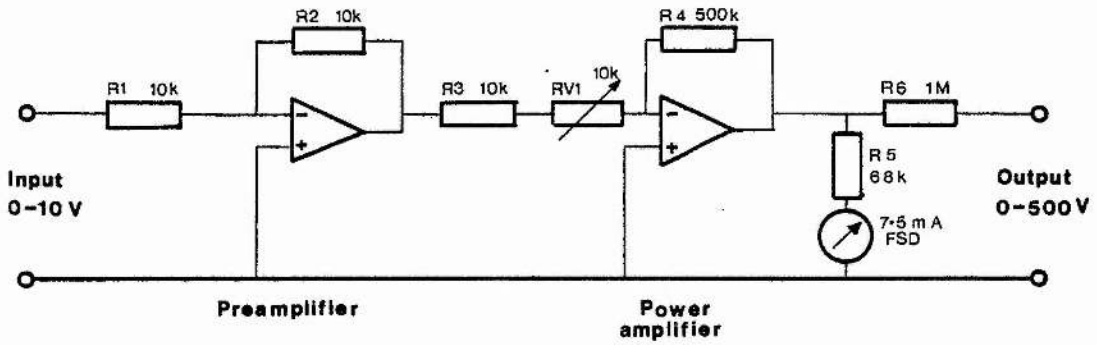

FIGURE 3.5 High voltage amplifier circuit

chart recorder, together with the output from the film drive unit. The off-balance signal was also connected to the film drive unit as part of the feedback path.

The programmable DC power supply used to drive the upper cell capacitor C_1 was a Kepco model OPS500B, capable of a maximum output voltage of 500V. It consisted of a low voltage preamplifier followed by a power amplifier. Figure 3.5 shows the connection of these two stages.

The preamplifier was configured as a unity gain inverter. The power amplifier was also connected as an inverter, with an adjustable gain controlled by RV_1. The gain could be varied from 25 up to 50, and was typically kept constant at 40. A 1MΩ resistor R_6 was inserted in series with the output in order to increase the output impedance, since only very little current was required by the capacitive load even when the output (V_1) was changing at its maximum rate. R_6 prevented damage to delicate wiring in the cryostat in the event of an accidental short circuit.

3.6 The Film Drive Unit

The six signal sources feeding the summing amplifier in the film drive unit were: a ramp generator, a short pulse generator, a long pulse generator, a differentiator, an amplifier/attenuator and a general purpose external signal. The function and the working of each of these sources will be described individually. Component numbers refer to figure 3.6.

The purpose of the ramp generator was twofold: to provide a means of altering the equilibrium levels in the capacitors, and to initiate and maintain flow at a predetermined transfer rate. The ramp generator had three modes, controlled by front-panel pushbuttons: a) 'run', when the output increased or decreased at

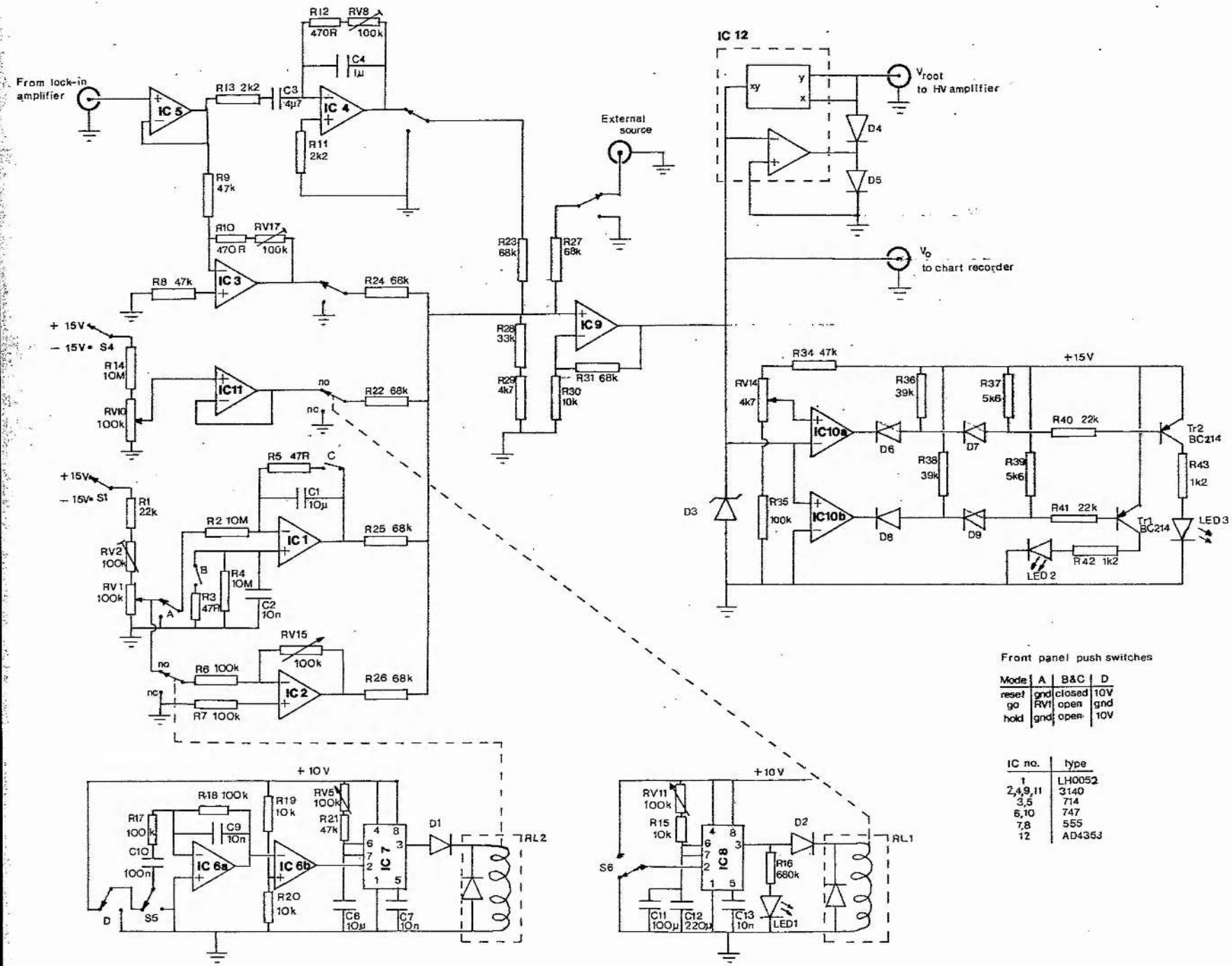

Front panel push switches

Mode	A	B&C	D
reset	gnd	closed	10V
go	RV1	open	gnd
hold	gnd	open	10V

IC no.	type
1	LH0052
2,4,9,11	3140
3,5	714
6,10	747
7,8	555
12	AD4353

FIGURE 3.6
The Film Drive Unit. ICs 1 to 5, 9, 11 and 12 have offset adjustment pots connected, and ICs 2, 4 and 9 have frequency compensating capacitors. These have been omitted for clarity, and they account for the missing component numbers.

a constant rate; b) 'hold', when the output was maintained at a constant value; and c) 'reset', when the output was forced to zero.

The ramp generator consisted of an integrator (IC_1,R_2,C_1) of time constant 100s, supplied (in 'run' mode) from the slider of a 10-turn potentiometer RV_1. The sign of the input voltage, and therefore the direction of change of the integrator output, was selected by S1. By adjusting RV_1, any required voltage ramp rate could be generated. The linearity of the integrator output was better than 0.1%. The ramp rate scaled linearly with the setting of RV_1 to 0.25%. An imbalance in the positive and negative supply lines caused the 'up' rate and the 'down' rate to differ by 0.4% for a given setting of RV_1.

In 'hold' mode, the integrator input was grounded, and the charge on C_2 maintained the output voltage at its previous value. In order that the output voltage should not 'droop' excessively in this mode, careful selection of components C_1 and IC_1 was essential. To minimise the leakage conductance of C_1, a polyester dielectric type was chosen, with a dielectric resistance greater than $3 \times 10^{10}\Omega$. This corresponded to a calculated time constant of more than 3.5 days. The measured 'droop' rate of the integrator output was $5\ \mu Vs^{-1}$ at an output voltage of 3.1V. The actual time constant was therefore 7.1 days.

In 'reset' mode, C_1 was discharged through R_5 and the output brought to zero.

We now turn to the long pulse generator. The presence of inertial oscillations in the helium film is often an unwanted side effect; for instance when studying steady flow. An electronic means of eliminating the oscillations was therefore attractive. The long pulse generator provided such a facility. An output pulse of adjustable height and duration could be


FILM DRIVE UNIT
EXT
on
on
ATTEN
+
–
on
start
LONG
on
man.
SHORT
up
down
adjust
RAMP
POWER
ON
on
DIFF
height
time
height
go
reset
hold
hi
lo

initiated using switch S_6. Section 4.3 describes the effect of the pulse on the oscillations.

The timing of the pulse was controlled by IC_8. Depressing the start button S_6 caused pin 3 on IC_8 to go high, illuminating LED_1 and operating relay RL_1, thus causing the output of the voltage-follower IC_{11} to be fed to the summing amplifier. The duration of the pulse was controlled by RV_{11} and could be varied from 3 to 30 seconds. The pulse height was adjustable up to 150mV using RV_{10}. The direction of the pulse was controlled by S_4.

The transition from a stationary equilibrium situation to a state of constant sub-critical transfer rate initiates inertial oscillations, because the film cannot accelerate to the required flow rate instantaneously. In order to eliminate oscillations generated in this manner, a short voltage pulse could be applied to the drive capacitor whenever the ramp generator entered 'run' mode. A pulse of (suitably short) constant duration and of height proportional to the transfer rate provided sufficient impulse to accelerate the film to the required flow rate. Section 4.3 describes the effect of the short pulse on the oscillations.

The pulse timing was controlled by IC_7, RV_5, R_{21} and C_6. A pulse width of 2 seconds was used. With the short pulse facility enabled (using S_5), whenever the 'run' mode of the ramp generator was selected relay RL_2 was energised, presenting the voltage on the slider of RV_1 (which was proportional to the transfer rate) to the inverting amplifier IC_2. For a fixed setting of RV_1, the height of the pulse was controlled by RV_{15} in the feedback loop of IC_2.

The 10V power supply for both the short and long pulse control logic ($IC_{7,8}$, $RL_{1,2}$) was kept separate from the analog

power supply (-15V and +15V) in order that any switching transients should not affect the latter.

I am obliged to J G M Armitage for suggesting both pulse techniques for eliminating the oscillations.

We now consider the remaining inputs to the summing amplifier. The output from the lock-in amplifier was connected to the FDU to complete the feedback loop. After a voltage follower stage (IC_5) to reduce the impedance, the lock-in signal was fed to an inverting amplifier (IC_3) with a gain variable between 0.5 and 100, controlled by RV_{17}. The lock-in signal was also fed to a differentiator (IC_4,C_3,RV_8) with a time constant adjustable up to 500ms using RV_8. R_{13} and C_4 limited the high frequency response of the differentiator to approximately 20Hz.

The polarity of the lock-in amplifier output could be reversed by means of a front panel pushbutton on the amplifier. It was thus possible to select positive or negative feedback. It will be shown in Chapter 4 how feedback through the amplifier/attenuator affected the period of the inertial oscillations, while feedback through the differentiator introduced either additional damping of the oscillations (if negative feedback), or exponential growth of the oscillations (if positive feedback).

An extra input to the summing amplifier was provided, but not used during the experiments.

The output V_0 of the summing amplifier IC_9 was available externally for monitoring on a chart recorder. Two front-panel indicators (LED_1 and LED_2) were used to show when V_0 was at the top or bottom of its permitted range of 0 to 10V. The zener diode D_3 prevented V_0 from rising above 10V.

The square-root function was implemented with an Analog Devices 435J transconductance multiplier module. The multiplier

inputs (X and Y) were both connected to the output of the internal amplifier A, which was configured as an inverter with the multiplier in the feedback loop. Analysis of this configuration gives the output voltage V_{root} in terms of the input V_0:

$$V_{root} = - \sqrt{10 (V_0 - \varepsilon)} \qquad (3.2)$$

where ε represents errors associated with the multiplier. Diodes D_4 and D_5 prevented the output from going positive, which would 'latch up' the circuit.

The measured performance of the square-root stage was:

$$V_{root} = - 0.997 \sqrt{10 (V_0 - 0.004)} + 0.014 \qquad (3.3)$$

The 14mV offset of V_{root} had the effect of a constant level difference between the capacitors and therefore did not affect the performance of the FDU. Neglecting this offset, the square - root stage was accurate to better than 0.4% over 90% of its range.

CHAPTER 4

EXPERIMENTAL PROCEDURE

4.1 Calibrating the Capacitors

The quantities actually measured in the experiment were the value of the measurement capacitor C_2 and the voltage V_1 applied to the drive capacitor C_1. In order to relate these to the physically interesting quantities of level difference and flow rate, knowledge of the capacitor geometry was important. The width and length of the capacitors were determined by measurement prior to assembly. The exact capacitor plate separations were however not known.

In order to obtain an estimate of d_2, the separation of the measurement capacitor plates, a preliminary experiment was carried out. Prior to mounting C_2 on the cell, it was placed on its own in a cryostat and cooled to 1.1K. Measurements were made of its value both in the liquid helium bath and out of it. The difference between these two values ($\Delta C = 0.62 \pm 0.005$ pF) together with the known areas of the capacitor plates and the Melinex spacers, was used to determine the mean value of d_2. ($d_2 = 123 \pm 3\,\mu$m.)

Once the cell had been assembled and filled, the relationship between level difference and the value of C_2 could be determined by measuring the latter as a function of the voltage applied to C_1. The expected form of this relationship may be derived as follows.

Ignoring surface tension, the chemical potential of the liquid helium in the upper and lower capacitors is given by

$$\mu_1 = g\,(h_0 + x_1 \sin\theta_1) - (\chi\varepsilon_0/2\rho).(V_1/d_1)^2 \qquad (4.1)$$

$$\mu_2 = g\,x_2 \sin\theta_2 - (\chi\varepsilon_0/2\rho).(V_2/d_2)^2 \qquad (4.2)$$

where the symbols have the following meanings:

g = acceleration due to gravity

h_0 = vertical separation of the two capacitors

$x_{1,2}$ = displacements of the liquid levels from the bottoms of the capacitors, measured parallel to the capacitor plates

$\theta_{1,2}$ = the angles made by the capacitors to the horizontal

$d_{1,2}$ = mean separation of the capacitor plates in the region occupied by the liquid helium

$w_{1,2}$ = mean widths of the capacitor plates in the region occupied by the liquid helium

$V_{1,2}$ = voltage applied to the capacitors

$(1+\chi)$ = dielectric constant of liquid helium

The total volume of liquid in the capacitors is:

$$V = w_1 x_1 d_1 + w_2 x_2 d_2 \qquad (4.3)$$

At equilibrium, $\mu_1 = \mu_2$. Combining equations (4.1), (4.2) and (4.3), and differentiating with respect to x_2, we obtain:

$$(\chi \varepsilon_0 / 2\rho g)\, dV_1^2/dx_2 = - d_1^2 d_2 w_2 / A \qquad (4.4)$$

where we have defined the "reduced area" A as:

$$A = (\sin\theta_1/w_1 d_1 + \sin\theta_2/w_2 d_2)^{-1} \qquad (4.5)$$

Expressing C_2 in terms of w_2, d_2 and x_2, and substituting in equation (4.4), we obtain:

$$\frac{dC_2}{dV_1^2} = - \frac{(\chi \varepsilon_0)^2}{2\rho g} \frac{A}{d_1^2 d_2^2} \qquad (4.6)$$

If d_1 and d_2 are independent of x and our other assumptions hold,

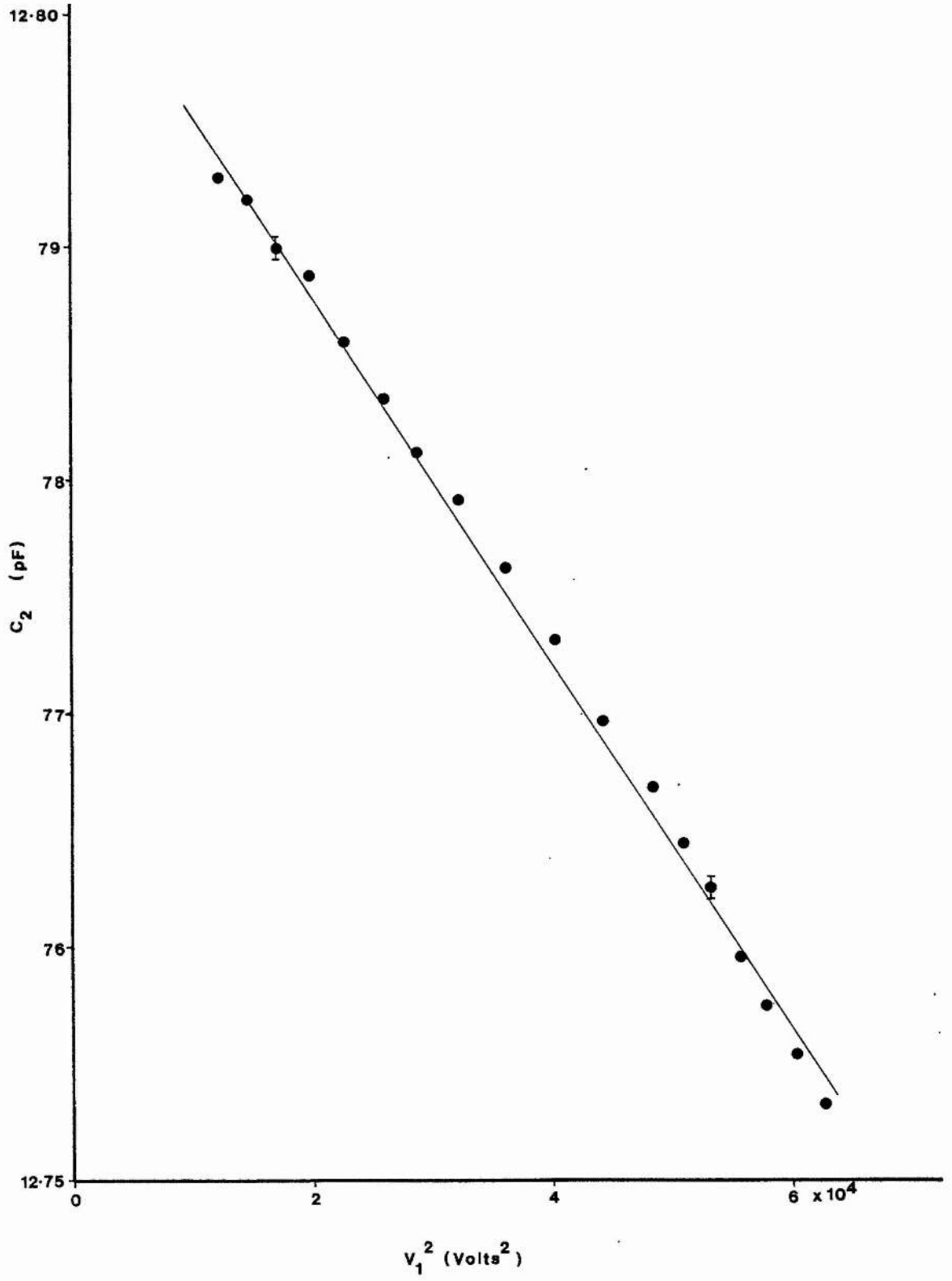

FIGURE 4.1 Capacitor calibration

then a graph of C_2 against V_1^2 should be a straight line, with a slope given by (4.6).

In order to verify this prediction, the filled cell was cooled to 1.1K and the temperature stabilised as described in section 3.2. V_1 was increased from zero using the film drive unit (FDU). To take a reading at a particular value of V_1, the FDU was put into "hold" mode, and once the inertial oscillations of the film had died away, the value of C_2 was measured.

Previous experience had shown that dielectric breakdown in the drive capacitor could occur at approximately 300V. This corresponded to a mean electric field of 3×10^6 Vm^{-1}, which is the approximate dielectric strength of helium gas. The field near the edges of the upper capacitor plate would exceed this value. For this reason, the voltage applied to C_1 was kept below 250V.

Figure 4.1 shows the results obtained. A number of points arise from this graph.

The range of C_2 (from completely empty to completely full) was 12.615 to 13.235 pF. The usable range over which the liquid level could be varied appears from figure 4.1 as 12.753 pF to 12.794 pF, ie only 0.041 pF, 8% of the total available range. (The repeatability of these "constants of the apparatus" was $\pm$0.01pF from run to run. The accuracy to which a particular value of C_2 could be measured was $\pm$0.0005pF.) Secondly, the graph appears to be slightly curved, rather than straight as predicted by equation (4.6). Possible factors contributing to these observations will now be described.

The actual capacitor plate separations were found to be approximately 20% larger than the designed value of 100 μm. Due to the strong dependence of dC_2/dV_1^2 on the plate spacing, this derivative was reduced by a factor of 2 from its designed value.

The maximum achievable value of V_1 was also reduced by a factor of 2 due to dielectric breakdown. Both these factors reduced the accessible range of the capacitors.

The effect of the Melinex spacers in the capacitors was to lower the value of the reduced area A by approximately 6% when the spacers intersected the liquid surface. The known size and approximate position of the spacers in the capacitors enabled the values of C_2 at which they would have this effect to be calculated. Below 12.675 pF and above approximately 12.83 pF, the spacers would be expected to alter the value of A. The cell was filled with enough liquid to ensure that the usable liquid level range was well away from these limits, and the spacers could be ignored.

The mean value of dC_2/dV_1^2 over the range 12.752 to 12.790 pF, where most of the experiments took place, was estimated from figure 4.1 to be $(7.85 \pm 0.25) \times 10^{-7}$ pFV^{-2}. Substituting this value, together with the mean value of d_2 derived earlier (page 4.1) into equations (4.5) and (4.6) yields the following values for d_1 and A within the above range:

$$d_1 = 113 \pm 7 \ \mu m$$

$$A = (3.05 \pm 0.15) \times 10^{-2} \ cm^2$$

It should be emphasised that the values of d_1, d_2 and A calculated above are average values, and may vary over the length of the capacitors. 'Rags' of unequal size on the Melinex spacers would cause d (and thus the slope of figure 4.1) to vary from one place to another, as would any distortion of the upper capacitor plate caused by the retaining leaf-spring. From figure 4.1, the value of dV_1^2/dC_2 varied by approximately 6%. This indicates the extent of variation in the capacitor parameters over the accessible range. For the inertial oscillations, which took

place over a comparatively small range of the capacitors, this variation was unimportant. The steady flows were carried out over part of the range where the variation was only 3%. No change in measured transfer rate which could be ascribed to capacitor parameter variation was observed.

We can now work out the relationship between C_2 and H, the vertical difference between the liquid levels in the two capacitors. Using the geometry of the capacitors together with equation (4.3), we obtain:

$$dC_2/dH = \chi\varepsilon_o A/d_2^2 \qquad (4.7)$$

Substituting the calculated values of A and d_2, we obtain $dC_2/dH = 1.07 \pm 0.07$ pF cm^{-1}.

The rate of change of C_2 with time can be related to the film transfer rate σ which is given by

$$\sigma = w_2\dot{x}_2 d_2/p_{min} \qquad (4.8)$$

where $p_{min} = 0.188 \pm 0.002$ cm is the perimeter of the flow path at the constriction. Using equation (4.8), we obtain for the rate of change of C_2:

$$\dot{C}_2 = (\chi\varepsilon_o p_{min}/d_2^2)\,\sigma \qquad (4.9)$$

The proportionality constant is 6.6 ± 0.5 pF cm^{-2}.

4.2 Steady Flow

Because of the small range over which the liquid level could be varied, only relatively short steady flows could be studied. Flows generally lasted no longer than 40s before the end of the available range was reached. In practice, to keep within the range and to minimise the effect of variations in the capacitor sensitivity, the runs were limited to approximately 30s,

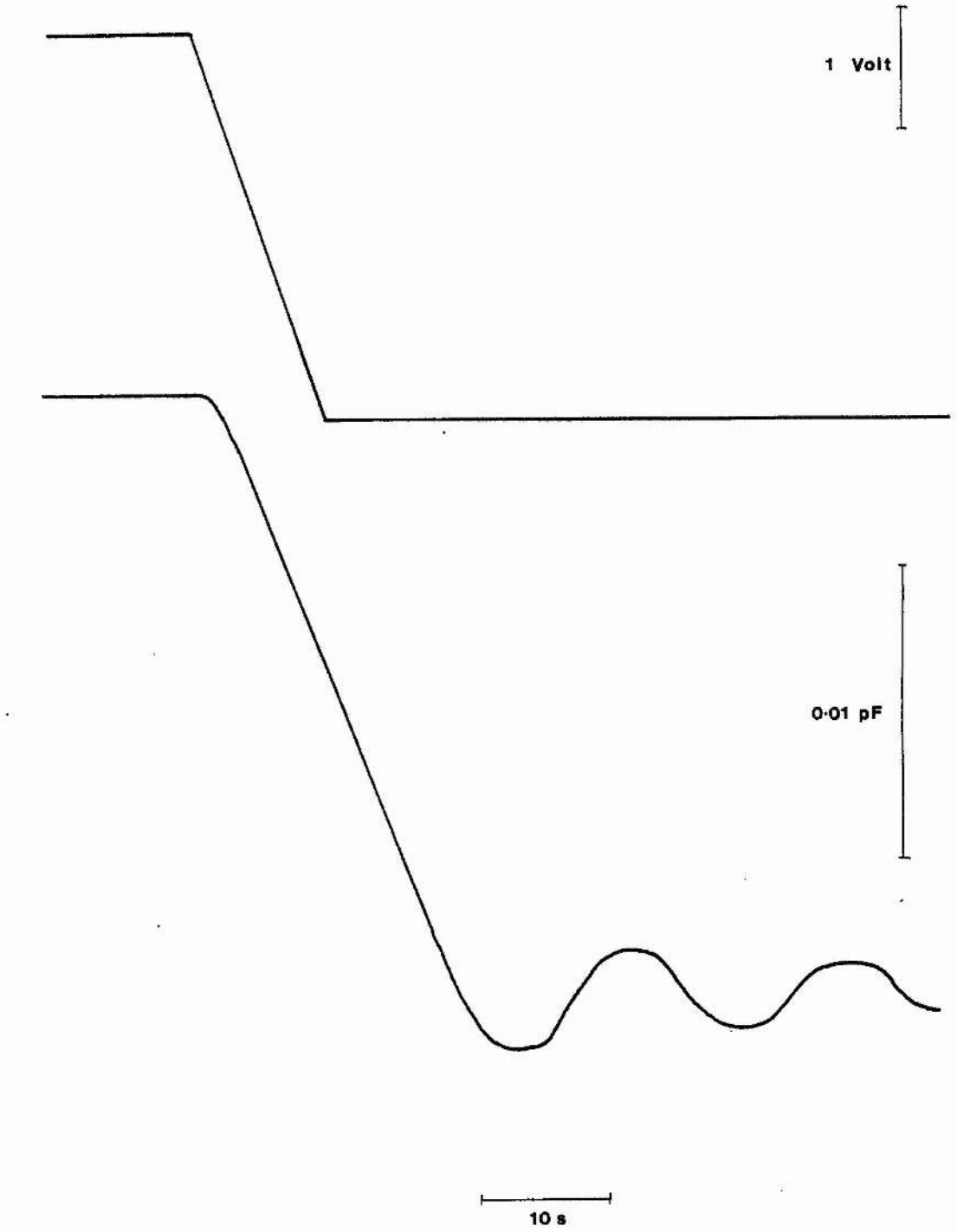

FIGURE 4.2 Tracing of V_0 ramp (top) and C_2 (bottom), showing critical flow followed by inertial oscillations.

depending on the flow rate.

V_1 was held constant until the inertial oscillations of the film had died away and the liquid level was stationary. The FDU was then put into 'run' mode, thus ramping V_1^2 at a predetermined rate. The ramp was stopped at a point corresponding to an equilibrium liquid level within the measurement range of the ratio-arm transformer bridge, so that it was not necessary to change the bridge setting during the flow. The liquid level was recorded on a chart recorder along with the linear output V_0 of the FDU. A tracing of a typical flow and V_0 ramp is shown in figure 4.2.

Because of the uncertainties in the linearity of the capacitors and the limited time over which the steady flows took place, detailed investigation was not attempted; preference was given to the study of the inertial oscillations. The results which were obtained are discussed in section 5.1.

4.3 Operation of the Pulse Generators

The long pulse was an attempt to cancel out the inertial oscillations of the film by altering the effective zero level about which they took place, for a time equal to half the oscillation period.

For purposes of illustration, we consider oscillations about a fixed level difference. Figure 4.3(a) shows the effect of the pulse. The pulse length was adjusted to exactly half an oscillation period. The pulse was started manually with a pushbutton when the liquid level was at its maximum, whereupon the level started to oscillate about its new effective zero position. If the pulse height (in terms of liquid level equivalent) was exactly half that of the oscillations, after one half period, the oscillating level reached its previous mean

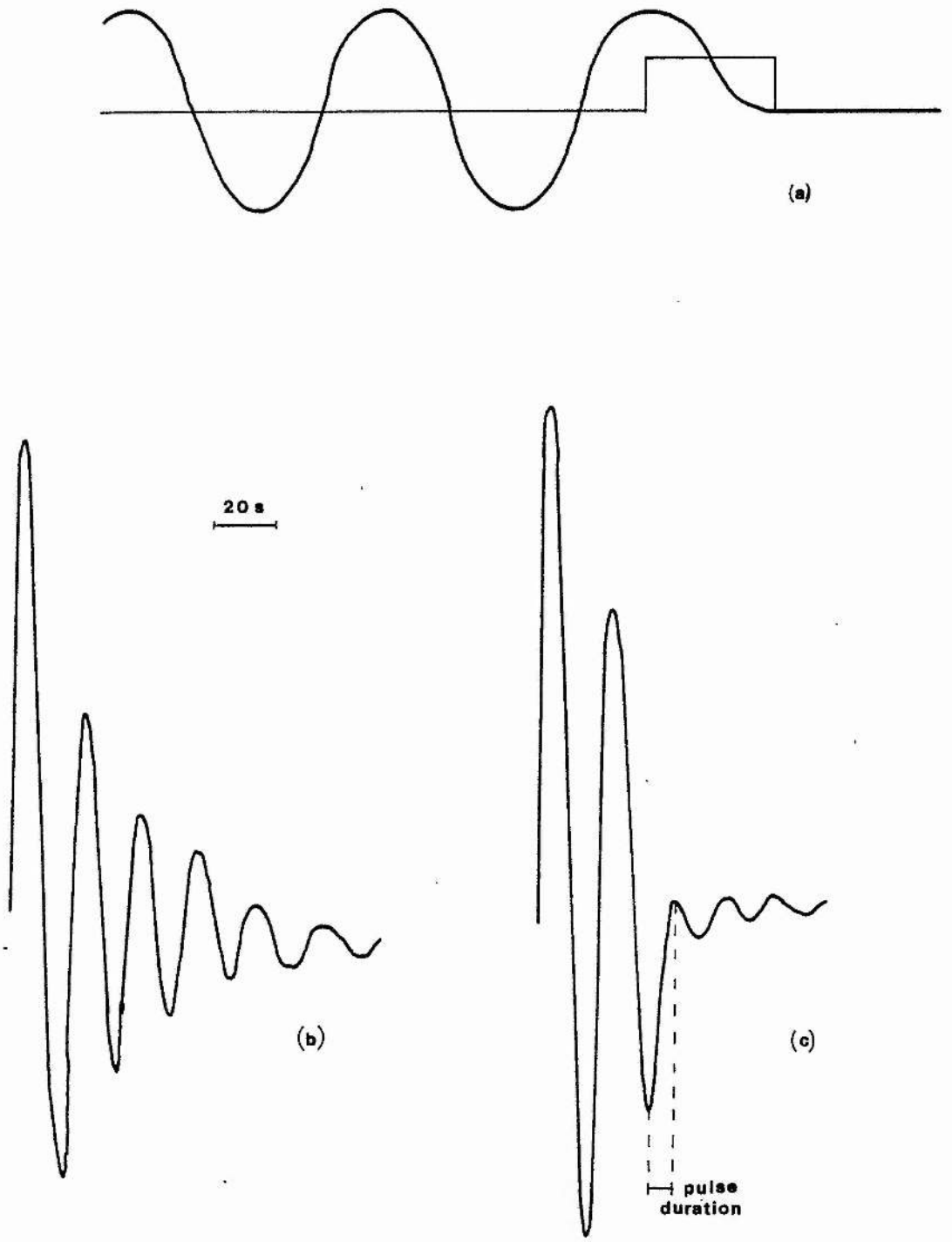

FIGURE 4.3 The long pulse method for eliminating inertial oscillations. (a) The ideal situation. (b) Decay of oscillations without pulse. (c) Decay of oscillations with pulse.

level with zero velocity. At this time the pulse automatically switched off, leaving the film stationary at the original mean level.

The oscillation period was measured, and the pulse duration adjusted to exactly half the period. Oscillations were initiated using the short pulse generator for convenience. Due to Robinson thermal damping, they decayed as shown in figure 4.3(b) over approximately 8 cycles. In 4.3(c), the long pulse was started just as the level difference reached its maximum value. After the pulse was over, the oscillations were considerably reduced in amplitude.

Adjusting the pulse length to the correct value presented no problems. However, the pulse height was more difficult to adjust correctly. Because of the rapid decay of the oscillations, the best method was found to be to set the pulse height, and wait for an oscillation of suitable amplitude on which to start the pulse. At lower temperatures, where the Robinson damping is ineffective and the decay of the oscillations therefore much slower, it would be easier to set the pulse height. In such a case, the long pulse facility would be essential in order to avoid a long wait while the oscillations died away.

It was found to be very difficult to tell exactly when the peak amplitude of the cycle was attained. Experience showed, however, that starting the pulse at any time within a 'window' approximately 3 seconds wide around the extremum was effective.

The reduction of oscillation amplitude was usually between 70% and 90%. In addition to the difficulty in setting the pulse height, the decay of the oscillations was another factor causing there to be a finite residual amplitude.

The short pulse was designed to enable a sub-critical steady flow to be started without the accompanying inertial oscillations

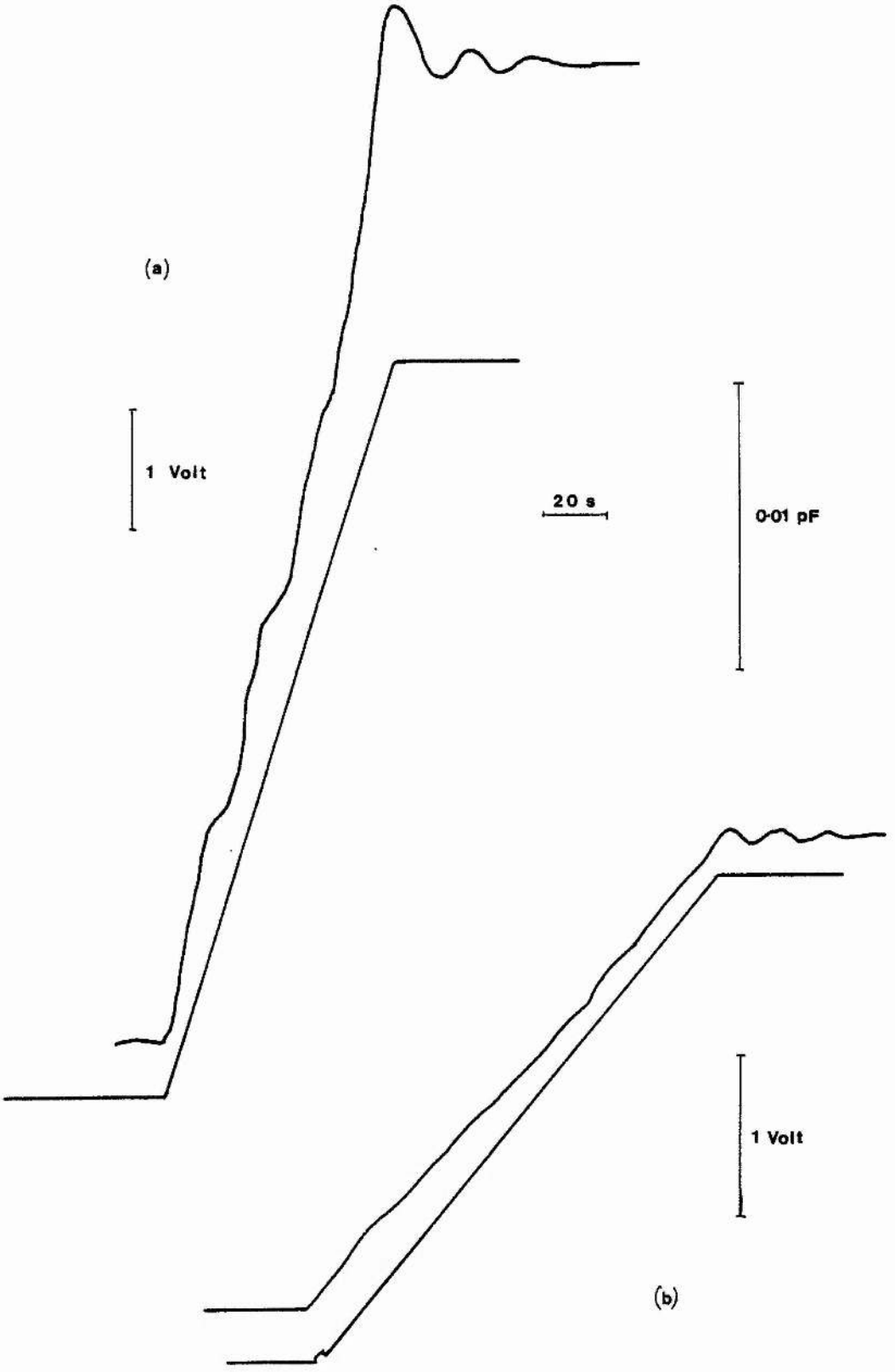

FIGURE 4.4 Sub-critical flow (a) without and (b) with a short voltage pulse at the beginning of the ramp. Note that the voltage scales are different in the two cases.

superimposed. By accelerating the film to the required velocity in the first two seconds of flow, the oscillations could be suppressed. Section 3.6 describes the operation of the short pulse generator electronics. Figure 4.4 shows sub-critical flow with and without the pulse.

Careful adjustment of the pulse height (at a fixed ramp rate) was necessary in order to eliminate the inertial oscillations. It was found that the short pulse was less effective at other sub-critical transfer rates, even though the pulse height was automatically adjusted in proportion to the drive rate.

4.4 Feedback

In order to discuss the effect of feedback through the differentiator and the attenuator in the FDU, we must first derive the equation of motion of the film for sub-critical flow.

The superfluid driving force is the chemical potential gradient, ie:

$$D\underline{v}_s/Dt = -\nabla\mu \qquad (4.10)$$

where D/Dt is the "co-moving derivative":

$$D/Dt = d/dt + \underline{v}_s.\nabla \qquad (4.11)$$

The second term in equation (4.11) (together with a term in the chemical potential proportional to v_s^2) gives rise to the Kontorovich film thinning effect when (4.10) is applied to a liquid helium film. Film thinning is most important at high velocities and will therefore be ignored at this stage in the analysis.

The superfluid velocity v_s may be related to the film transfer rate σ, which is defined as the rate of change of

volume in one reservoir divided by the minimum perimeter of the path (p_{min}). Conservation of mass requires that at any point in the film,

$$\rho \sigma p_{min} = \rho_s v_s dp \tag{4.12}$$

should be a constant. Here d is the film thickness and p the perimeter of the flow path at any point. Integrating equation (4.10) over the length of the film and using equations (4.1), (4.2), (4.8) and (4.12), we obtain:

$$\frac{\rho}{\rho_s} I\ddot{h} = -\frac{g}{A} h - \frac{\chi \varepsilon_a \sin \theta_2}{2\rho\, w_2\, d_2} \frac{V_1^2}{d_1^2} \tag{4.13}$$

where the integral

$$I = \int \frac{dl}{pd} \tag{4.14}$$

is along the flow path. It is a geometry dependent quantity, calculable for any known geometry and film thickness. The variable $h = h_2 = x_2 \sin \theta_2$ is the vertical height of the liquid level in the measurement capacitor (to within an additive constant).

Since V_1^2 is proportional to V_0 (the linear output of the film drive unit), we may lump all the prefactors together and obtain:

$$\ddot{h} + \omega_0^2 h = \alpha V_0 \tag{4.15}$$

where

$$\omega_0^2 = \frac{\rho_s}{\rho} \frac{g}{IA} \tag{4.16}$$

If V_0 is a constant, this is just the equation of free simple harmonic motion (SHM) at angular frequency ω_0. The effect of

feedback can now be clearly seen. For feedback through the attenuator, V_0 is proportional to h, thus altering the period of the oscillations by an amount depending on the attenuator gain.

In the case of feedback through the differentiator, V_0 is proportional to $\dot{h}$, thus introducing damping into equation (4.15). A positive damping coefficient (negative feedback) corresponds to exponentially decreasing oscillations, while a negative damping coefficient (positive feedback) corresponds to exponentially increasing oscillations. The sense of the feedback is changed by inverting the output signal from the Brookdeal lock-in amplifier. In practice, since Robinson damping, also proportional to $\dot{h}$, is present, increased positive feedback is required to produce oscillation growth.

With the liquid levels at equilibrium, the differentiator gain was set to the required value, and it was then enabled. Small perturbations due to electronic noise soon initiated small oscillations which increased in amplitude exponentially, until non-linear dissipation limited growth. After a suitable number of oscillations had been recorded, the feedback was either removed, or reversed in sign, and the oscillations decayed.

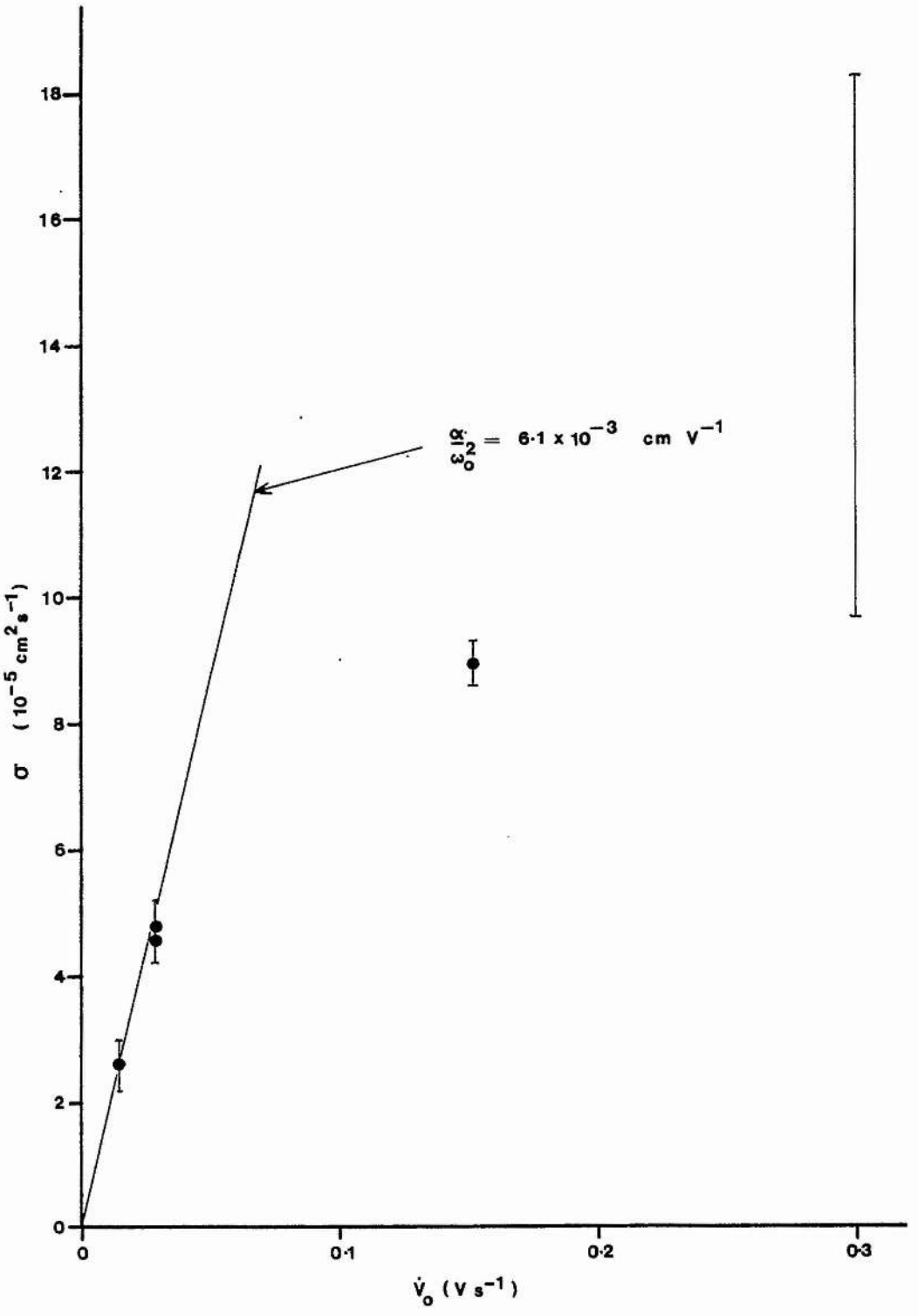

FIGURE 5.1 Transfer rate v voltage ramp rate

CHAPTER 5

THE EXPERIMENTAL RESULTS

5.1 Steady Flow

Sixteen driven steady flows, produced as described in section 4.2, were studied. The cryostat temperature for all flows was 1.14K. The results from these runs are tabulated in table 5.1. σ is the film transfer rate. V_0 refers to the linear output voltage from the FDU, while ΔV_0 is the total change in V_0 over the duration of the run. Δh is the total change in vertical liquid level in the measurement capacitor during the run. The quantity Σ is defined later in this section.

It was found that at low drive rates, the transfer rate at constant drive rate was reproducible to $\pm 5\%$ from run to run. However, at a higher drive rate ($\dot{V}_0 = 0.31\ Vs^{-1}$), a range of transfer rates was observed. Thus, despite the limited data available, we can divide up the flow into critical and sub-critical regimes.

Figure 5.1 is a graph of transfer rate against the drive rate $\dot{V}_0$. In the sub-critical region (drive rate below approximately $0.1 Vs^{-1}$), the results show a linear relationship between the drive rate and the transfer rate. These sub-critical flows have inertial oscillations superimposed on them, and are typified by the example shown in figure 4.4(a).

At a drive rate of $\dot{V}_0 = 0.31\ Vs^{-1}$, the run to run variation in transfer rate was 9.7 to 18.2 $\times 10^{-5}\ cm^2 s^{-1}$. There was no correllation between σ and ΔV_0 or Δh. The mean transfer rate was $13.8 \times 10^{-5}\ cm^2 s^{-1}$ and the standard deviation was $2.8 \times 10^{-5}\ cm^2 s^{-1}$. A typical flow of this type is shown in figure 4.2. The transfer rates were approximately 30% higher than expected, indicating the possible presence of an

Table 5.1

Sense of flow	$\dot{V}_0$ Vs^{-1} ± 0.005	$\sigma \times 10^5$ $cm^2 s^{-1}$ ± 0.4	ε μm ± 2	ΔV_0 Volts ± 0.05	Δh μm ± 2
in	0.31	12.2	150	3.05	183
out	0.31	17.3	---	3.12	189
in	0.31	9.7	144	3.00	179
in	0.31	10.2	110	2.17	133
in	0.31	13.6	72	1.40	83
out	0.31	14.8	70	1.20	79
in	0.31	11.7	67	1.30	77
out	0.31	16.3	77	1.57	95
in	0.31	15.8	75	1.57	95
out	0.31	18.2	---	1.85	---
in	0.31	10.8	---	2.35	---
out	0.31	15.6	83	1.60	102
in	0.153	8.9	60	1.63	96
out	0.029	4.8	---	2.15	131
out	0.029	4.6	---	2.20	135
out	0.014	2.6	---	1.80	110

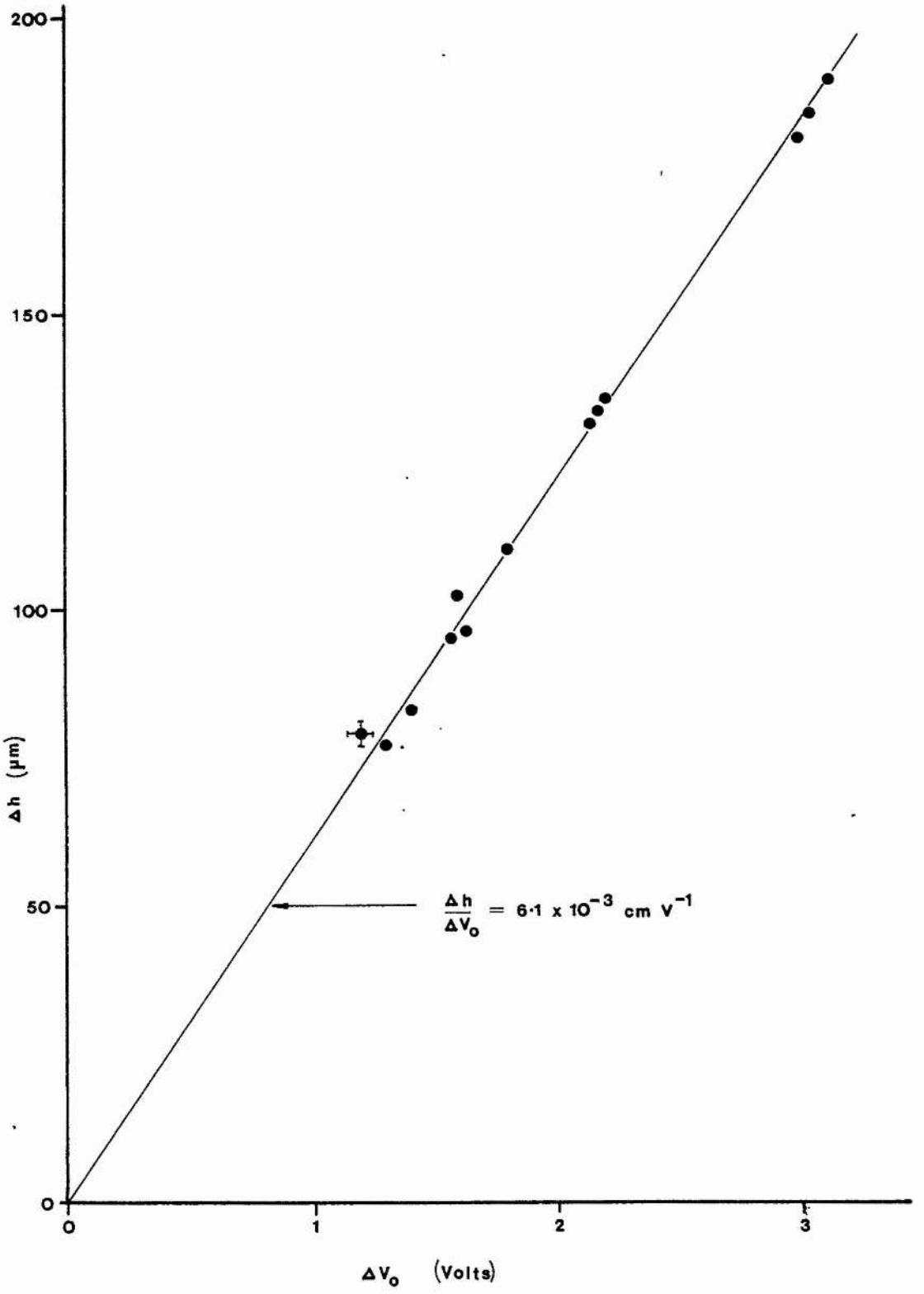

FIGURE 5.2 Voltage step $\underline{y}$ level change

unidentified systematic error. Although other workers[35] have observed transfer rates much higher than those reported here, the normal range of σ is generally between 9 and 13 x 10^{-5} cm^2s^{-1}. The uncertainty of up to 10% in the capacitor calibration (equation 4.9) could not account for all of this discrepancy. However, a preliminary experiment to investigate flow over a machined Stycast 1266 surface showed that high transfer rates of the order of 17 x 10^{-5} cm^2s^{-1} could occur. The geometry of the constriction may also be conducive to high flow rates (see Chapter 6).

At equilibrium, before and after the steady flow, equation (4.15) predicts a linear relationship between V_0 and h. Figure 5.2 is a graph of Δh against ΔV_0, showing that this is found to be the case. From equation (4.15), the slope of the graph gives the value of α/ω_0^2:

$$\alpha/\omega_0^2 = (6.1 \pm 0.2) \times 10^{-3} \text{ cmV}^{-1}$$

If we introduce a dissipative chemical potential difference $\Delta\mu_D$ into the analysis in section 4.4, we obtain:

$$\ddot{h} + \frac{\omega_0^2 \Delta\mu_D}{g} + \omega_0^2 h = \alpha V_0 \qquad (5.1)$$

We now have two cases to consider: critical flow, observed at $\dot{V}_0 = 0.31$ Vs^{-1}; and sub-critical flow, observed for $\dot{V}_0 < 0.1$ Vs^{-1}. (It is believed that the point at $\dot{V}_0 = 0.153$ Vs^{-1} is in the transition region between the two regimes.) An important quantity in the following discussion is ξ, which is defined as the difference between the value of h when the driving ramp is switched off at t_1, and the subsequent equilibrium value of h. Figure 5.3 makes this clear. ξ is tabulated in table 5.1.

For sub-critical flow, the data is not inconsistent with the

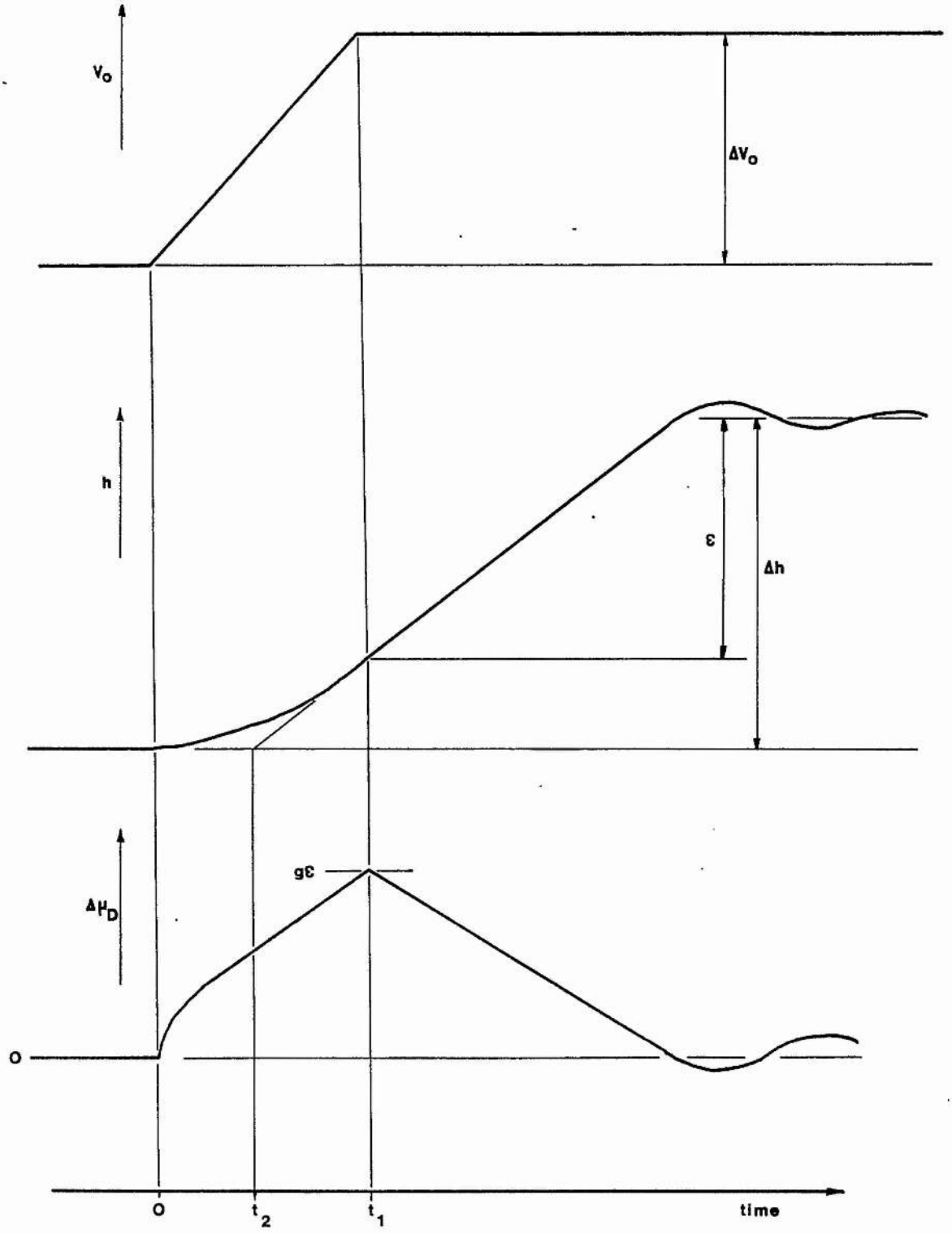

FIGURE 5.3 Voltage ramp, liquid level and dissipation

assertion that the dissipation is a function solely of the superfluid velocity and thus of $\dot{h}$:

$$\ddot{h} + F_{diss}(\dot{h}) + \omega_0^2 h = \alpha V_0 \qquad (5.2)$$

To illustrate this, let us choose initial conditions such that $h=0$, $\dot{h}=0$ and $V_0=0$. At time $t=0$, we start to drive the film at a constant rate $\dot{V}_0$. After the inertial oscillations (due to the $\ddot{h}$ term) have died away, the solution of (5.2) becomes:

$$h = (\alpha \dot{V}_0/\omega_0^2)t - F_{diss}(\alpha \dot{V}_0/\omega_0^2)/\omega_0^2 \qquad (5.3)$$

Thus we expect $\dot{h}$ (and therefore the transfer rate σ) to be proportional to the drive rate $\dot{V}_0$. The second term in the above equation is equal to ε, which for these sub-critical flows was too small to be measurable (less than about 2μm).

Taking the time derivative of equation (5.3) and using (4.8), we obtain for the transfer rate:

$$\sigma = \frac{w_2 \; d_2}{p_{min} \sin\theta_2} \frac{\alpha}{\omega_0^2} \dot{V}_0 \qquad (5.4)$$

Using the value of α/ω_0^2 from figure 5.2, we can draw a line on figure 5.1 representing equation (5.4). The data acquired at low drive rates (below $0.1 Vs^{-1}$) lie on the line, confirming equation (5.4).

We now consider the critical flow data. In this case, the transfer rate varied independently of $\dot{V}_0$ and equations (5.2) to (5.4) do not hold. The interpretation of ε is also different.

For these critical flows, the dissipation is so large that the film cannot "keep up with" the driving chemical potential produced by the V_0 ramp. In other words, the chemical potential difference is being increased faster than the ability of the film to decrease it by transferring liquid between the reservoirs.

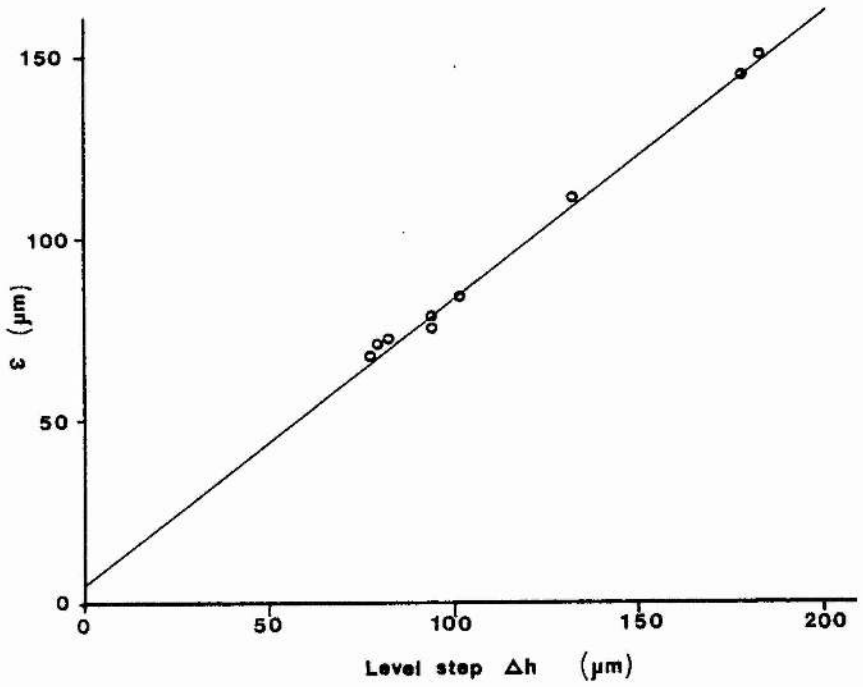

FIGURE 5.4 Level step $\underline{v}$ ϵ

Figure 5.3 illustrates this. The chemical potential difference between the reservoirs rises to a maximum of $\mathcal{E}g$, when the ramp is switched off and the chemical potential difference falls as the liquid levels approach equilibrium at a new value of V_0.

The transfer rate is almost constant throughout this process, implying that it is very weakly dependent on dissipation (or equivalently that dissipation is strongly dependent on transfer rate) in this regime. However, σ is not reproducible from run to run. This implies that for critical flows, the dissipation is not specified uniquely by the transfer rate.

Figure 5.4 shows that $\mathcal{E}$ is approximately linearly related to Δh. This relationship is explained in Appendix E. It does not yield any important information about dissipation in the film, and merely confirms the self-consistency of the measurements.

5.2 Oscillatory Flow

Figure 5.5 is a tracing of a typical series of oscillations, obtained as described in section 4.4. At time t_1, the differentiator was switched on, and the oscillations grew until at time t_2, the non-linear dissipation limited the film velocity and hence the oscillation amplitude. Oscillations continued until t_3, when the differentiator was switched off. The oscillations then decayed. These three divisions will be referred to as the growth stage, the intermediate stage, and the decay stage.

Table 5.2 gives the details of the sixteen series of oscillations recorded. They are referenced by a number of the form RxSy, where x is the number of the experimental run, and y is the number of the series within the run. The series have been divided into four groups (column 5 in the table); the

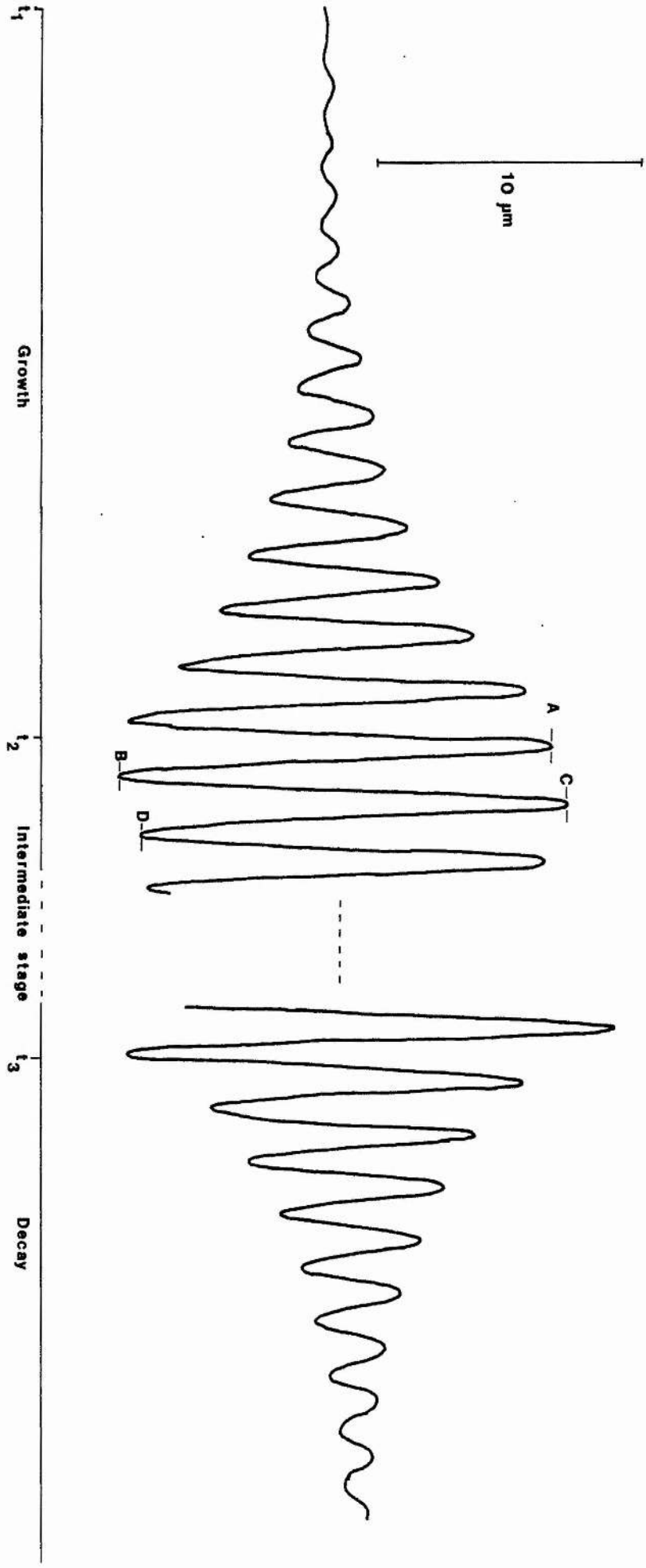

FIGURE 5.5 Tracing of R3S8

Table 5.2

Ref.No.	Temp. ±0.01 ^{o}K	No.of Oscs.	Period ±0.3 s	Group	Growth Rate s^{-1} ±7%	Decay Rate s^{-1} ±7%	FB.	$\lvert\gamma_F\rvert$ s^{-1}	γ_R s^{-1}	Max. Ampl. μm	h_{onset} ± 0.4 μm
R3S1	1.18	30	18.4	1	0.027	0.026	0	0.053	0.026	14.6	14.6
R3S2	1.16	19	22.2	1	0.026	---	---	---	---	16.8	14.0
R3S3	1.16	57	16.8	2	0.0035	---	---	---	---	2.8	2.7
R3S4	1.16	65	18.0	2	0.0030	---	---	---	---	4.4	4.4
R3S4A	1.16	4	17.0	2	---	0.056	-ve	0.029	0.027	11.2	----
R3S4B	1.16	7	17.4	2	---	0.027	0			12.0	----
R3S5	1.16	47	18.7	2	0.0047	0.025	0	0.026	0.025	5.8	5.2
R3S6	1.14	24	20.5	3	0.019	0.056	-ve	0.038	0.019	13.5	12.5
R3S6A	1.14	9	19.6	3	---	0.017	0	---	0.017	7.0	----
R3S7	1.12	29	20.4	3	0.017	0.051	-ve	0.035	0.017	11.2	8.8
R3S8	1.12	31	19.8	3	0.017	0.017	0	0.035	0.017	9.4	7.4
R3S9	1.12	38	20.7	3	0.017	0.018	0	0.035	0.018	16.0	9.9
R3S10	1.11	48	20.8	3	0.016	0.060	-ve	0.038	0.022	14.7	13.3
R3S11	1.10	58	20.7	3	0.016	0.018	0	0.033	0.018	14.4	12.1
R3S12	1.10	112	21.1	3	0.016	0.018	0	0.034	0.018	13.0	11.2
R5S1	1.16	160	17.2	4	0.019	0.024	0	0.043	0.024	11.3	10.8

differentiator gain was changed for each group. Column 8 indicates whether the decay of the oscillations was under conditions of no feedback, or of negative feedback. Column 11 gives the maximum value of Δh during the series. The values of C_2 about which the oscillations took place were: groups 1 and 2, C_2 = 12.7540 pF; group 3, C_2 = 12.7720 pF; group 4, C_2 = 12.7616 pF. The oscillation amplitudes were up to 0.003pF.

Ignoring for the moment any non-linear dissipation, the Robinson damping will give rise to a dissipative term linear in the film velocity and thus in $\dot{h}$:

$$F_{diss}(\dot{h}) = 2\,\gamma_R\,\dot{h} \qquad (5.5)$$

When the differentiator is on, V_0 will also be proportional to $\dot{h}$, and we can define a constant γ_F such that:

$$V_0 = 2\gamma_F\,\dot{h} \qquad (5.6)$$

Substituting these two expressions into equation (5.2), we obtain:

$$\ddot{h} + 2(\gamma_R - \gamma_F)\,\dot{h} + \omega_0^2\,h = 0 \qquad (5.7)$$

If the positive feedback is so high that γ_F exceeds γ_R, then the oscillation amplitude will grow exponentially. A log-linear plot of the amplitude versus oscillation number should therefore be a straight line, with a slope equal to $(\gamma_F - \gamma_R)T$ where T is the period of the oscillations. With the differentiator switched off, γ_F becomes zero, and γ_R may be determined on its own. If the sense of the feedback is reversed, γ_F becomes negative, and the quantity $|\gamma_F| + \gamma_R$ may be determined.

The oscillation amplitude was quantified by measuring the peak-to-peak amplitude every half oscillation. Thus in figure

The following figures are plots of the oscillation amplitude on a logarithmic scale against oscillation number. The step/plateau nature of some of the data (eg in R3S5) is due to the finite resolution of the measurements made on the chart recorder tracings from which the data is derived. The resolution of the amplitude measurements is approximately ± 0.03 μmfor R3S3 and R3S4, and $\pm 0.1\mu$m for the rest.

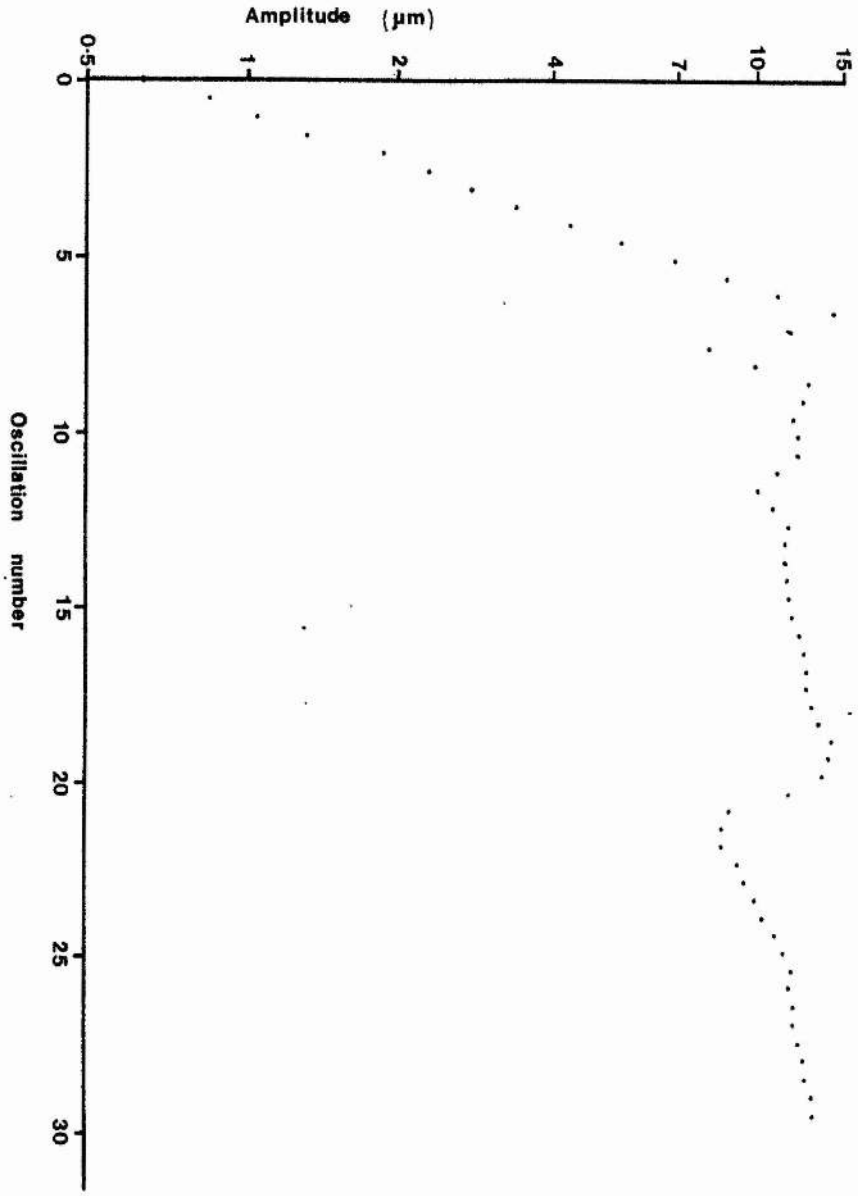

FIGURE 5.6 R3S1

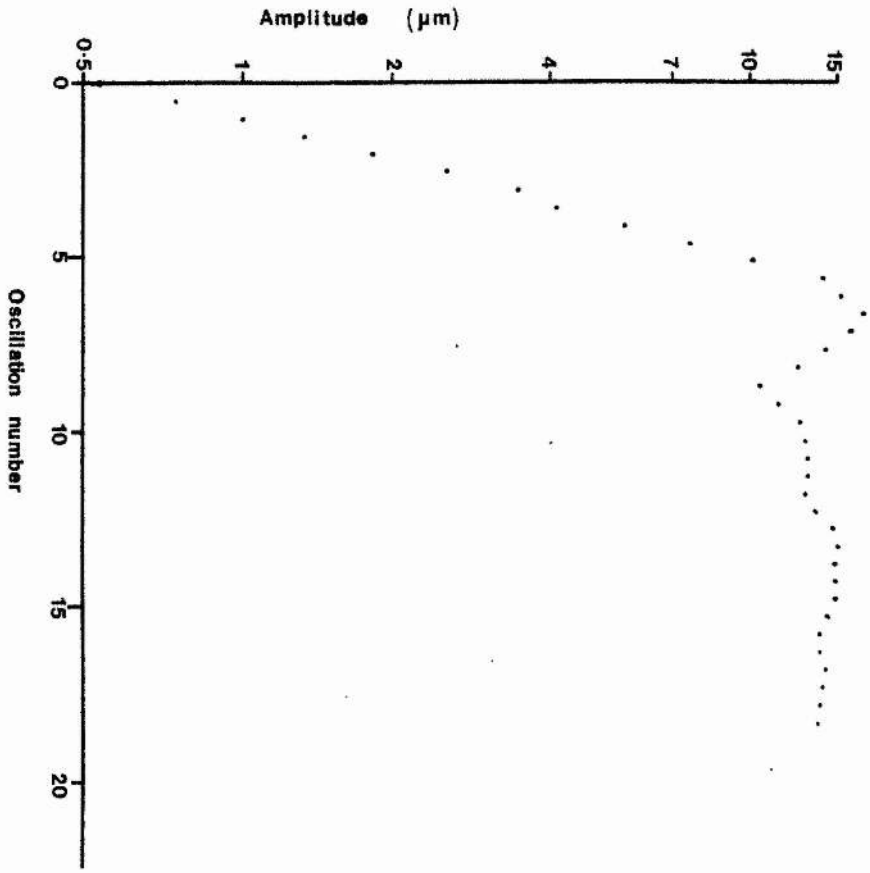

FIGURE 5.7 R3S2

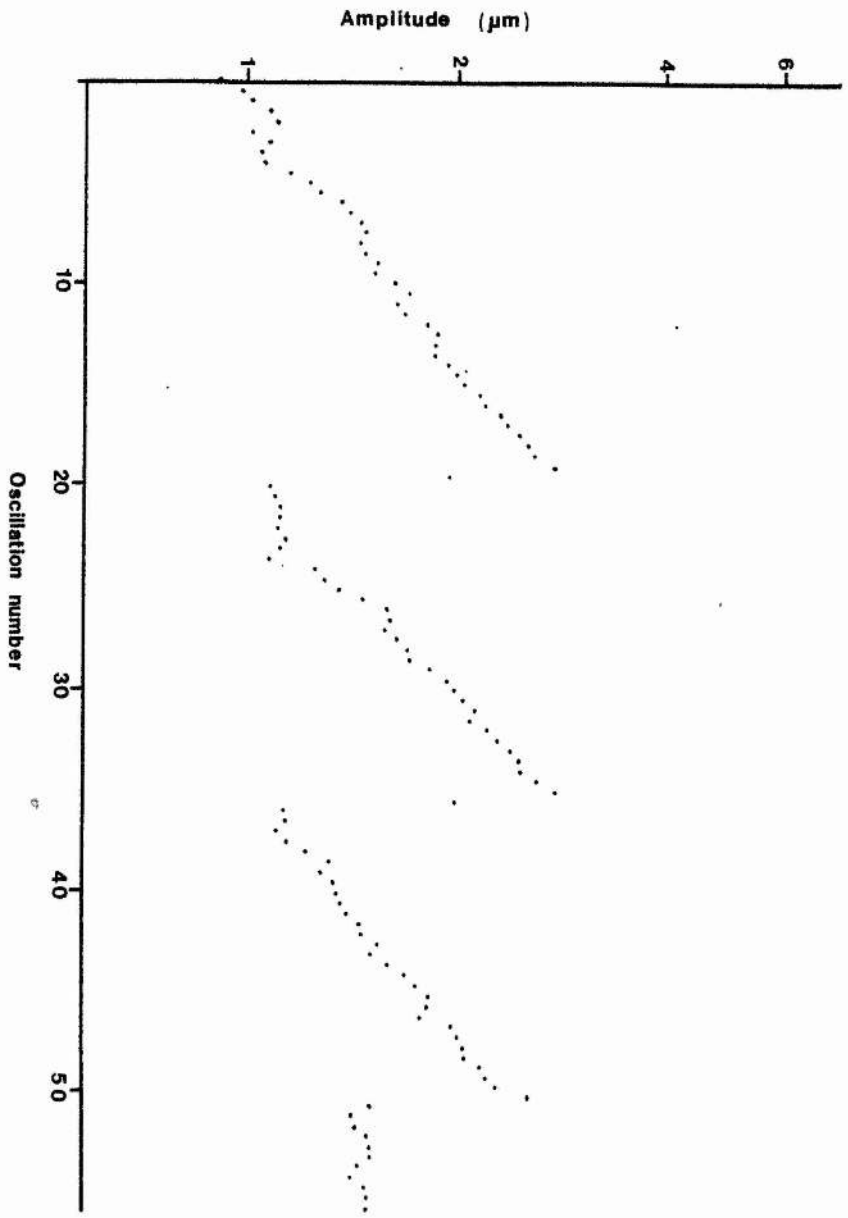

FIGURE 5.8 R3S3

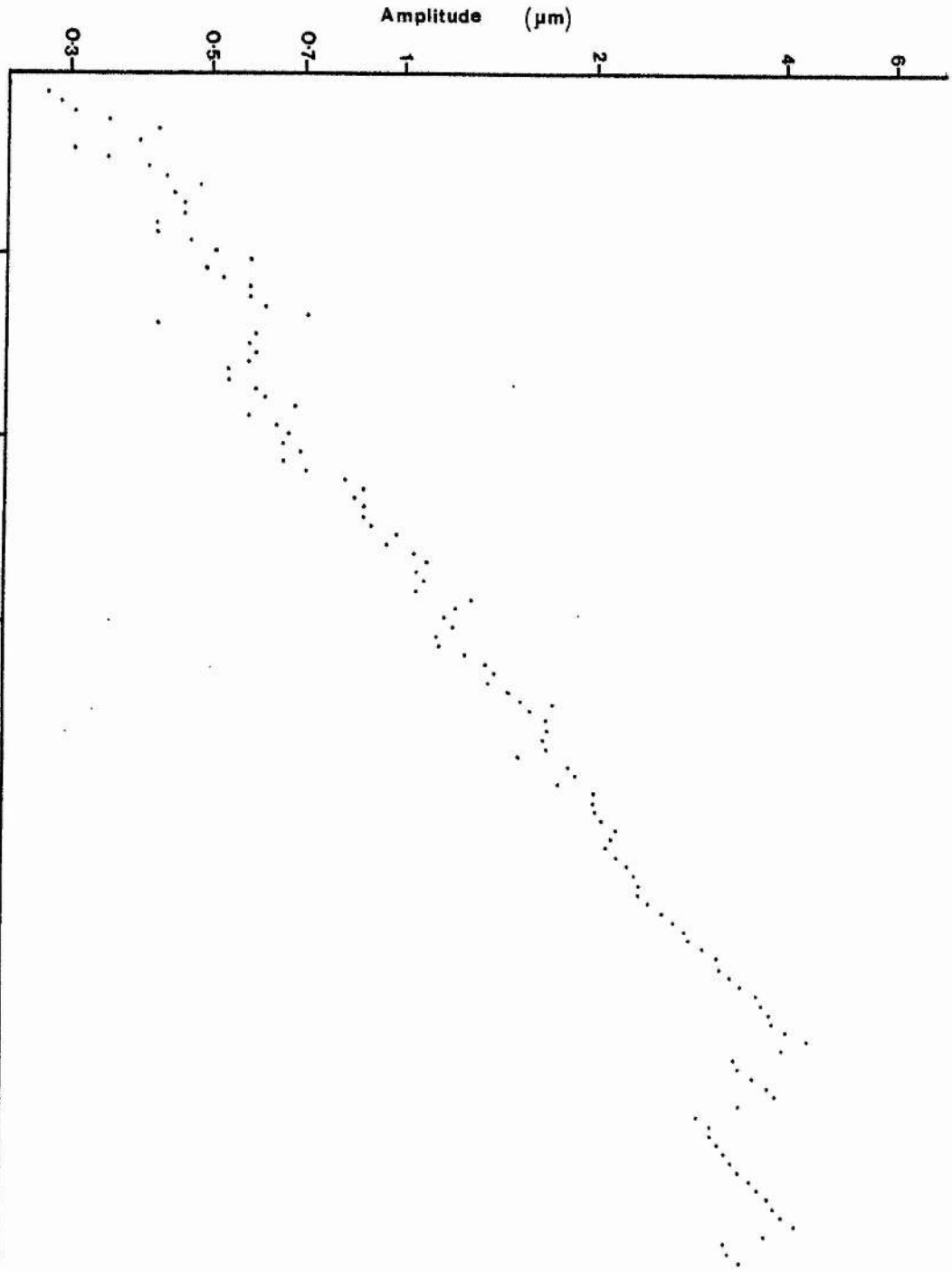

FIGURE 5.9 R3S4

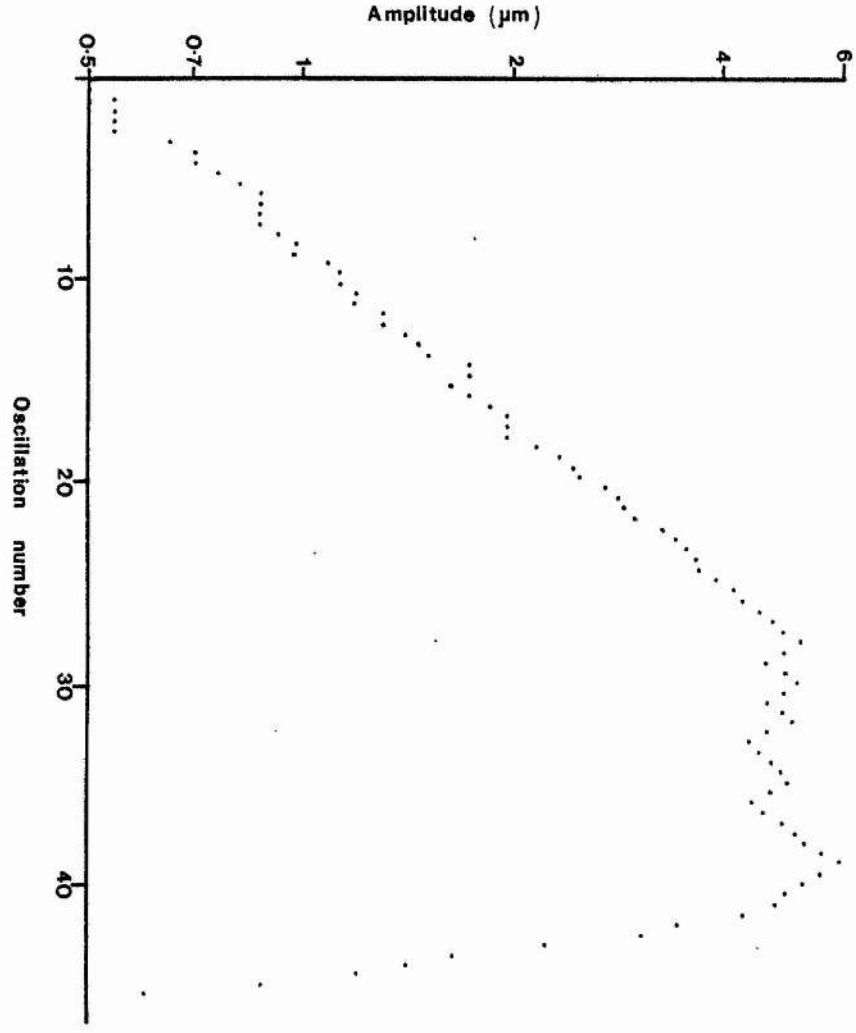

FIGURE 5.10 R3S5

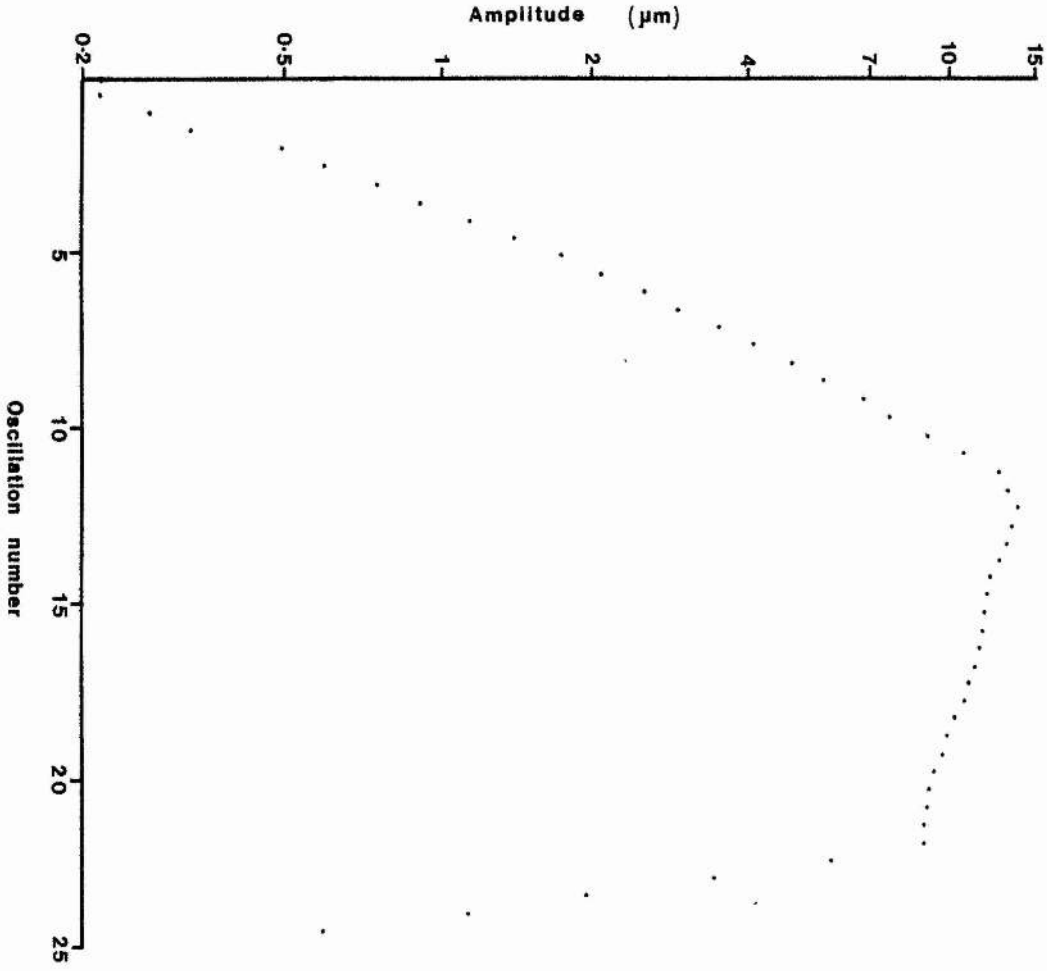

FIGURE 5.11 R3S6

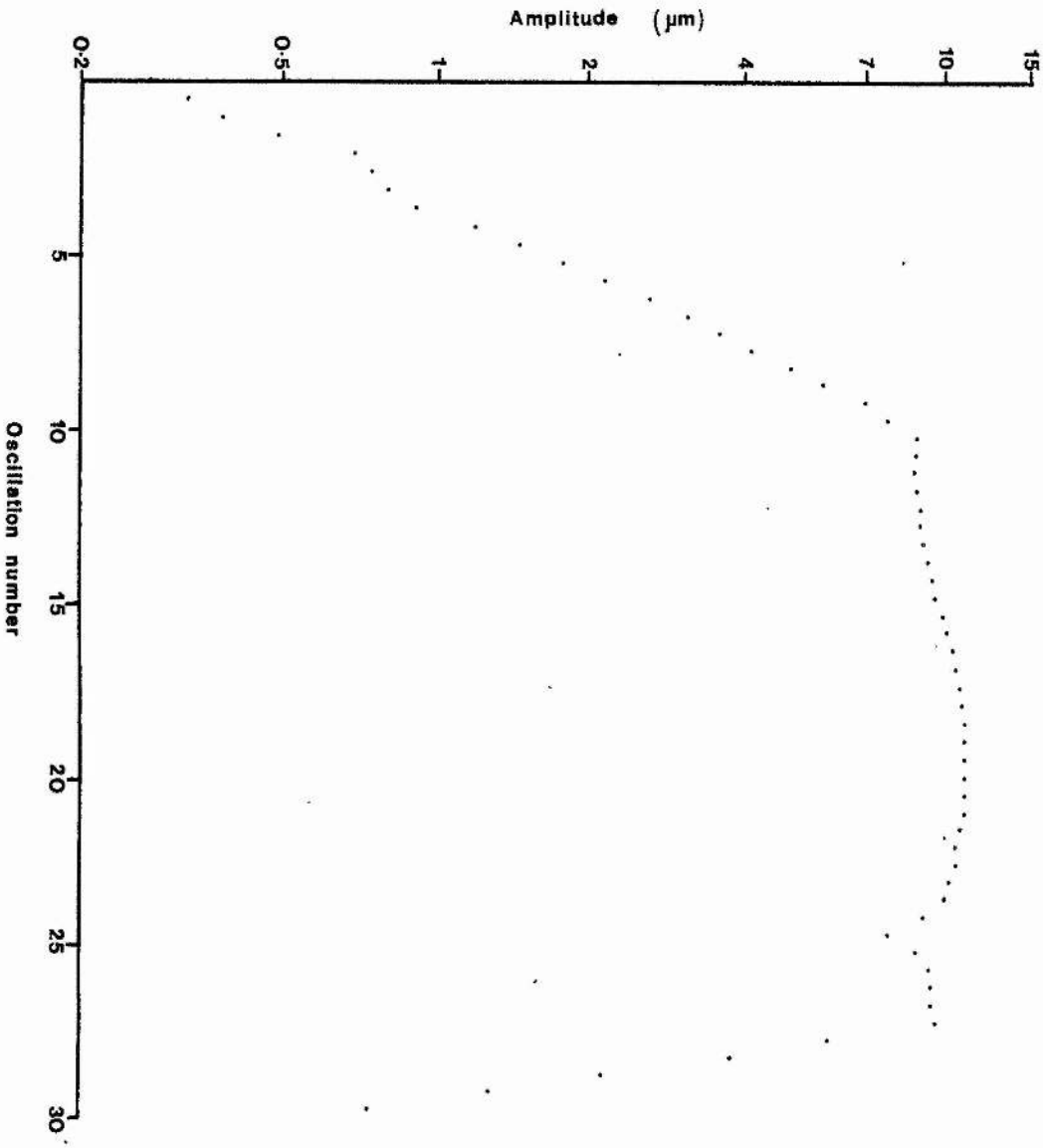

FIGURE 5.12 R3S7

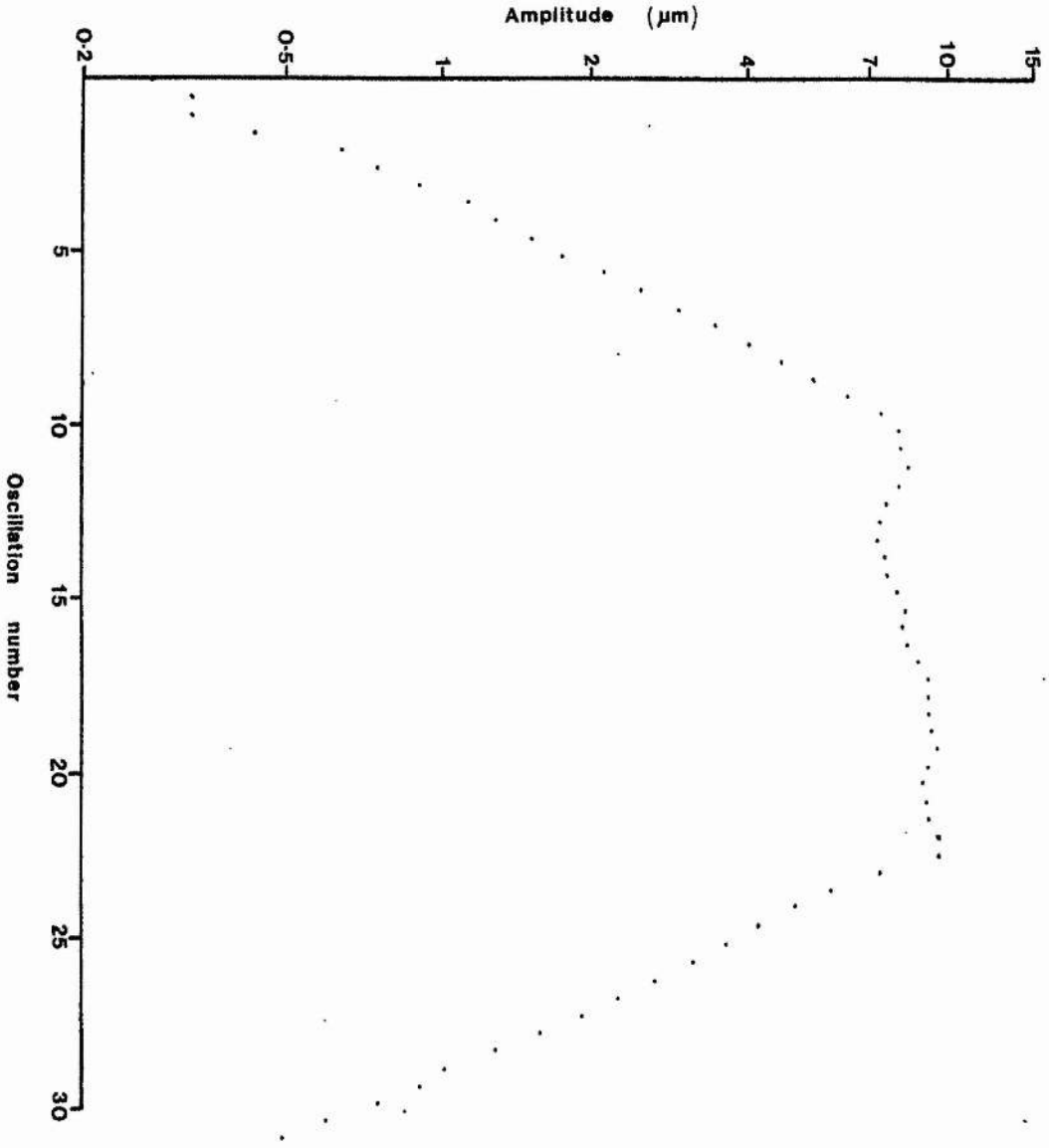

FIGURE 5.13 R3S8

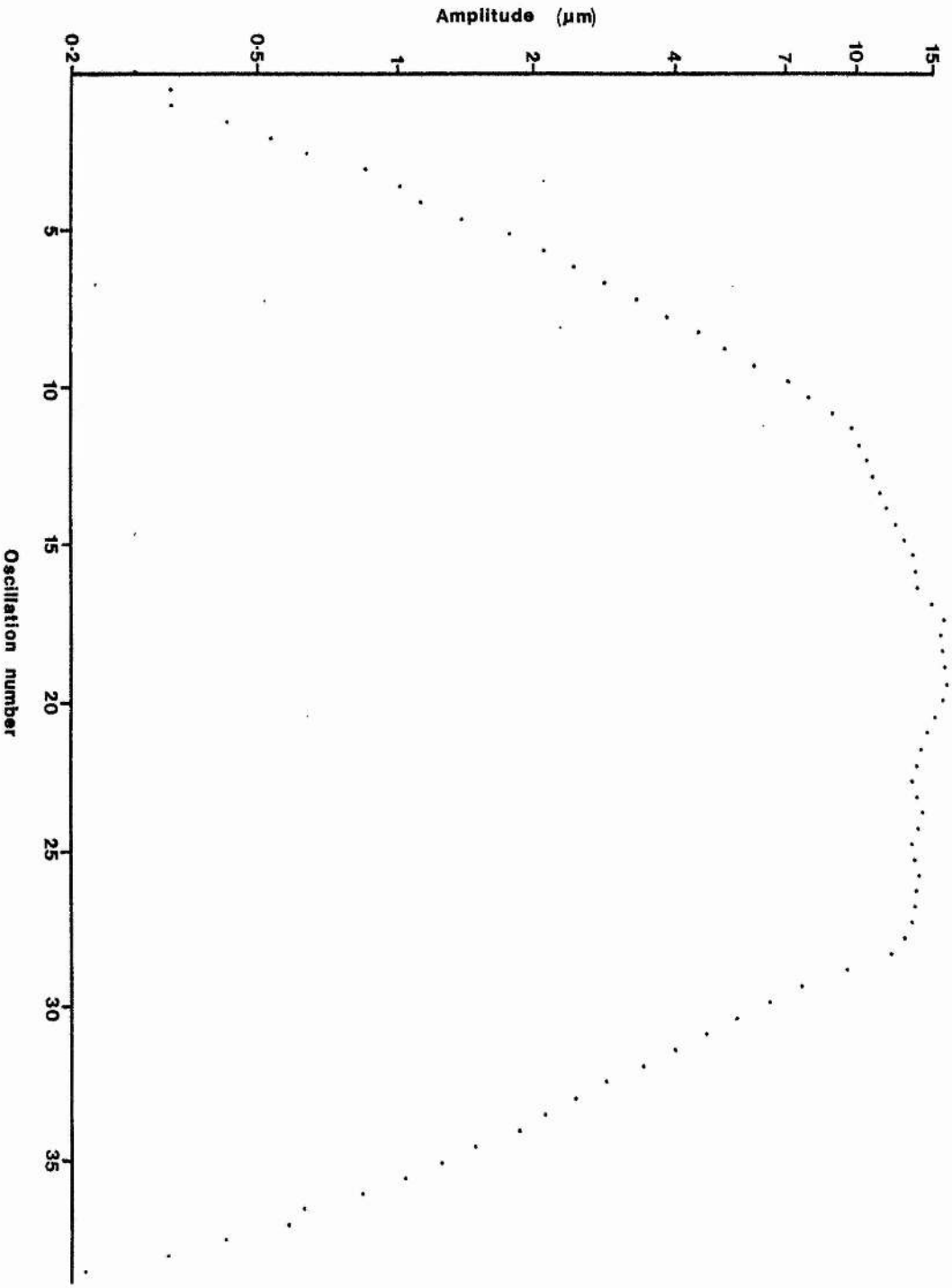

FIGURE 5.14 R3S9

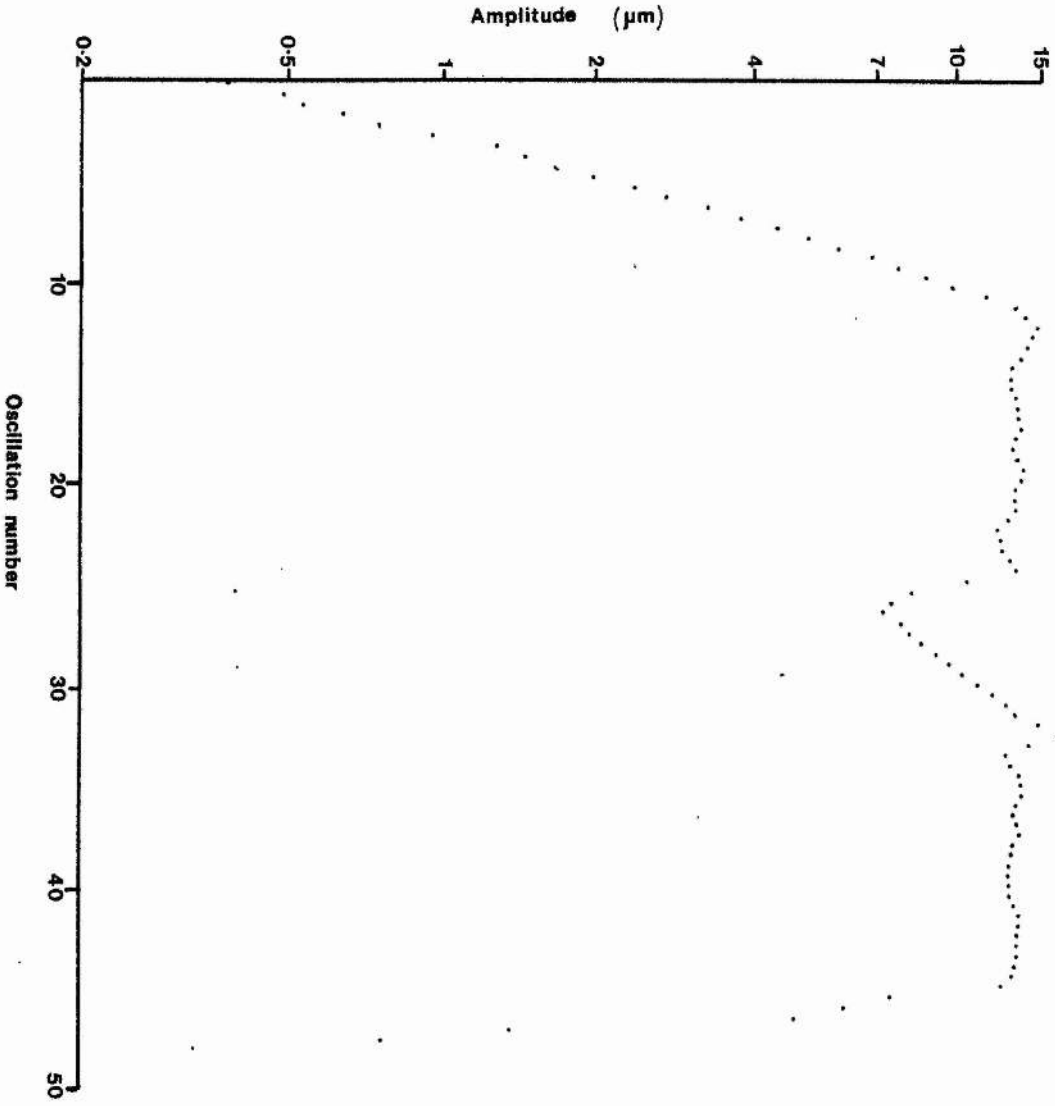

FIGURE 5.15 R3S10

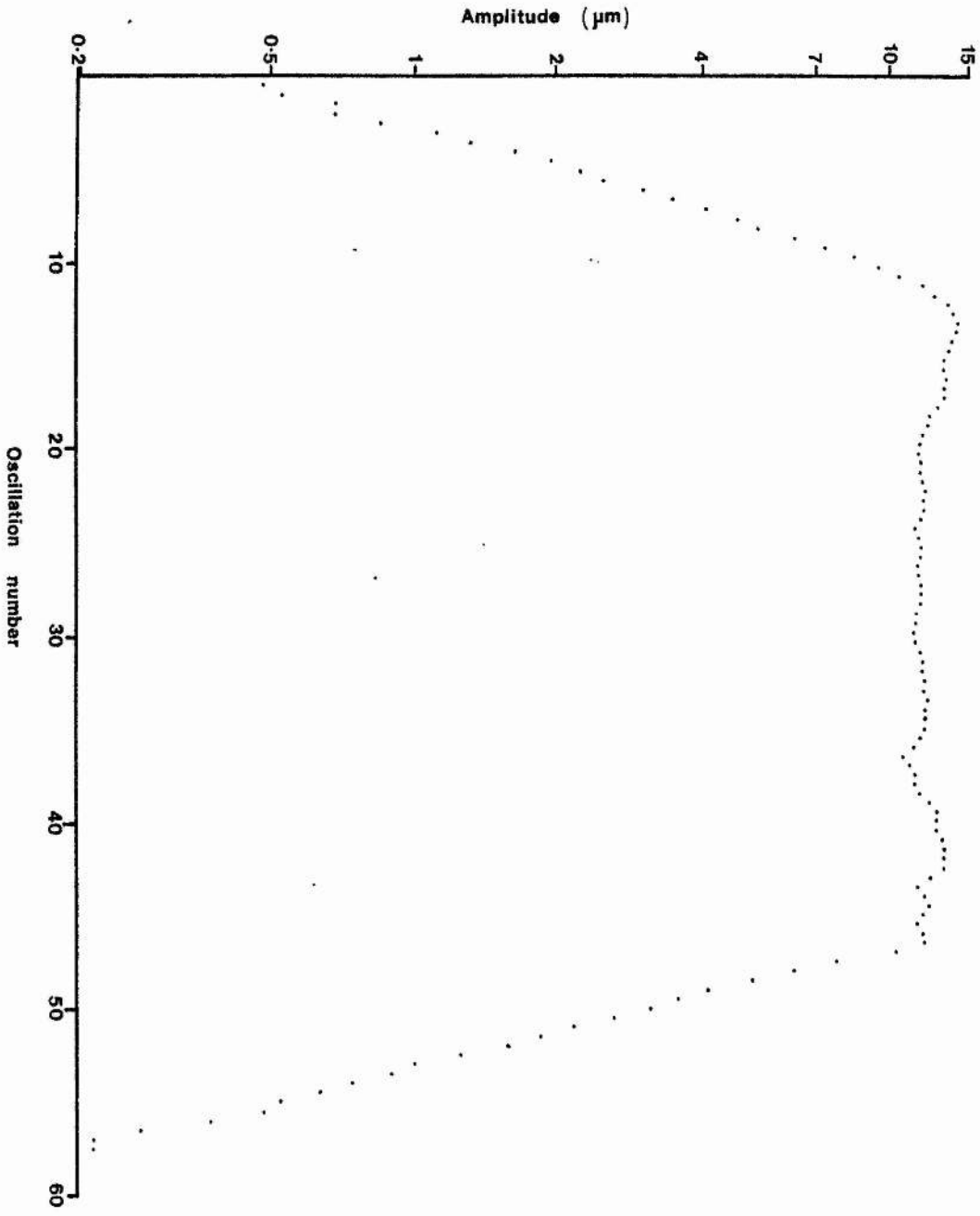

FIGURE 5.16 R3S11

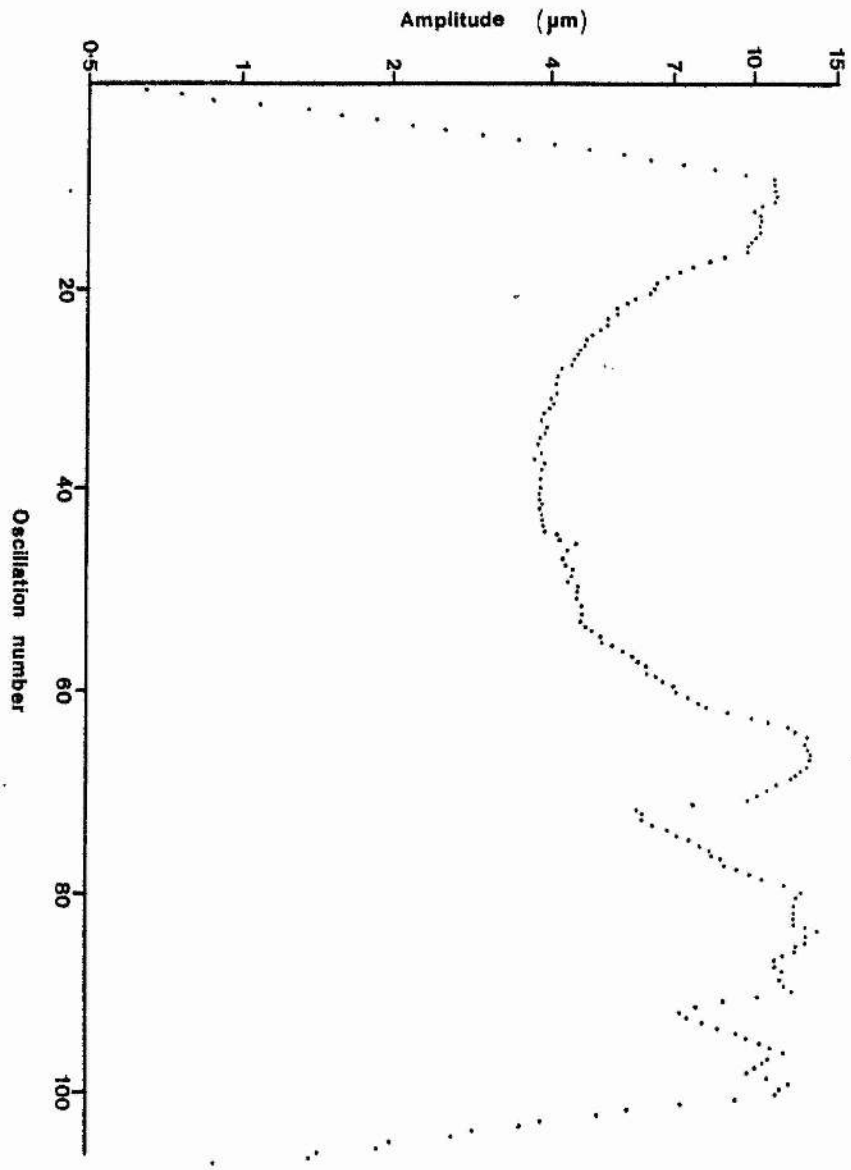

FIGURE 5.17 R3S12

FIGURE 5.18 R5S1

5.5, A to B, B to C, C to D and so on, were measured. This method largely eliminated any drift in the base line.

The amplitude of the oscillations is plotted on a logarithmic scale against period number in figures 5.6 to 5.18. It was observed that the oscillation amplitude in the intermediate range was by no means constant. The features of this amplitude variation are discussed in section 5.4.

Figure 5.19 shows the growth of R3S12 on an expanded scale. The experimental points lie closely on a straight line, as predicted by equation (5.7). (The slight negative curvature indicates the presence of a small amount of non-linear dissipation.) The slope of the line, divided by the oscillation period T, gives the value of the growth time constant:

$$\gamma_F - \gamma_R = 0.0047 \pm 0.0004 \ s^{-1} \quad \text{for R3S5}$$

Straight lines were also fitted to the growths and decays of the other series. The values of the growth and decay constants obtained are given in columns 6 and 7 in table 5.2. The uncertainties in determining the slopes of the graphs amounted to approximately 7%.

Knowing $|\gamma_F| - \gamma_R$ and $|\gamma_F| + \gamma_R$ (or just γ_R if no feedback) from the oscillation growths and decays respectively, we can calculate the values of γ_F and γ_R. These are shown in columns 9 and 10 in the table. Good agreement was found between values of γ_F obtained from oscillations in the same group. Table 5.3 summarises the values obtained. Note that in group 2, γ_F is nearly equal to γ_R, thus causing very slow growths in R3S3, R3S4 and R3S5.

The value of γ_R tends to fall with temperature, as shown in figure 5.20. This is a feature of Robinson damping. The data allows us to calculate the thermal time constant of the cell, and

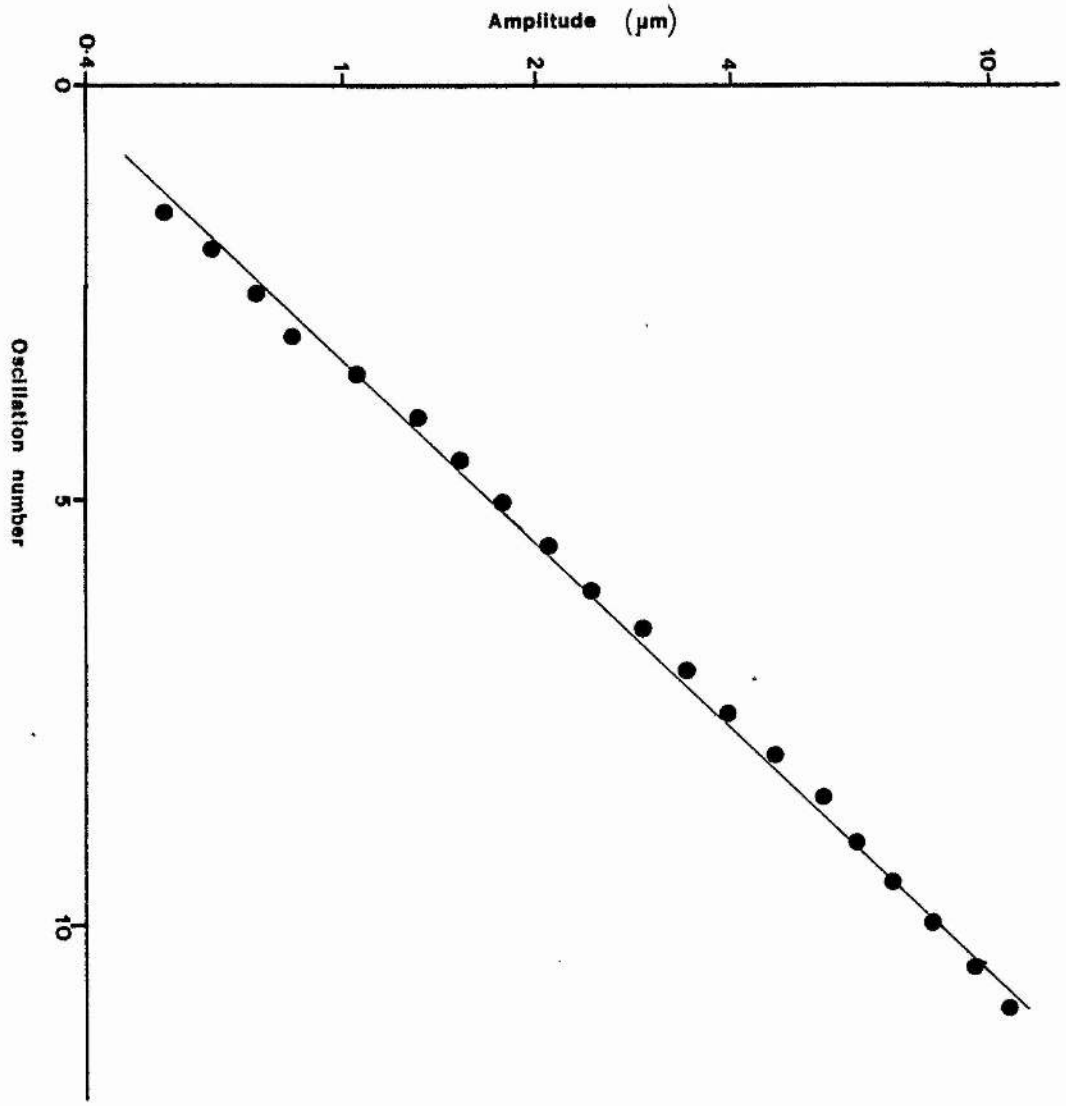

FIGURE 5.19 R3S12: growth stage

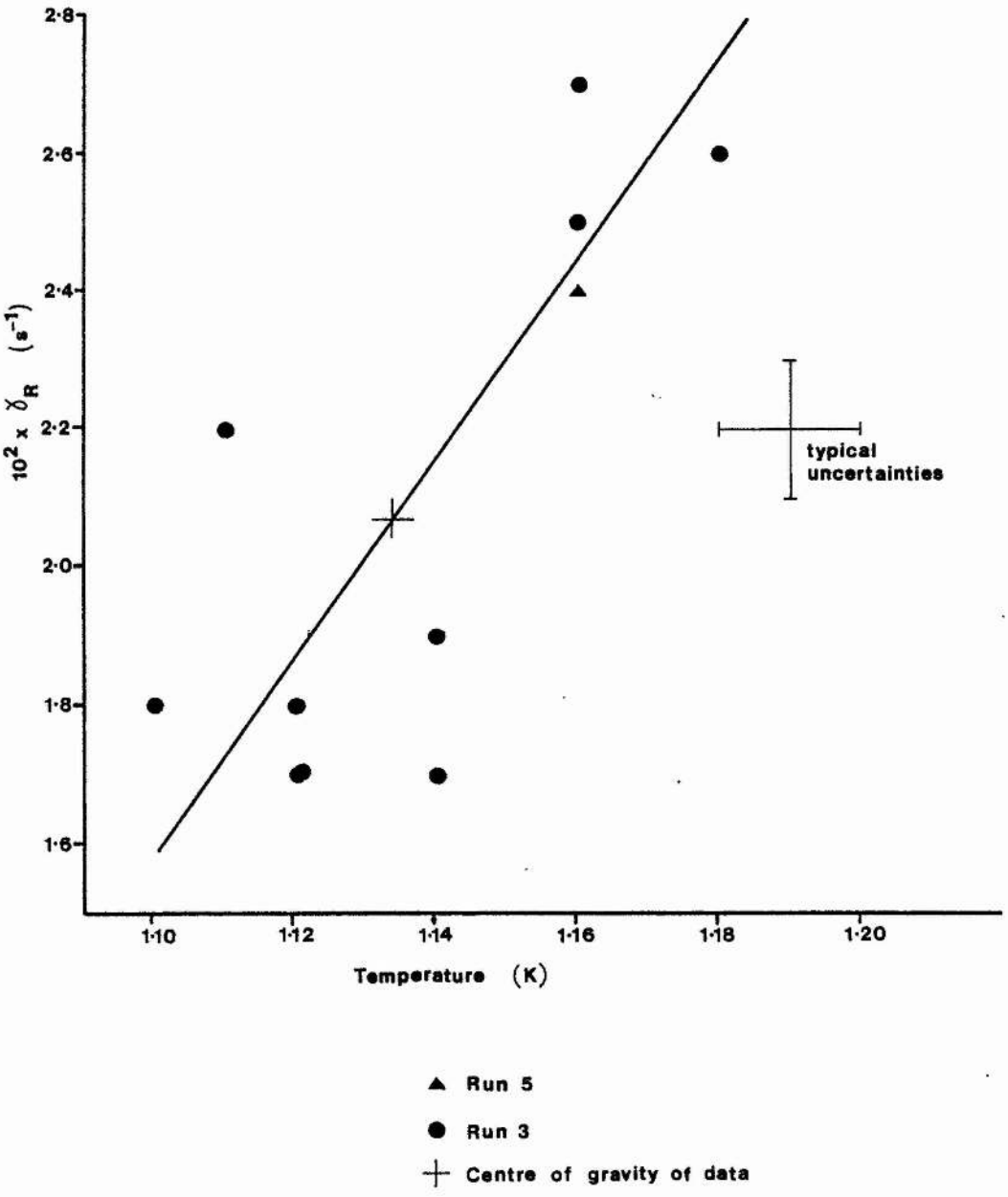

FIGURE 5.20 Thermal damping versus temperature

we do so in Appendix C. We also show that Robinson damping adequately explains the variation of δ_R.

The amplitude of the oscillation at the point where the growth breaks away from a simple exponential has been recorded in column 12 of table 5.2. This amplitude, h_{onset}, represents the onset point of non-linear dissipation. Approximating the oscillations to a sinusoid of constant amplitude, we obtain for the transfer rate at onset:

$$\sigma_{onset} = \frac{w_2 d_2 \omega_0}{p_{min} \sin\theta_2} h_{onset} \qquad (5.8)$$

The onset amplitude for R5S1 given in the table is the average of the onset amplitudes for the initial growth and all the intermediate growths which have the same slope as the initial growth. (See figure 5.18 and section 5.4). Similarly for R3S3.

In some of the series of oscillations, the onset of dissipation is more gradual than in others. For instance, the rate of growth of amplitude in R3S11 becomes slower gradually as the amplitude increases, making it difficult to specify exactly the onset amplitude. In R3S9, the rate of growth changes discontinuously at an amplitude of 9.9μm, indicating an abrupt increase in the rate of dissipation. For several oscillations after this, the amplitude continues to grow approximately exponentially, but at a slower rate, indicating that the dissipation is still linear in the velocity.

Even in those series (such as R3S7) where the onset of non-linear dissipation is abrupt, the onset amplitude is widely scattered within each group. There would appear to be no constant critical amplitude for the onset of dissipation.

To reduce the effect of the variation in onset, σ_{onset} was evaluated for all flows, and averaged for each group. The

Table 5.3

Group	γ_F (s^{-1})	Mean growth rate (s^{-1})	σ_{onset} ($cm^2 s^{-1}$)
1	0.053±0.004	0.0265±0.0005	12.7±1.5
2	0.028±0.005	0.0037±0.0007	4.1±1.2
3	0.035±0.002	0.017 ±0.001	9.2±1.5
4	0.043±0.003	0.019 ±0.001	11.0±0.9

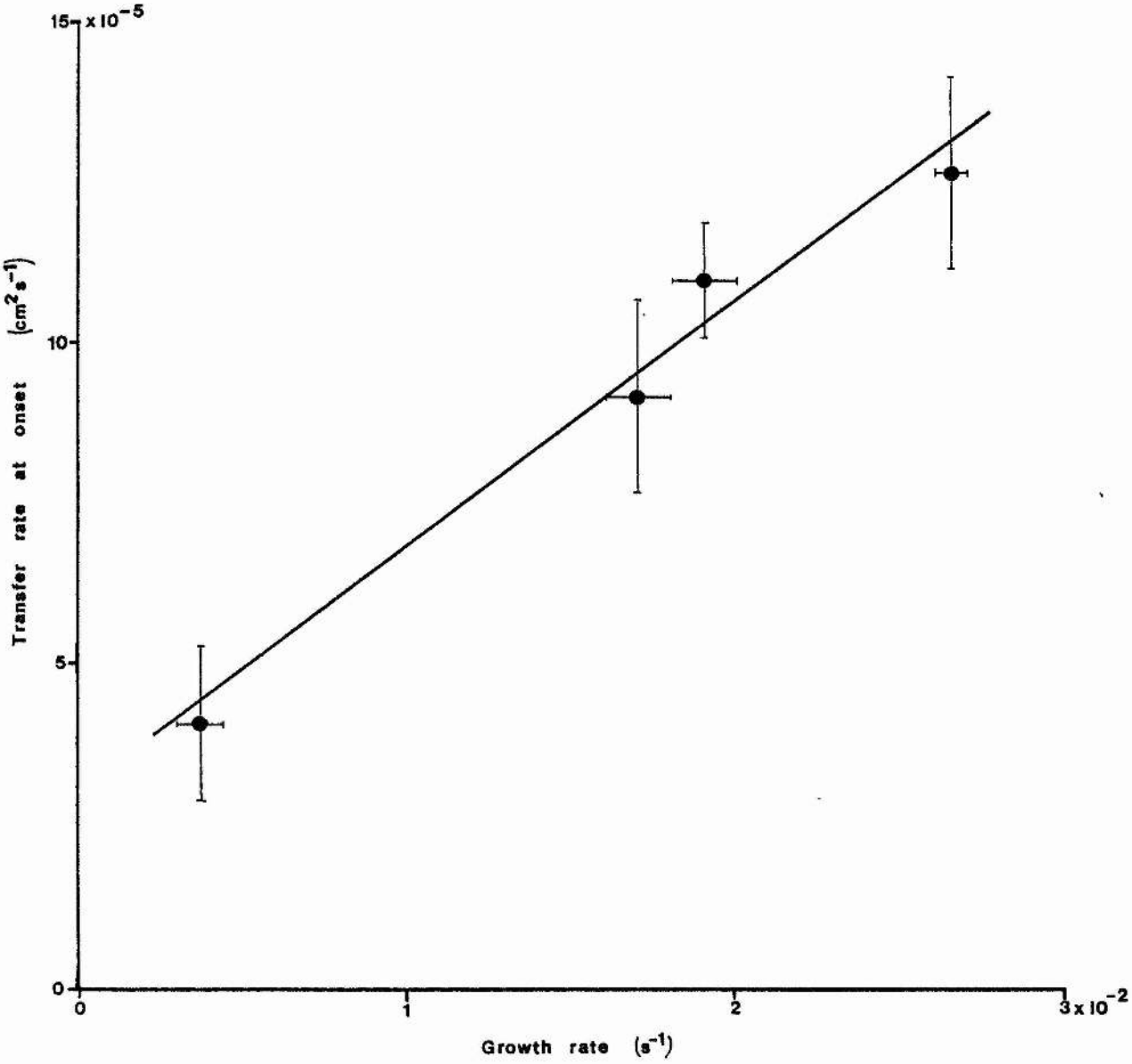

FIGURE 5.21 Transfer rate at onset of dissipation v growth rate

initial growth rate of the oscillations was also averaged for each group. The results are given in table 5.3, and σ_{onset} is plotted against growth rate in figure 5.21.

The points to note from figure 5.21 are these. Firstly, the experimental data lie nearly on a straight line of positive slope, which does not pass through the origin. Thus, as the differentiator feedback (and therefore the growth rate) is increased, higher and higher film velocities are accessible without non-linear dissipation setting in. Presumably, such behaviour will not continue indefinitely, and at sufficiently high growth rates, the line will flatten out.

Secondly, note that quite high transfer rates can apparently be obtained without non-linear dissipation occurring. These rates are nevertheless lower than those observed in the steady flows.

Thirdly, we observe the important fact that figure 5.21 demonstrates hysteresis in the film, in that dissipation sets in at a velocity which depends on the previous history of the film, rather than at some constant velocity. This point is elaborated on in sections 6.1 and 6.3.

5.3 The Period of the Oscillations

The period of the oscillations was measured for every series. The time taken for ten zero-crossings in the same direction was measured to obtain the average period over those oscillations. The results reported in column 4 of table 5.2 represent the mean period during the "intermediate" stage, when dissipation limited the oscillation amplitude. Care was taken to use oscillations where the amplitude did not vary far from the mean.

However, to quote a single figure for each series is

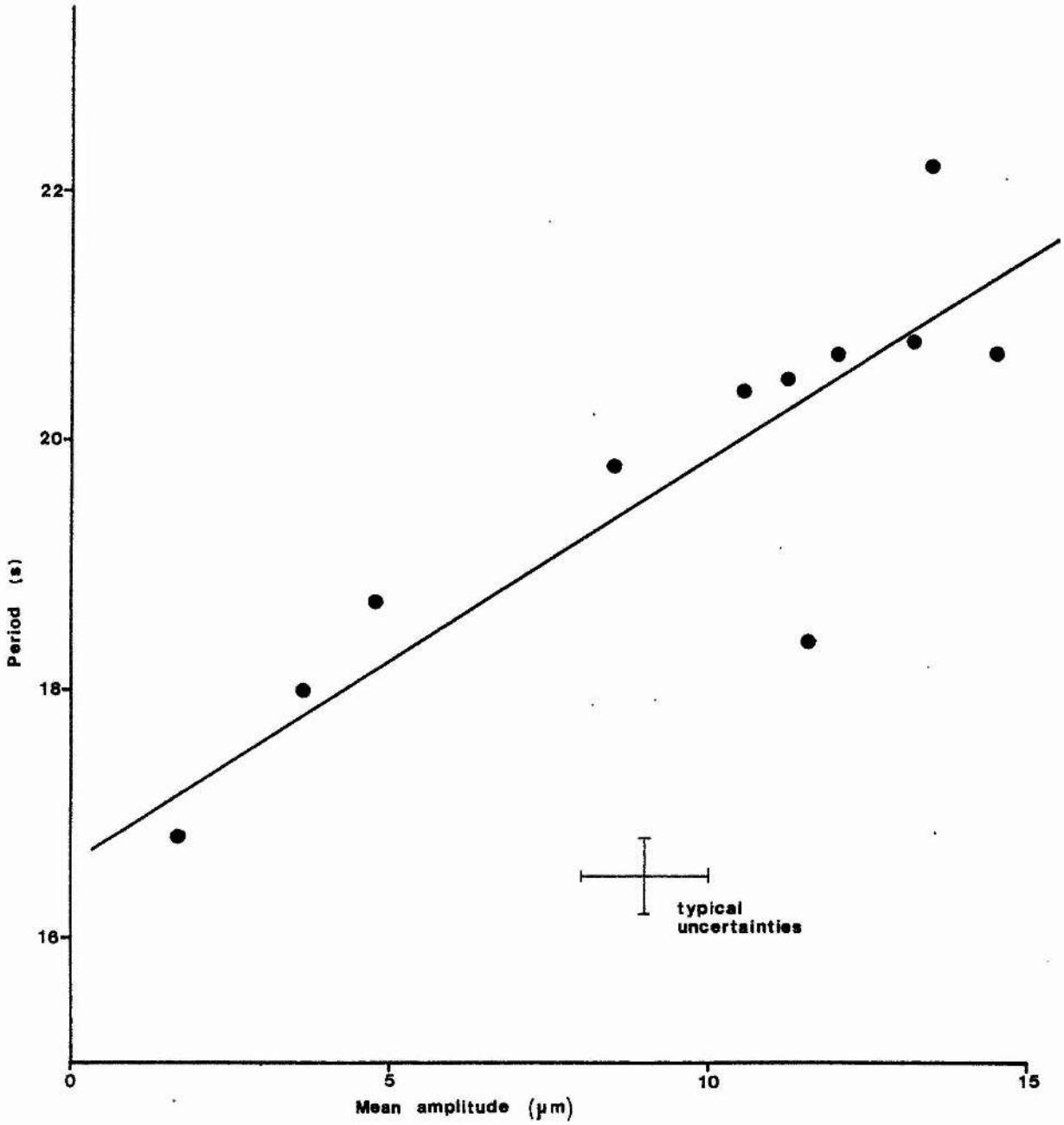

FIGURE 5.22 Amplitude v period (all series except R5S1. Line: T(seconds) = 16.6 + 0.33 h(microns)

misleading, in that the period was observed to increase with increasing amplitude. The mean period at low amplitude during the growth of the oscillations was typically about 5% less than the value given in the table.

The variation of the period from series to series can be explained by the different amplitudes of the series. Figure 5.22 is a graph of the period (as recorded in column 4 of the table) versus the mean amplitude during the ten cycles over which the period was measured. It incorporates all series except R3S12 and R5S1, which are discussed below. The graph shows a trend for the period to be greater at larger amplitude. A least-squares fitted straight line is drawn through the points. (Correlation coefficient = 0.850).

This effect is also clearly shown in R3S12, in the intermediate stage during the slow fall and then rise (see figure 5.19). Plotting the mean period over ten cycles against the mean amplitude during those cycles yields figure 5.23. A straight line has been fitted to the data; the least squares method gives the equation of the line as $T = a + bh$ where $a = 18.8$ s, $b = 2.15 \times 10^3$ s cm^{-1}. However, this line is evidently different from the variation in period between the series (figure 5.22).

In R5S1, during the slow fall and rise (see figure 5.18), the variation in period is almost zero. For a change in amplitude from 7.2 to 11.0 μm, the period changes from 17.1 to 17.4 s. This finding is consistent with the observed dependence of the velocity on amplitude in R5S1. For that series, the output of the differentiator was monitored on the chart recorder, and the peak to peak velocity swing measured every half-cycle. The velocity was found to be proportional to the amplitude over the entire amplitude range. This implies that the oscillations

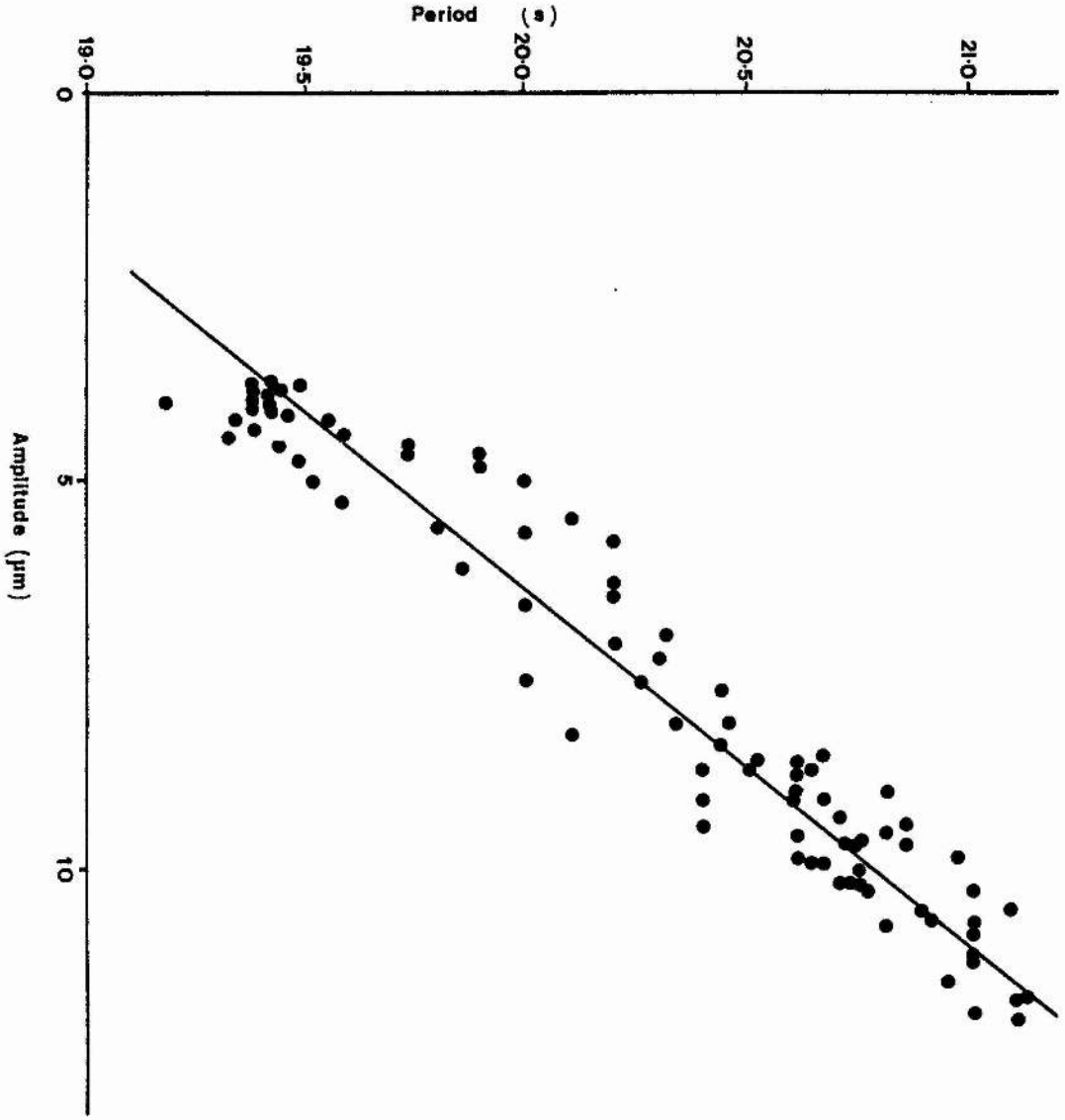

FIGURE 5.23 Period v amplitude (R3S12, slow fall and rise)

were sinusoidal and the frequency was constant during R5S1.

Thus, we can say that the period appears to vary linearly with amplitude, but the rate of such variation is not always the same. Film thinning as a possible source of the period variation is considered in section 6.4.

A theoretical prediction of oscillation period may be made using equation (4.16), provided that the integral I given by equation (4.14) is known. A film thickness profile of the form

$$d(z) = d_0 \, z^{-1/3} \qquad (5.9)$$

was used, where z is the height in centimetres of the film above the bulk liquid level and d_0 is the film thickness at a height of 1 cm. The integral was evaluated from the known cell geometry to be:

$$I_{calc} = (1.0 \pm 0.07) \times 10^6 \ \ cm^{-1}$$

where d_0 was set to 3.0×10^{-6} cm. Substituting this value of I into equation (4.16) gives an estimate of the oscillation period:

$$T_{calc} = 35 \pm 2 \ \ s$$

It should be noted that in the calculation of I , only 25% of the contribution to the integral comes from the Melinex disk and the constriction. Most of the kinetic energy of the film is thus located in the remainder of the flow path.

T_{calc} is nearly twice the experimental value T_{expt}. The most probable source of error of this magnitude is the integral I. Substituting the value of T_{expt} for group 3 into (4.16) yields:

$$I_{expt} = (3.3 \pm 0.1) \times 10^5 \ cm^{-1},$$

which is approximately three times smaller than the calculated

value.

Campbell[43] has noted that a leak, forming an additional parallel flow path between the reservoirs, can increase the oscillation frequency by providing extra area for the flow. The denominator in the expression for I becomes $(p_1+p_2)d_0$ where p_1 and p_2 are the perimeters of the main path and the leak respectively. In the present geometry, the only possible extra flow path between the two reservoirs would be a leak past the support-rings of the Melinex disk constriction. Any other leaking joints would leak into the main bath, which would lead to an immediate filling of the entire cell with liquid helium.

The decrease in I required to increase the frequency by a factor of two is 75%. This is a far greater change than would be obtained by removing the constriction entirely. A leak of this size would also lead to an overestimation of the transfer rate by several times. We can therefore conclude that there is no major leak between the resevoirs.

The possibility of a smaller leak contributing part of the difference between the experimental and calculated periods may also be considered. Such a leak might explain the higher transfer rates observed. However, Campbell[43] has shown that one characteristic of such a two-path situation is an asymmetry in the inertial oscillations between one flow direction and the other, which occurs when there is a persistent current through one path, returning through the other. Such a current will be created whenever the film is driven to the critical velocity along one of the paths. By looking at the inertial oscillations after steady flow in the critical regime, we can determine whether there is a leak or not. Examining the oscillations obtained in this manner, we find that the cell passes the test.

An anomalously high frequency has been reported by previous

investigators, who have usually explained it in terms of an increased film thickness. For instance, Glick and Werntz[40] used the oscillation frequency as a function of film height to determine the film thickness profile (equation 5.9). They inferred d_0 to be approximately 100 nm, three times as much as the value that is usually quoted and that was assumed earlier in this section. Again using the oscillation period, Hallock and Flint[42] found d_0 to be between 41 nm and 51 nm, depending on the substrate. In the present case, estimating d_0 from I_{expt} gives $d_0 = 90$ nm $\pm$ 10%. Our results are therefore not incompatible with those from previous experiments.

However, an alternative (or supplementary) explanation for this discrepancy is that the effective microperimeter of the flow path is considerably larger than the macroscopic geometry indicates. This could be caused by surface roughness created during machining of the Stycast 1266. Because of the relatively small contribution to the integral from the smooth Melinex disk, a larger perimeter in the remainder of the flow path would have a correspondingly large effect on the integral.

5.4 The Intermediate Oscillations

We discuss here the intermediate oscillations occurring after the initial growth has been checked by the onset of non-linear dissipation, but before the differentiator is switched off to allow the oscillations to decay away.

If (for the low frequencies reported here) dissipation was a universal, unchanging function of the superfluid velocity, one would expect that the oscillations would grow to such a size that the energy imparted to them by the driving force was equal to the energy dissipated, per cycle. This constant amplitude would be

maintained throught the intermediate stage. The non-linear dissipation would also lead to the introduction of odd harmonics into the oscillations. Such constant amplitude behaviour is observed, but it is far from being universal. The best example occurs in R3S11 (figure 5.16). This type of behaviour will be referred to as "normal" or "type I" behaviour. Other examples occur in R3S7 and R3S10 (figures 5.12 and 5.15).

A second type of behaviour is seen in R3S12 (figure 5.17, oscillations 16 to 25) and R5S1 (figure 5.18, oscillations 15 to 40). There is a slow fall to lower amplitude, which is maintained for a number of oscillations, and then a slowly accelerating growth. This results in a characteristic "U" shape in the amplitude/time graph. This behaviour will be referred to as "type II". It is possible that the slow decrease observed during the intermediate oscillations in R3S6 would have developed into this type of behaviour.

"Type III" behaviour occurs in R3S1, R3S10 and R3S12. It consists of a sharp fall in amplitude, followed by a slow rise. The dissipation causing the fall in amplitude all happens in one half-cycle; the data point half way down the fall is half the peak-to-peak amplitude of this half-cycle. The subsequent slow rise is exponential, but is at a slower rate than the initial growth rate (prior to onset).

"Type IV" behaviour is very similar to type III, except that the growth rate is equal to the initial growth rate, implying the absence of all intrinsic dissipation. Type IV behaviour is observed in R3S3 and in R5S1 (oscillations 40 to 90). In both cases, a number of such falls and subsequent growths occur together (thirteen in R5S1). The amplitudes at which the sudden falls occur have been averaged to obtain the transfer rate σ_{onset} in table 5.3 (see section 5.2).

It is believed that the four types of behaviour classified above describe all the major features of the intermediate amplitude behaviour. No previous experiment has supplied energy to the oscillations continuously, and these interesting types of behaviour have never been seen before. Further discussion of these observations is postponed until Chapter 7.

CHAPTER 6

VORTICES AND DISSIPATION (I)

6.1 Introduction

In this chapter and the following one, some theoretical ideas and analyses are presented which go towards an explanation of some of the experimental results described in the previous chapter. In section 6.2, the steady flows are discussed, and the likely effect of the experimental geometry on the transfer rate is elucidated. The onset of non-linear dissipation is discussed in section 6.3. Section 6.4 is a discussion of the possible origins of the observed variation of frequency with amplitude. Chapter 7 describes a theory of the intermediate oscillation behaviour. The present section contains preliminary remarks on features common to all the theoretical work in subsequent sections.

We first emphasise the need for a theory of dissipation in the saturated film which incorporates vorticity in the film as a variable (or variables) on the same footing as the superfluid velocity. Most previous theories have derived expressions for the dependence of dissipation on superfluid velocity, without allowing for a dependence on the vortex density. We have seen in the previous chapter that there is a multiplicity of flow rates for the same voltage ramp rate; that there is hysteresis in the onset of dissipation in the oscillations; and that the amplitude is not uniquely determined by the rate at which energy is supplied to the oscillations. These results show that the dissipation in the film cannot in general be described solely by the velocity.

Some previous experiments have also demonstrated hysteresis in the film. The transfer-rate transitions observed by (among

others) Allen and Armitage[19], Harris-Lowe and Turkington[35], and Toft[36], indicate that the velocity is not solely dependent on driving force. The persistent current experiment of Eckholm and Hallock[103] demonstrates that hysteresis can occur in the unsaturated film as well.

From these observations, it is obvious that at least one further variable is required to describe the behaviour of the film. That this variable is connected with the vorticity present in the film seems beyond doubt. It is also clear that the traditional method of presenting results in the form of a dissipation/velocity graph is not necessarily useful in all cases.

There are a variety of alternatives for the type of vorticity present in the film. A tangled mass of vortex lines - "spaghetti" - has been used to explain the flow of bulk liquid in broad channels[105]; in the helium film, however, the energy of such a tangle would be much higher, and it would therefore be unlikely to occur. Vortex lines parallel to the plane of the film have also been suggested[106], as have vortices pinned at one end and trailing downstream[32]; and perpendicular to the film but free to move[107].

For the present work, we have chosen the last of these possible situations. We assume the existence of vortices perpendicular to the plane of the film, which are not pinned to the substrate, but are free to move under the action of the forces acting on them. The reasons for this choice are as follows.

The success of the Kosterlitz-Thouless theory (see section 2.2) in describing the superfluidity of the unsaturated film in terms of two-dimensional vortices suggests that a three-dimensional extension of this situation might be relevant to the saturated film. Theoretical calculations by J G M Armitage and

the author[107] also used vortices with this orientation to predict the variation of transfer rate with temperature. A further point in favour is that the theoretical analysis of the perpendicular orientation is much simpler, whereas the parameters of a vortex line parallel to the film have not yet been calculated[32]. Finally, this orientation provides a simple parameter which is easy to define and calculate - the vortex density, which we define as the number of vortices of either sign per unit area of film.

Since the energy required to create a vortex of circulation κ is proportional to κ^2, we assume that only vortices of unit circulation are present. It is also worth noting that such a vortex whose end becomes pinned to the substrate will remain there, perpendicular to the film, unless it can acquire sufficient energy from the flow to either leave the pinning site[89], or to increase its length, depart from the perpendicular and start to be swept downstream[32]. We do not find it necessary to include explicitly pinning behaviour in order to explain the experimental results.

The hydrodynamics of a quantised vortex line in liquid helium has been worked out by several authors[89,94,108,109]. In the frame of reference where the normal fluid is stationary (the laboratory frame in the case of the helium film), the vortex is acted on by four forces. These are: a normal-fluid drag and a normal-fluid lift, arising from the scattering of thermal excitations from the vortex core; a Magnus force, due to the relative motion of the vortex line and superfluid; and possibly an external force per unit length $\underline{f}$. The sum of all these forces must be zero, since a vortex is just a flow configuration and has no intrinsic mass.

Let $\underline{v}_s$ represent the superfluid velocity evaluated at the vortex core, and $\underline{v}_L$ the vortex line velocity. The balance of the forces can then be written:

$$\rho_s \underline{\kappa} \times (\underline{v}_L - \underline{v}_s) - \nu \underline{v}_L - (\nu'/\kappa)\underline{\kappa} \times \underline{v}_L + \underline{f} = 0 \quad (6.1)$$

where $\underline{\kappa}$ is the circulation of the vortex, and ν and ν' are constants representing respectively the normal-fluid drag and lift forces per unit length. For a vortex in two dimensions, this equation can be solved[108] for $\underline{v}_L$, which we resolve into two components $v_{\parallel}$ and $v_{\perp}$, respectively parallel and perpendicular to the superfluid velocity $\underline{v}_s$:

$$\begin{aligned} v_{\parallel} &= \delta v_s + \beta f/\kappa\rho_s \\ v_{\perp} &= \beta v_s - \delta f/\kappa\rho_s \end{aligned} \quad (6.2)$$

where

$$\begin{aligned} \delta &= \xi\eta^2/[1+(\xi\eta)^2] \\ \beta &= \pm\eta/[1+(\xi\eta)^2] \\ \xi &= 1 - \nu'/\kappa\rho_s \\ \eta &= \rho_s\kappa/\nu \end{aligned} \quad (6.3)$$

β and η take the sign of the vortex circulation. In deriving equations (6.2), we have assumed that $\underline{f}$ has no component perpendicular to $\underline{v}_s$.

Campbell[108] gives the value of ξ as 1 except very near the lambda point, so the third term in equation (6.1) can be ignored. The value of η is strongly temperature dependent; at T=1.15K, $\eta = 10^2$. Thus $\beta = 10^{-2}$.

For a free vortex, the contributions to v_s at the vortex core from other vortices in the film will average out, and v_s is just given by the overall superfluid velocity u_s due to bulk transport. However, two vortices may approach so closely that the vortex contribution to v_s is comparable to u_s. The

characteristic distance at which this occurs is given by $R \sim \kappa/u_s$. Depending on the relative signs of the vortex lines, they may scatter off each other, or may bind or annihilate each other.

The discrete nature of the thermal excitations which interact with the vortex core to produce the terms in ν and ν' in the equations, means that a "noise" term $\int(t)$ should be added to equation (6.2). This term is effectively the Brownian motion of the vortices in the surrounding gas of thermal excitations, and is important in the unsaturated film[87,94]. Due to this Brownian motion, vortices will diffuse through the film with a diffusion constant D given by:

$$D = \frac{k_B T}{\rho_s \kappa} \beta \qquad (6.4)$$

(see Ambegaokar et al., reference 94, second paper, equation (2.4) and appendix B). For the unsaturated film, because of a lack of experimental data, D has been estimated from dimensional arguments[94] to be of order $\kappa \sim 10^{-3}$ cm^{2}s^{-1}. For the saturated film (and also bulk liquid helium), the experimental results of Rayfield and Reif[56] have been interpreted by Campbell[108] who obtains the value of β given above at T=1.15K. This implies that the value of D is approximately 10^{-14} cm^{2}s^{-1}, and we see that diffusion due to Brownian motion is negligible in the saturated film at this temperature.

Equations (6.2) contain terms in an external force f per unit length, parallel to v_s. Such a force will arise from any change in the film thickness d. The energy of a vortex line of length d is:

$$E = \rho_s \kappa^2 d \ln(a/R) / 4\pi$$

where a is the vortex core radius and R is a cut-off radius,

equal to the mean separation of the vortices. Therefore, if the vortex is in a region where there is a film thickness gradient ∇d parallel to $\underline{v}_s$, it will experience a force per unit length due to stretching of the vortex line:

$$\underline{f} = \rho_s \kappa^2 \nabla d \ln(a/R) / 4\pi d$$

Changes in the film thickness will arise from the requirement that the chemical potential on the film surface must everywhere be the same (in the absence of dissipation). In a vertical region of the film on a flat substrate, this will lead to a film profile given by equation (5.9). If there is an internal "corner" on the substrate, it will fill with liquid, held there by surface tension to form a meniscus. This will produce a very large ∇d. The shape of such a meniscus is calculated in Chapter 8.

6.2 The Effect of the Experimental Geometry

The presence of the Melinex disk in the flow path causes the film to flow radially inwards to the central hole, through the hole, and radially outwards on the downstream side. Conservation of mass requires that the velocity at radius r is:

$$v_s(r) = v_0 r_0 / r \qquad (6.6)$$

where v_0 is the velocity at the hole, which has radius r_0. There is thus a large velocity gradient in the vicinity of the hole. This experimental arrangement was originally chosen with the intention of confining the largest velocity and hence the dissipation to the hole. We shall show that this is not the case.

We will consider for the present steady flow (v_s = constant). It is useful to estimate the approximate vortex

density required to produce the dissipation observed in the flow. The starting point is Anderson's phase slippage requirement that the number of vortices per second crossing a streamline ($\dot{N}$) should be related to the consequential dissipative chemical potential difference by:

$$\Delta\mu_D = \kappa \dot{N} \tag{6.7}$$

(See section 1.3.) The number of vortices crossing a streamline per second per unit length of streamline is just $nv_\perp$ where n is the vortex density. N is therefore $nv_\perp$ integrated along a streamline from one reservoir to the other, and thus we have:

$$\Delta\mu_D = \kappa \int n\, v_\perp\, dl \tag{6.8}$$

For the purpose of showing it not to be the case, we now assume that the dissipation and hence the vorticity is confined to the immediate vicinity of the hole. Specifically, let us assume that n is zero except over a length L = 30μm parallel to the flow. If we take for $\Delta\mu_D$ the quantity $g\epsilon$ with ϵ = 100μm, we obtain from equations (6.8) and (6.2) that $n = 10^7 cm^{-2}$. The mean vortex separation is therefore $1/\sqrt{n} = 3\mu m$. However, in travelling L = 30μm downstream, a vortex will move (in the absence of any external force) a distance of only $\beta L = 0.3\mu m$ perpendicular to the flow. This is only one-tenth of the inter-vortex separation, and (on average) will not bring vortices of opposite sign close enough together for annihilation to occur. Therefore, vortices will move downstream from the hole, and the remaining 90% of the streamlines will be crossed further down the flow path. This particular experimental geometry thus separates the region of maximum velocity from the region of maximum dissipation.

It is possible to derive an estimate of the minimum extent of the dissipation region based on the above considerations. We make the approximations n = constant and v_s = constant within the dissipation region, which is of length L. From (6.8) and (6.2) we have $n = \Delta\mu_D/\kappa\beta v_s L$. However, βL must be at least as long as $1/\sqrt{n}$ in order that vortices of opposite sign annihilate before leaving the dissipation region. We therefore obtain for the length of the dissipation region:

$$L > \kappa v_s/\beta\Delta\mu_D \qquad (6.9)$$

For $\beta = 10^{-2}$, $v_s = 30\text{cms}^{-1}$ and $\Delta\mu_D/g = 100\mu\text{m}$, we obtain L > 0.3cm. Because of the approximations noted above, (6.9) is not directly applicable to our experimental geometry.

All previous experiments on film flow have been performed in geometries where the minimum flow perimeter p_{min} was maintained for a considerable length (generally greater than the RHS of (6.9)). Effectively all the dissipation occured within the minimum perimeter region, and p_{min} was therefore an important parameter. The definition of transfer rate as $\sigma = \dot{V}/p_{min}$ (where $\dot{V}$ is the rate of change of volume in one reservoir) allowed the velocity in the dissipation region to be calculated as simply $v_s = (\rho/\rho_s)\sigma/d$ with d the film thickness.

However, in the present situation, the velocity in the dissipation region is lower than the velocity at the point of minimum perimeter. Since dissipation limits the superfluid velocity, it is reasonable to assume that the velocity in the dissipation region is the same in the present radial flow situation as in the usual case of linear flow. The velocity at the central hole (and thus the calculated transfer rate) will therefore be greater than in the linear flow case. In other words, to compare the transfer rates in the two cases, we should

use the flow perimeter in the dissipation region rather than the minimum perimeter of the path in our calculation of σ.

The transfer rates listed in table 5.1 were calculated using p_{min}. The considerations above show why the values obtained are higher than those found in other experimental geometries.

In order to make a more precise comparison of the two situations (radial flow and linear flow), we will allow the vortex density to vary over the length of the film. For definiteness, we consider a linear flow experiment on (or in) a tube of constant perimeter $2\pi r_0$, ℓcm long. The radial flow path is an annulus of inner radius r_0 and outer radius r_1. In the experimental geometry, $r_0 = 0.03$cm and $r_1 = 0.30$cm. Our object is to calculate the dissipation in each case.

We shall assume that vortices are created at a rate R per second at the upstream end of the flow path. They are annihilated at a rate Cn^2 where C is a constant (see section 7.2). First of all, we calculate the vortex distribution as a function of ℓ or r. The starting point is the differential equation for the vortex density:

$$\frac{D_L n}{D t} = \frac{\partial n}{\partial t} + \underline{v}.\nabla n = -Cn^2 \qquad (6.10)$$

For steady flows, we shall assume that $\partial n/\partial t = 0$; in other words, we ignore vortex relaxation effects. From equations (6.2) and (6.6), we obtain in the radial case:

$$dn/dr = -Cn^2 r/v_0 r_0 \qquad (6.11a)$$

and in the linear case:

$$dn/d\ell = -Cn^2 r/v_0 \qquad (6.11b)$$

Integrating these equations, we obtain:

$$n(r) = n_0[1+Cn_0(r^2-r_0^2)/2v_0r_0]^{-1} \qquad (6.12a)$$

$$n(\ell) = n_0[1+Cn_0\ell/v_0]^{-1} \qquad (6.12b)$$

where n_0 is the vortex density at the upstream end of the path. n_0 may be calculated from the rate R as follows. At the upstream end of the path, there will be $R/2\pi r_0$ vortices created per second per cm width of film. In width dw of film, one vortex will be created every $2\pi r_0/Rdw$ seconds, by which time the previously created vortex will have moved downstream a distance $dl = v_0 2\pi r_0/Rdw$. There is thus one vortex every dl.dw cm^2, so the vortex density at the start is:

$$n_0 = R/2\pi r_0 v_0 \qquad (6.13)$$

We now calculate the dissipation using equations (6.1), (6.2), (6.8) and (6.12). We obtain in the radial and linear cases respectively:

$$\Delta\mu_D = \frac{\beta\kappa v_0 r_0 n_0}{2-Cn_0r_0/v_0} \ln\left\{\frac{r_1^2/r_0^2}{1+(r_1^2-r_0^2)Cn_0/2v_0r_0}\right\} \qquad (6.14a)$$

$$\Delta\mu_D = (\beta\kappa v_0^2/C) \ln [1+Cn_0\ell/v_0] \qquad (6.14b)$$

Various functional forms for the dependence of vortex creation rate on superfluid velocity have been proposed in the past (see Chapters 1 and 2). Provided such functions vary sufficiently quickly with v_s, film flow experiments are often unable to determine which functional form is correct. We are therefore free to choose any suitably fast function for $R(v_0)$ without fear of unduly predjudicing the final result. For algebraic simplicity, we choose:

$$R = R_0 v_0^{\lambda} \qquad (6.15)$$

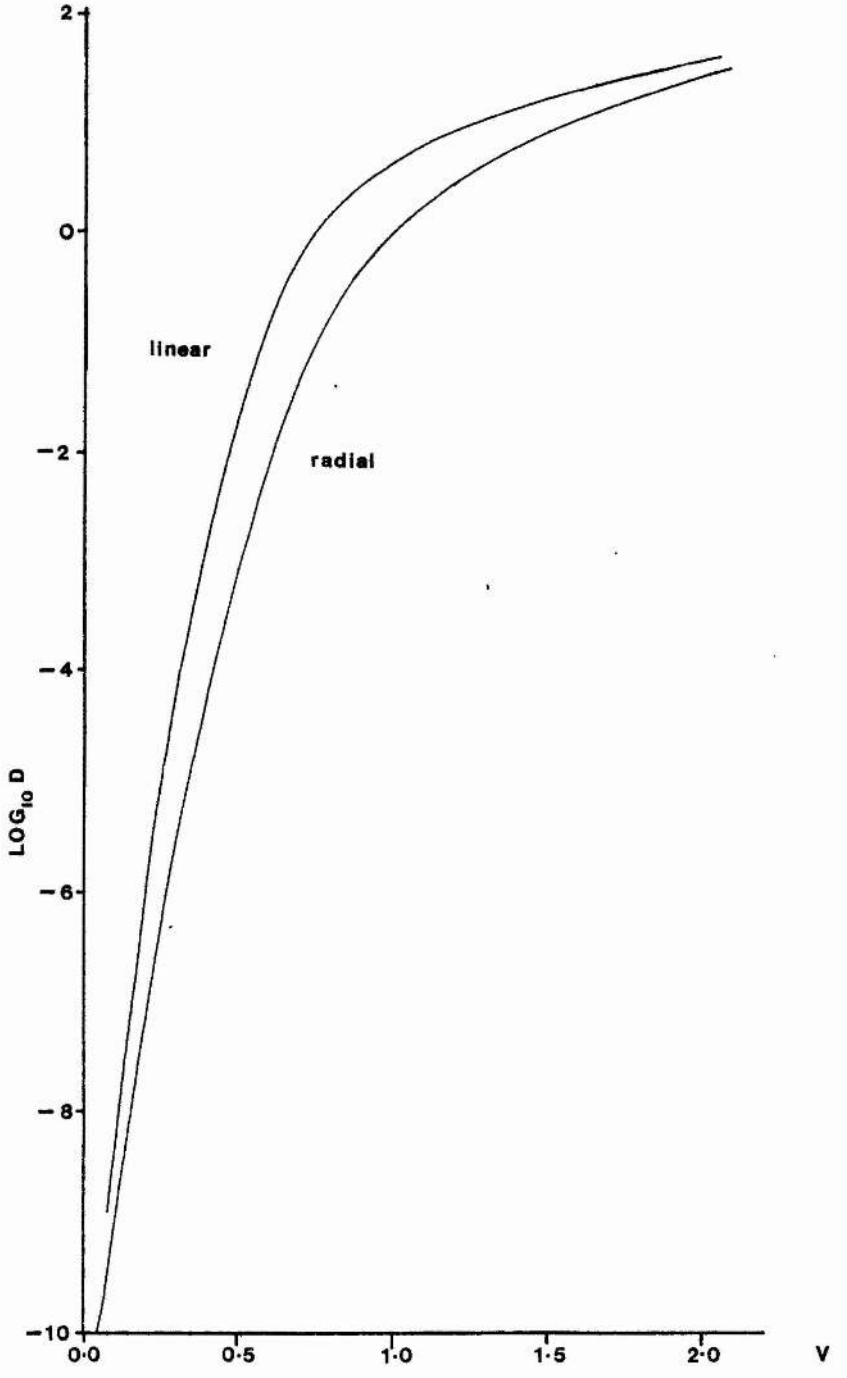

FIGURE 6.1 Dissipation v velocity
(linear and radial cases)

where R_0 is a constant and $\lambda>2$ in order that equations (6.14) should not diverge (see section 7.2).

To compare the two situations realistically, we must choose a suitable value for ℓ. Two choices suggest themselves: that the length of the dissipation region should be the same in both cases ($\ell=r_1-r_0$); or that the vortex density at the end of the flow path should be the same in both cases. The latter alternative is chosen for algebraic simplicity. There is no qualitative difference in the results if the other option is selected. Setting (6.12a) equal to (6.12b) yields:

$$2\ell/r_0 = A-1 \tag{6.16}$$

where $A = r_1^2/r_0^2 = 100$ in our experimental geometry. For convenience, we define a dimensionless velocity V and a dimensionless dissipation D by:

$$V^{\lambda-2} = v_0^{\lambda-2}CR_0/4\pi$$

$$D = (\Delta\mu_D/\kappa\beta C) \cdot (CR_0/4\pi)^{2/(\lambda-2)}$$

Substituting these equations into (6.14), we obtain

$$D_R = \frac{V^{\lambda-2}}{1 - V^{\lambda-2}} \ln \{A/[1+(A-1)V^{\lambda-2}]\} \tag{6.17a}$$

$$D_L = V^2 \ln \{1+(A-1)V^{\lambda-2}\} \tag{6.17b}$$

The dissipation is always less in the radial case than in the linear case (see Appendix A). Figure 6.1 is a graph of D versus V for the two cases, with A = 100 and $\lambda = 12$.

If $D_R = D_L$, the ratio between the radial and linear velocities is approximately $V_R/V_L = 1.3$ for $V < 1.2$. At larger V, the ratio becomes smaller. The value $\lambda = 12$ has been chosen so that this ratio corresponds to the observed discrepancy between the transfer rate in our geometry, and the lower transfer

rates observed in most linear flow experiments (see section 5.1).

At low values of V, the dissipation is proportional to V^{λ}. At large V, however, it varies much more slowly: $D \propto V^2 \ln V$. This is true in both situations. Because the dissipation in the steady state is known to be a steep function of V, it is likely that we are in the regime $V \ll 1$.

From equations (6.12), we see that for $V \ll 1$, most of the vortices survive to reach the outer rim of the Melinex disk. At the rim, there exists a surface tension meniscus, in the corner between the disk and its supporting epoxy ring. On reaching the meniscus, the vortices will experience a force due to their increasing length. v_s will fall as the film becomes thicker, and $v_{||}$ will also fall. $v_{\perp}$ will tend to fall because of the reduced v_s, but this will be more than offset by a rise due to its dependence on f.

Using the simple quadratic expression $d = d_0 + kz^2$ for the film thickness, where z is the distance from the top of the meniscus (compare equation (8.15)), we obtain:

$$v_{||} = v_1 d_0 (1-\beta^2 sz)/(d_0+kz^2)$$
$$v_{\perp} = v_1 d_0 (1+sz)/(d_0+kz^2)$$

where v_1 is the superfluid velocity at the start of the meniscus and $s = 2k\kappa \ln(R/a)/2\pi\beta v_1 d_0$. We find that $k/d_0 \sim 4\times10^{-5}\text{cm}^{-2}$, and $s \sim 8\times10^{4}\text{cm}^{-1}$, and we are therefore free to ignore the term in kz^2 in the denominator of the above equations.

Note that v becomes negative for $z > 1/\beta^2 s \sim 0.1$cm. This means that the vortices are confined to the region $z < 1/\beta^2 s$, and must all annihilate within it. Since the presence of vortices may alter the shape of the meniscus, the problem becomes extremely complicated, and is unsuitable for analytic solution. We can say that if $V \ll 1$, meniscus dissipation becomes important,

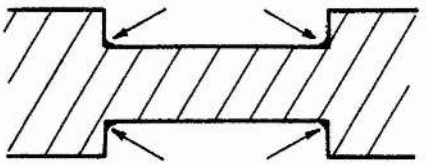

(a)

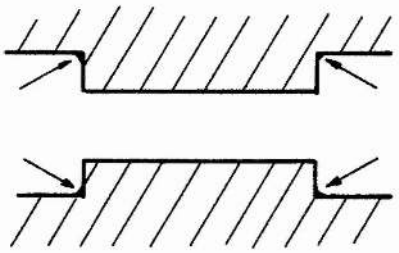

(b)

FIGURE 6.2 Flow (a) outside and (b) inside a cylindrical tube. The positions of the surface tension menisci are arrowed.

and indeed may dominate the dissipation on the disk. However, the considerations described at the beginning of this section will still apply, and the radial dissipation will be less than the linear dissipation for the same v_0.

A further source of possible inaccuracy in our results is that we have taken into consideration vortex creation at only one point in the film. In the radial flow case, the large velocity gradient near the hole, combined with the strong dependence of creation rate on v_s, ensures that very few vortices will be created elsewhere in the film. In the linear case, there may be vortex creation over the entire length of the dissipation region: this can only increase the dissipation, and the result that the radial flow is less dissipative than the linear flow still holds.

The analysis does not account for the large variation in transfer rate from flow to flow. Such a variation could come from a change in C or R_0. It is difficult to see how vortex relaxation could play a part, since each flow takes place at constant velocity.

There is an interesting consequence of our results which has implications for linear flow experiments. If the linear flow takes place on the outside of a cylindrical tube (figure 6.2a), there will be a meniscus at either end of the tube, at the minimum flow perimeter. However, if the flow is on the inside of the tube (figure 6.2b), the meniscus will occur at some larger perimeter where the superfluid velocity is smaller. If our model of the dissipation is correct and meniscus dissipation is important, the dissipation will be greater in the former case, and one would expect a lower transfer rate to be observed.

6.3 The Onset of Dissipation

We now turn to the inertial oscillations described in

section 5.2. Exponential growth of the oscillations under positive feedback from the differentiator is terminated by the sudden onset of non-linear dissipation. In section 5.2, we found that the oscillation amplitude at which this occurred was related linearly to the growth rate of the oscillations. It is clear that the non-linear dissipation does not occur at a critical flow rate.

However, it is obvious that the onset of dissipation occurs at a critical value of "something" - some unknown physical quantity X which builds up as the amplitude of the oscillations increases. We can conceive of X as the density of some sort of vorticity. When X exceeds a certain critical value X_c, dissipation will occur. We assume that X is created by superfluid flow, and therefore obeys an equation of the form:

$$X = f(v_s) \text{ or } f(\dot{h}) \tag{6.18}$$

where $f(0) = 0$. We are restricted to even functions $f(\dot{h})$, since we wish X to be monotonically increasing with time. Given $f(\dot{h})$, the above equation may be integrated to obtain X(t) or X(m) where $m = t/T$ is the period number. We can then determine the value of m when $X = X_c$, and hence the amplitude h_{onset} at that point. For $f(\dot{h})$, we assume the form:

$$f(\dot{h}) = A\,|\dot{h}| \tag{6.19}$$

h and $\dot{h}$ are given by:

$$h = h_0 e^{\gamma t} \sin \omega t \quad \text{and} \quad \dot{h} = \omega_0 h_0 e^{\gamma t} \sin(\omega t + \phi)$$

where $\sin \phi = \omega/\omega_0$ and $\cos \phi = \gamma/\omega_0$

Integrating equation (6.18), we obtain:

$$X(m) - X_0 = A\,\omega_0 h_0 \int_0^{2\pi m/\omega} e^{\gamma t} |\sin(\omega t + \phi)|\, dt$$

The integral may be evaluated to give:

$$X(m) = X_0 + Ah_0(\omega/\omega_0)(e^{4km}-1)\coth k$$

where $k = \pi\gamma/2\omega = \gamma T/4$ (see Appendix B). The value of m for which $X(m) = X_c$ is thus given by:

$$4km = \ln\{1+(X_c-X_0)(\omega_0/\omega Ah_0)\tanh k\}$$

and the corresponding amplitude h_{onset} is therefore:

$$h_{onset} = h_0 e^{4km} = h_0 + (X_c-X_0)(\omega_0/\omega A)\tanh k$$

For our experiment, $k \ll 1$, so we can approximate the above equation to

$$h_{onset} = h_0 + (k+O(k^3))(X_c-X_0)/A$$

If X_c is constant or zero, then a plot of h_{onset} against k (or equivalently σ_{onset} against γ) should be a straight line. Figure 5.21 is such a graph; it yields the following approximate values of the parameters:

$$h_0 = 3.8\,\mu m$$
$$(X_c-X_0)/A = 73\,\mu m$$

The function $f(\dot{h}) = A\dot{h}^2$ was also tried, but was found to lead to a quadratic dependence of σ_{onset} on γ, which is not supported by the experimental data. We can therefore infer that X obeys an equation of the form (6.18) with $f(h) = A|\dot{h}|$.

We can only speculate as to the nature of the quantity X. It can certainly be said that it is not equal to n, the density of free vortices, since dissipation will always occur when n is non-zero - there is no critical value n_c which must be exceeded. It might be that X is some form of "trapped" vorticity, which when

it reaches a critical density, escapes and is able to cause dissipation. The flow of the film would then require three parameters to describe it fully: the velocity, and the densities of the two different kinds of vorticity. Dissipation would be a two-stage process; the creation of trapped vorticity due to flow; and its subsequent escape to form free vortices capable of causing dissipation. There is insufficient data at present to be able to say whether this is more than speculation.

6.4 The Variation of the Oscillation Period

It is convenient to include here a discussion of the variation of period with oscillation amplitude that was mentioned in section 5.3. Figure 5.23 shows that the period varies apparently linearly with the amplitude, increasing by 7% up to the maximum amplitude of 12μm. This type of behaviour has been observed by other workers. Flint and Hallock[51] observed a variation of up to 3% in the period, while Campbell et al.[44] observed a 5% change.

Flint and Hallock were able to explain their results in terms of the kinetic thinning of the film. As the amplitude increases, so the mean square superfluid velocity rises, causing the average film thickness to decrease. The period, which is inversely proportional to the square root of the film thickness (see equation (4.16)), will then increase. We can calculate the magnitude of this effect as follows.

Let d(l) be the film thickness at a distance l along the flow path. $d_s(l)$ is the static film thickness, given by (5.11). The Kontorovich equation for the film thinning is:

$$d = d_s\,(1+\rho_s v_s^2/2\rho gz)^{-1/3} \qquad (6.20)$$

We can express v_s in terms of σ, the perimeter p, and p_{min} using

equation (4.12), in which we substitute d_s for d. (6.20) is then approximately:

$$d = d_s\ (1-\rho p_{min}^2\ \sigma^2/6gz\rho_s p^2 d_s^2) \qquad (6.21)$$

In equation (4.16) for the oscillation period, the film thickness appears only in the integral I. We can now calculate I using (6.21) and (4.14):

$$I = \int \frac{dl}{d_s p(1-A/zp^2 d_s^2)}$$

where $A = \rho p_{min}^2 \sigma^2/6\rho_s g$. We obtain:

$$I = I_s\ (1+AI_d/I_s) \qquad (6.22)$$

where I_s is the value of I ignoring kinetic thinning, and I_d is the integral:

$$I_d = \int \frac{dl}{zp^3 d_s^3}$$

From the geometry of the experimental cell, and using equation (5.15) for the film profile, we calculate $I_d = 5.1/d_0^3$. From (6.22) and (4.16) we have:

$$\omega^2 = \omega_0^2(1-\rho p_{min}^2\ \sigma^2 R/6g\rho_s)$$

where R is the ratio $I_d/I_s = 1.9\times10^{11}\,cm^{-5}$. We replace σ^2 by its average value, and the fractional change in period is thus:

$$\frac{\Delta T}{T} = \frac{\rho p_{min}^2\ \overline{\sigma^2}}{\rho_s\ 12\ g} R$$

which is proportional to the mean square transfer rate and hence to the square of the amplitude. At $\sigma = 10^{-4} cm^2 s^{-1}$ we obtain a value of $\Delta T/T \sim 0.6\%$, much less than the observed variation.

The effect of film thinning on the oscillation frequency is

thus negligible in our experiment. This is because so much of the flow path has a large perimeter, and therefore a low superfluid velocity. The only significant change in film thickness due to kinetic thinning occurs in the region of the constriction. However, this region does not contribute very much to the kinetic energy integral I on which the period depends, and thus the effect is very small. The experimental geometry of Flint and Hallock[51] had a relatively long region where v_s was high, and this contributed most to the integral I. The effect of film thinning was therefore more pronounced in their experiment.

It should be noted that the predicted change in period is proportional to the square of the amplitude. The scatter of the data in figure 5.23 does not allow us to reject completely the possibility that the observed relationship is really quadratic. The unexpectedly large variation in period has also been observed by Campbell et al.[44] They reported a change in period eight times larger than the predicted change due to film thinning. Unfortunately, they did not say whether the change observed was linear or quadratic in the amplitude.

CHAPTER 7

VORTICES AND DISSIPATION (II)

7.1 The Equation of Motion in the Phase Plane

In this chapter, a theoretical model of intrinsic dissipation during the inertial oscillations is presented. By combining the equation of motion (5.1) of the liquid level h with an equation of motion for the vortex density, the time development of the oscillation amplitude may be calculated. The calculation is performed by computer, using the numerical method of analytic continuation. The details of this method of solving a differential equation are given in section 8.3.

For convenience, we again set down the equation of motion of the film under positive feedback through the differentiator:

$$\ddot{h} + 2\gamma\dot{h} + \omega_0^2 h = -\omega_0^2 \Delta\mu_D/g \qquad (7.1)$$

where $\gamma = \gamma_R - \gamma_F < 0$ and $\Delta\mu_D$ is the intrinsic dissipation in the film. Our object is to solve (7.1) numerically. The disadvantage of applying the method of analytic continuation to this equation directly is that the desired oscillatory solutions have large second derivatives at their extrema. In order to maintain accuracy, it would therefore be necessary to include at least the second derivative in the Taylor expansion of h(t) (see equation (8.16)) at the expense of computing time. For this reason, the calculations were carried out in the phase plane, and only the first derivative was used.

Let us define dimensionless quantities x and y, proportional to h and $\dot{h}$ respectivly:

$$x = \omega_0 h/B \qquad y = \dot{h}/B \qquad (7.2)$$

where B is a constant with the dimensions of a velocity, which we

leave undetermined for now. From (7.2), we have that $\dot{x} = \omega_0 y$. x and y are Cartesian coordinates in a phase plane. We can eliminate time from (7.1) to obtain the equation of the phase trajectory:

$$\frac{dy}{dx} + a + \frac{x}{y} = -\frac{\omega_0 4\mu D}{B\, g\, y} = -\frac{D}{y} \qquad (7.3)$$

where D represents the dissipation, and a is a dimensionless constant proportional to the growth rate:

$$a = 2\gamma/\omega_0 \qquad (7.4)$$

For positive feedback, a will be negative. D must always have the same sign as y. If a and D are zero, the solution of (7.3) is just a circle, representing simple harmonic motion at constant amplitude.

It is more convenient to work in polar coordinates (r, θ). Rewriting (7.3) in these coordinates, we obtain:

$$\frac{dr}{d\theta} = \frac{(ay + D)\, y}{r + (ay + D)\cos\theta} \qquad (7.5)$$

We have retained y in the equation as shorthand for $r.\sin\theta$. The case D=0 is simple harmonic motion with a damping term a. In that case, the solution to (7.5) may be determined analytically:

$$r(\theta) = r_0[1 + (a/2)\sin 2\theta]^{-1/2}\, e^{F(\theta)}$$

where (7.6)

$$F(\theta) = \int_0^{2\theta} \frac{d\phi}{(2/a + \sin\phi)} = \frac{2\gamma}{\omega} \tan^{-1}\left\{\frac{\omega_0}{\omega}(\tan\theta + a/2)\right\}$$

r_0 is a constant of integration. For $|a/2| \ll 1$, (7.6) reduces to the spiral $r = r_0 e^{a\theta}$.

We shall also find it necessary to work out the time at which a point on the curve is reached. Since $\dot{x} = \omega_0 y$, we have that $\omega_0 dt = dx/y$. Now, $x = x(r, \theta)$, and r and θ are both

functions of t. Therefore

$$\frac{dx}{dt} = \frac{dr}{dt}\frac{\partial x}{\partial r} + \frac{d\theta}{dt}\frac{\partial x}{\partial \theta} = -r\dot{\theta}\sin\theta + \dot{r}\cos\theta$$

Multiply by dt/y to obtain:

$$\omega_0 dt = dx/y = -d\theta + \cot\theta\, dr/r \qquad (7.7)$$

In the case where a and D are both zero, the path is a circle, and hence dr=0. We thus have $\omega_0 dt = -d\theta$, and we see that the system point moves clockwise as time proceeds. To obtain the time at any point on the path, (7.7) may be integrated from any suitable starting point.

To obtain the oscillation period T, we integrate (7.7) over $d\theta$ from 0 to -2π, using (7.5):

$$\omega_0 T = 2\pi - \int_0^{2\pi} \frac{(ay+D)\cos\theta}{r+(ay+D)\cos\theta}\, d\theta \qquad (7.8)$$

When D=0 it is easy to show that (7.8) reduces to the expected formula $2\pi/T = \omega_0[1-(a/2)^2]^{1/2}$.

A computer program (similar to that in Appendix D) was written to solve equation (7.5). Given a point $[r(\theta), \theta]$ on the phase trajectory, an adjacent point $[r(\theta+\Delta\theta), \theta+\Delta\theta]$ is calculated from the Taylor series expansion, retaining only the first order term in $\Delta\theta$ (see section 8.3 for details of analytic continuation):

$$r(\theta+\Delta\theta) = r(\theta) + \Delta\theta\, dr/d\theta \qquad (7.9)$$

where $dr/d\theta$ is given by (7.5). $\Delta\theta$ is set to -1.0°, so that $r(\theta+\Delta\theta)$ is later than $r(\theta)$. The difference in the results between using a value of -5° and -1° for $\Delta\theta$ was 2% over five cycles. r is printed out every 180°, when the velocity is zero and the displacement x is at an extremum. These values of r are

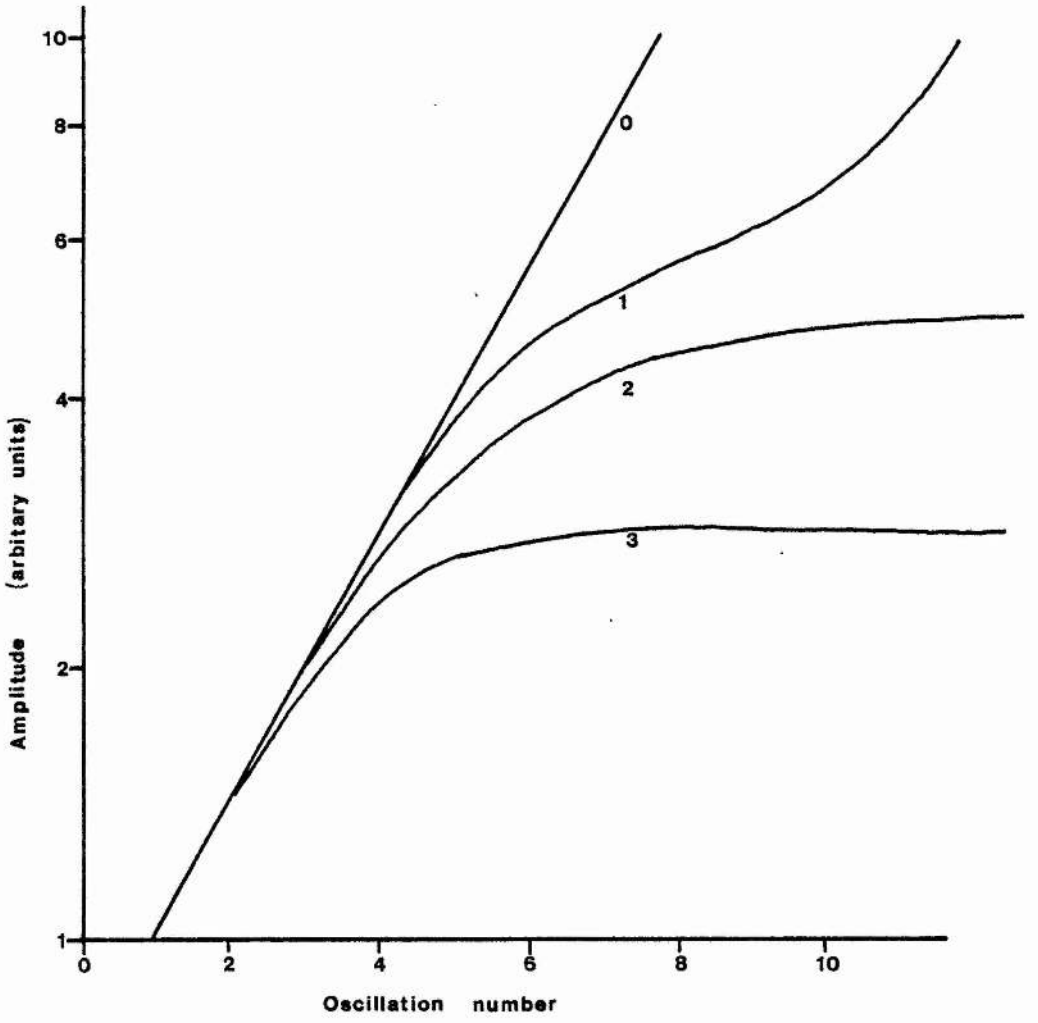

FIGURE 7.1 Oscillation amplitude y period number, with a=-0.109, dissipation function $D(y) = D_0 \exp(-1/|y|)\,\mathrm{sign}(y)$.
0: $D_0=0$ 1: $D_0=0.2$ 2: $D_0=0.5$ 3: $D_0=1.5$

thus the amplitudes of every half-cycle of the oscillations, and correspond to the measured amplitudes plotted in figures 5.6 to 5.18. The period was calculated by converting the integral (7.8) to a summation over the intervals $\Delta\theta$.

The program was tested by setting D=0, when exponentially increasing oscillations should be obtained. Using the value a=-0.109, corresponding to the group 3 oscillations, a plot of the logarithm of the calculated amplitude against the period number gave a straight line of slope $\pi|a|$, as expected (curve 0 in figure 7.1).

The consequences of using a dissipation function D which depends only on velocity was also investigated. Three dissipation functions were tried:

$$D(y) = \text{sign}(y)\, D_0\, e^{-1/|y|} \qquad (7.10a)$$

$$D(y) = \text{sign}(y)\, D_0\, |y|^{\lambda}, \quad \lambda = 10 \qquad (7.10b)$$

$$D(y) = \text{sign}(y)\, D_0\, H(|y|-1) \qquad (7.10c)$$

where H is the Heavyside unit step function.

The first of these exhibits saturation at large y. Examining (7.5), we see that if $-a > D(y)/y$ for all y, the amplitude of the oscillations will increase without limit. The maximum value of $e^{-1/|y|}/y$ is 1/e at y=1, and thus if $D_0 < -2.7a$, energy is supplied to the oscillations faster than the dissipation can remove it. This behaviour could be reproduced on the computer (curve 1 in figure 7.1).

For $-a < D_0/e$, the oscillation amplitude rose exponentially for $r \ll 1$, and then flattened off at a "plateau" value x_c dependent on the value of D_0 (curves 2 and 3 in figure 7.1). This constant amplitude x_c is determined by the requirement that the energy supplied to the oscillations per cycle should be equal

to the energy dissipated per cycle. Multiplying equation (7.1) by $\dot{h}$, using (7.2), and integrating over one period, we obtain the energy equation for the oscillations. At constant amplitude, it reduces to:

$$a\langle y^2 \rangle = \langle yD(y) \rangle \qquad (7.11)$$

where $\langle\ \rangle$ indicates the average value over one period. This is an equation for the oscillation amplitude on the plateau in terms of D_0, and is applicable to any dissipation function D(y).

The plateau corresponds to type I behaviour as discussed in section 5.4. The oscillations contain odd harmonics, and the period of oscillations on the plateau are larger than the oscillation period at low amplitude by approximately 0.2%. Unfortunately, it is not possible to deduce a value for D_0 and hence the attempt frequency ν of section 2.1 from the experimental results, since we can measure only the plateau amplitude in μm. We do not know the value of B (equation (7.2)) which for the ILF dissipation function (7.10a) is proportional to v_B (see equation (2.5)).

The dissipation function (7.10b) exhibits behaviour very similar to curves 2 and 3 in figure 7.1. Since it does not saturate at large y, the oscillation amplitude always limits whatever the value of D_0.

The discontinuous dissipation function (7.10c) was also tried in an attempt to reproduce type IV behaviour (sudden drop in amplitude followed by growth at the usual exponential rate). In this case, B is interpreted as the critical velocity for the onset of dissipation. If $D_0 > -a$, the oscillation amplitude limits in the manner described above. If $D_0 < -a$, the amplitude continues to grow exponentially, at a lower rate. No type IV behaviour is observed.

A variation on the discontinuous dissipation function (7.10c) is to incorporate a hysteresis band. Dissipation commences at a rate D_0 when $|y|$ exceeds a critical value y_1, and does not stop until $|y|$ falls below a value $y_2 < y_1$. This "function" was also tried in the program, but it was found that as in the other cases, the oscillation amplitude quickly reached a plateau value.

Considering these results, it is likely that any function D(y) dependent only on velocity will lead to type I behaviour. In order to explain the other types of behaviour observed, we must introduce an extra variable.

7.2 Vortex Density Changes

In this section, we introduce an equation of motion for the average vortex density n. The actual physical distribution of vortices will not appear in the calculation, since any theory which incorporates vortex density gradients must also take into account the presence of surface tension menisci, and the problem at once becomes extremely complex. By using just the average density n, we retain the major features of such a theory, while realising that the numerical values of any parameters we derive will be subject to correction. We are thus considering here a "global" theory as opposed to a "local" theory such as that described in section 6.2.

The dissipation in the film is given by equation (6.8), which with n and $v_\perp$ constant gives:

$$\Delta\mu_D = \kappa n v_\perp l$$

where l is the length of the dissipation region. The dissipation function D of (7.3) is thus:

$$D = \beta\omega_0\kappa n v_s l/Bg \tag{7.12}$$

where we have substituted βv_s for v_l. We now use equations (4.12) and (7.2) to express v_s in terms of y, to obtain:

$$D = kny \tag{7.13}$$

where

$$k = \frac{\beta\omega_0\kappa}{g}\frac{\rho}{\rho_s}\frac{w_2\ d_2}{\sin\theta_2}\frac{1}{pd}$$

$$= 5 \times 10^{-5}\ cm^2$$

where we have used the (experimental) value of I (equation (4.14)) for the term 1/pd.

It is convenient to define a dimensionless vortex density N as follows:

$$N = kn/|a| \tag{7.14}$$

Substituting (7.13) and (7.14) into (7.5) and remembering that a is negative, we obtain:

$$\frac{dr}{d\theta} = \frac{a\ (1-N)\ y^2}{r+a(1-N)y\ \cos\theta} \tag{7.15}$$

Clearly, for $N < 1$ the oscillations will grow, while for $N > 1$ they will decay. Using (7.14), N=1 corresponds to $n = 2 \times 10^3$ vortices per cm^2 in the film. This should be regarded as a very approximate correspondence, in view of the approximations made in deriving the value of k.

The next step is to introduce an equation for the time development of N:

$$dN/dt = R_c(N,y) - R_a(N,y) \tag{7.16}$$

where R_c and R_a are vortex creation and annihilation rates respectively. The time development of the oscillations is

determined by solving (7.15) and (7.16) simultaneously, with specific functions for R_a and R_c.

Four creation rate functions were tried:

$$R_c = R_{c0}\, e^{-1/|y|} \qquad (7.17a)$$

$$R_c = R_{c0}\, e^{|y|} \qquad (7.17b)$$

$$R_c = R_{c0}\, |y|^{\lambda} \quad , \lambda = 10 \qquad (7.17c)$$

$$R_c = R_{c0}\, H(|y|-1) \qquad (7.17d)$$

(7.17a) is just the rate of vortex ring creation by thermal fluctuations, according to the ILF theory (section 2.1). For $y \ll 1$, the function increases steeply with y, but flattens off for $y \gg 1$. (7.17b) is appropriate to a situation where there is a large reservoir of pinned vortices which acts as a thermally activated source of free vortices[89]. The third function (7.17c) is the dissociation rate of two-dimensional bound vortex pairs[87], and is appropriate to the unsaturated film, when λ is given by (2.11). The fourth function (7.17d) is just a step function in the velocity. It was chosen to try to reproduce the abrupt changes in dissipation observed during the oscillations, and currently lacks any theoretical justification.

Two different annihilation rates were used:

$$R_a = R_{a0}\, N^{3/2}\, |y| \qquad (7.18a)$$

$$R_a = R_{a0}\, N^2 \qquad (7.18b)$$

The first of these is dependent on the velocity, and was used in reference 107 with regard to dissipation in beaker film flow. It can be derived as follows. The lifetime of a vortex is proportional to the time it takes to travel one inter-vortex separation perpendicular to the flow (whereupon it annihilates with a vortex of the opposite sign). This is just $\tau = N^{-1/2}/v_\perp$.

The annihilation rate R_a is therefore proportional to $N/\tau = N^{3/2}v_\perp$.

The above derivation assumes that vortex motion is determined only by the bulk flow of the film. It also has the disadvantage that at zero velocity the vortices do not annihilate, which is at best only approximately true. For these reasons, (7.18b) was also tried. The randomness of vortex distribution means that the probability per second of one vortex annihilating is proportional to the number of vortices N/2 with which it can annihilate. The total annihilation rate is therefore this probability times the total number of vortices N. R_a is thus proportional to N^2. (7.18b) has been used by a number of authors[88,89,95,104] in connection with the unsaturated film, where as remarked in section 6.1, Brownian motion is dominant and therefore the equation is certainly valid. Although we have shown in that section that Brownian motion is not dominant in the saturated film, it is nevertheless unclear whether (7.18a) or (7.18b) is the appropriate expression for the annihilation rate.

7.3 The Computed Results

Equations (7.15) and (7.16) were solved simultaneously by a Fortran program running on a System 3 Cromemco microcomputer. The latest version of the program is given in Appendix D. The equations are analytically continued from predetermined starting conditions, which are usually r=1, θ=0 and N=0. Increments Δr and ΔN are calculated by multiplying the right-hand sides of (7.15) and (7.16) respectively by $\Delta\theta = -1.0^\circ$.

The program listing is followed by a sample of its output. Four columns are printed on each line; the logarithm of r, the logarithm of N, the elapsed time t (in seconds) and the difference between the current time and the time of the

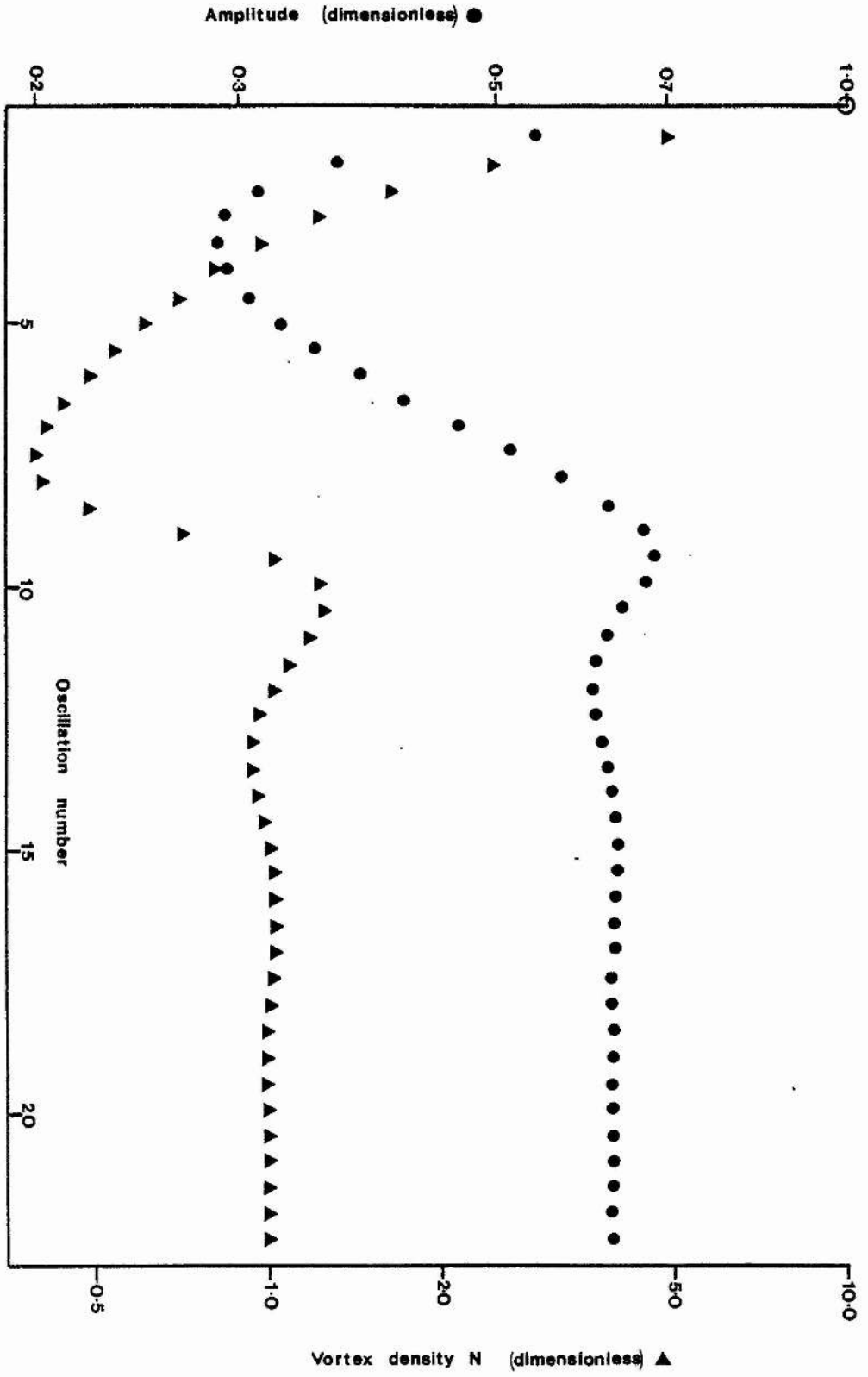

FIGURE 7.2 $R_c = 10.0\ |y|^{10}$ $R_a = 0.02\ N^2$

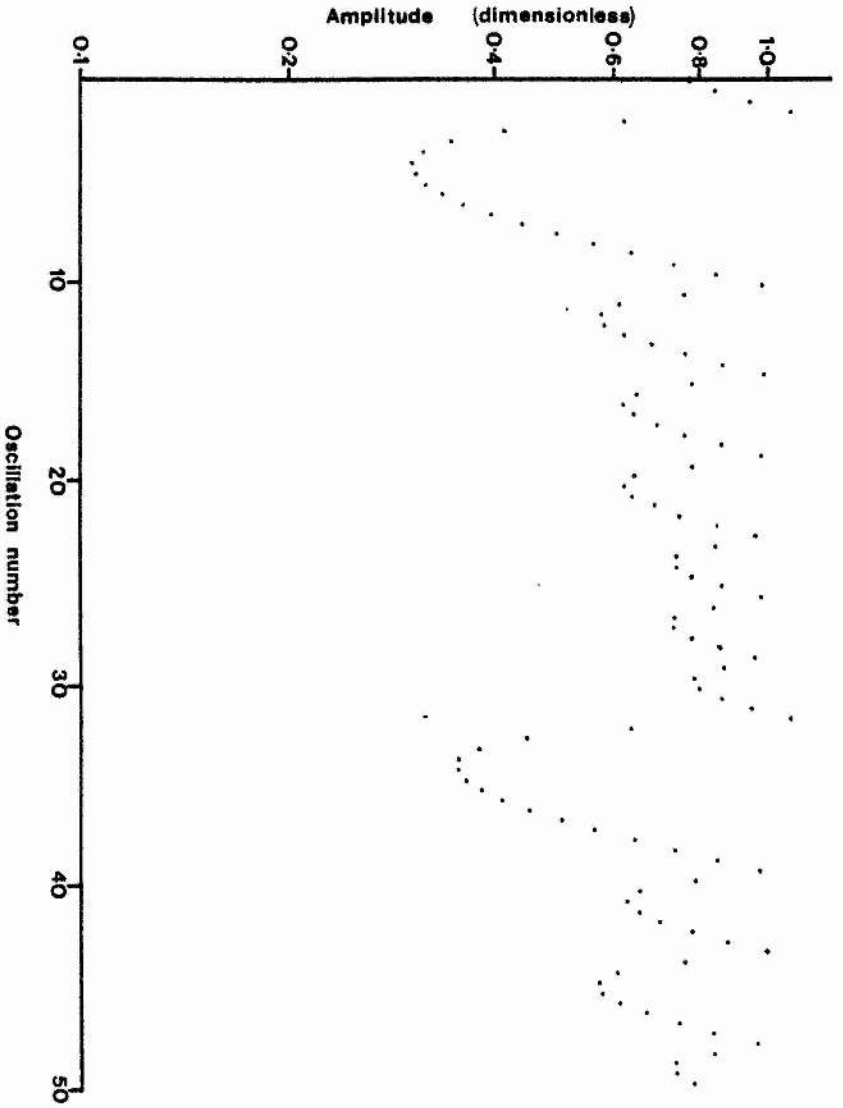

FIGURE 7.3 $R_c = 10.0\ H(|y|-1)$ $R_a = 0.1\ n^{3/2}|y|$

previously printed line. One line is output every 180°, and the fractional difference in period is printed out every 360°. This is defined as $(T-T_0)/T_0$ where T is the period of the computed cycle and $T_0 = 2\pi/\omega_0$. The program stops after a predetermined number of cycles, with twenty oscillations taking up to approximately two hours, depending on the form of R_c.

The continuous creation functions (7.17a, b & c) were tried in the program. Figure 7.2 is typical of the results obtained. There is little essential difference between the results using the three functions. After some initial amplitude "bounce", the oscillations settle down to a constant amplitude dependent on the values of R_{a0} and R_{c0}. The vortex density exhibits similar variation before stabilising near N=1. The fractional change in period is greatest when N is large, but it never exceeds 1.5%.

The results are much the same whether (7.18a) or (7.18b) is used for the annihilation rate, except that with the former, it is possible to have a situation where the oscillations go into a decay from which they cannot recover. As the amplitude (and hence $|y|$) falls, vortices are annihilated more and more slowly, and N may never fall below 1. Thus from (7.15), the oscillations will continue to decrease indefinitely. Such behaviour was never observed experimentally.

We now leave the continuous creation rate functions to concentrate on the step function creation rate (7.17d), which gives very different results from the other three functions. Figure 7.3 shows the time development of the oscillation amplitude and vortex density for (7.17d), with (7.18a) for the annihilation rate. The similarity between figure 7.3 and the experimental data in (eg) figure 5.17 or 5.18 is apparent.

If there are few vortices in the film (low R_{c0}), then the

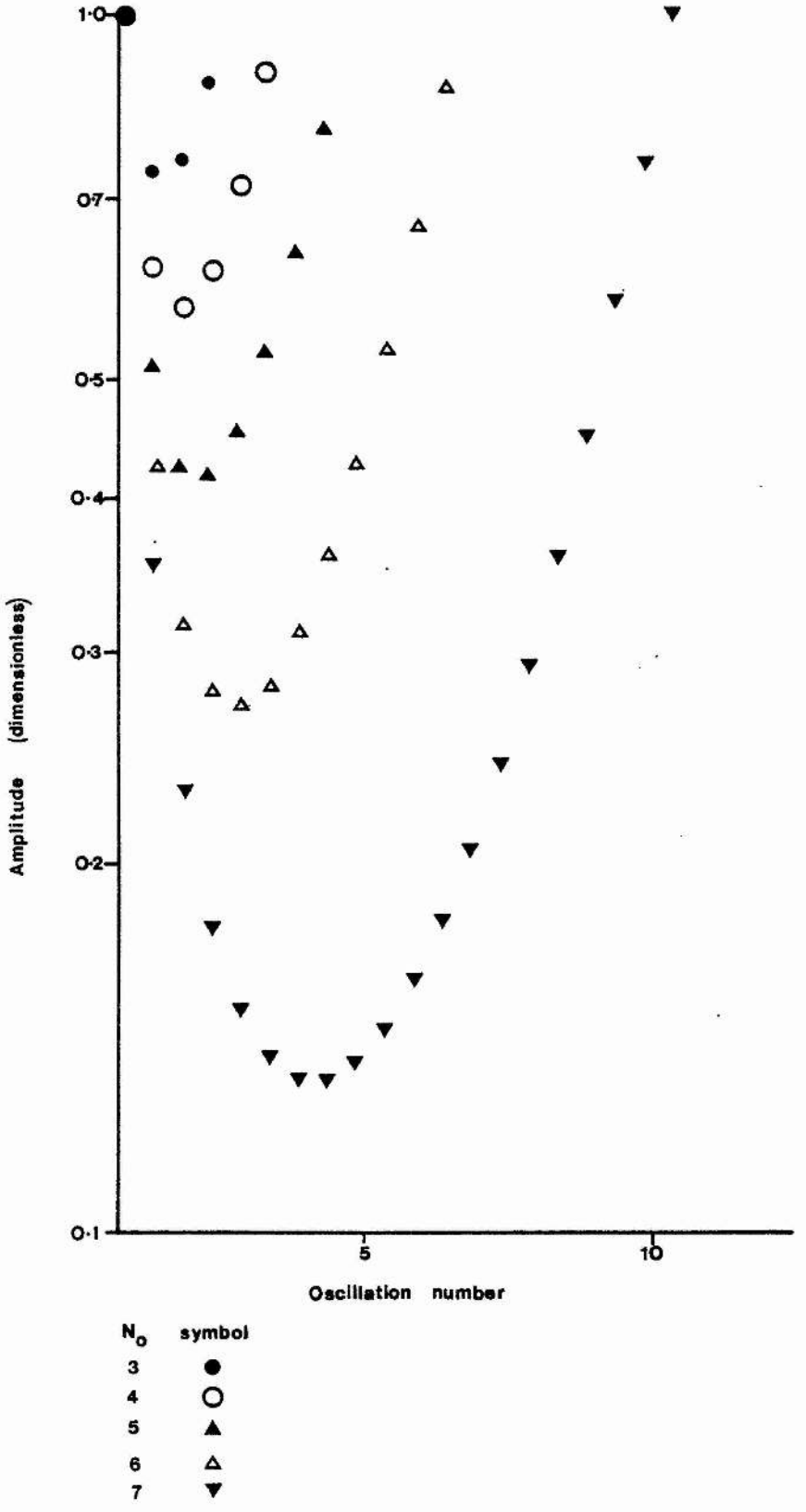

FIGURE 7.4 $R_a = 0.06\ N^{3/2}|y|$

amplitude stays approximately constant near r=1, with only very small "dips". This sort of behaviour is very similar to the type I constant amplitude behaviour of section 5.4.

The depth and duration of each amplitude "dip" is determined by R_a and by N_0, the number of vortices in the film at the start of the dip. Even at constant R_{c0}, N_0 will vary depending on the length of time the system has spent in the vortex creation region $|y| > 1$. For this reason, it is more convenient to start with a known N_0 and perform the calculation only in the region $r<1$, where there is no vortex creation. When r exceeds 1, the calculation terminates. We can then investigate the effect on the amplitude of altering N_0 and R_{a0}. R_{c0} does not enter into the calculation for $r<1$.

Figure 7.4 is a graph of the amplitude against the period number at $R_{a0}=0.06\ s^{-1}$ for various values of N_0. Equation (7.18a) was used for the annihilation rate. As N_0 increases, the depth of the amplitude dip, the time for the amplitude to reach the bottom, and the time for it to recover its initial value (ie r=1) all increase.

It is clear that at small N_0, the amplitude variation closely resembles the type IV behaviour observed experimentally. All the dissipation occurs within the first cycle (or first 1.5 cycles at the most), and thereafter the amplitude rises at the original rate determined by γ_F and γ_R.

At larger N_0, the recovery time is many cycles long, and the amplitude falls below 0.2. This is similar to the type II behaviour of R5S1 in terms of the timescale of the recovery, but the experimentally observed depth of the dip (down to approximately 0.6 of the initial value) is much less than the computed depth.

Increasing N_0 further results in a non-recoverable fall in

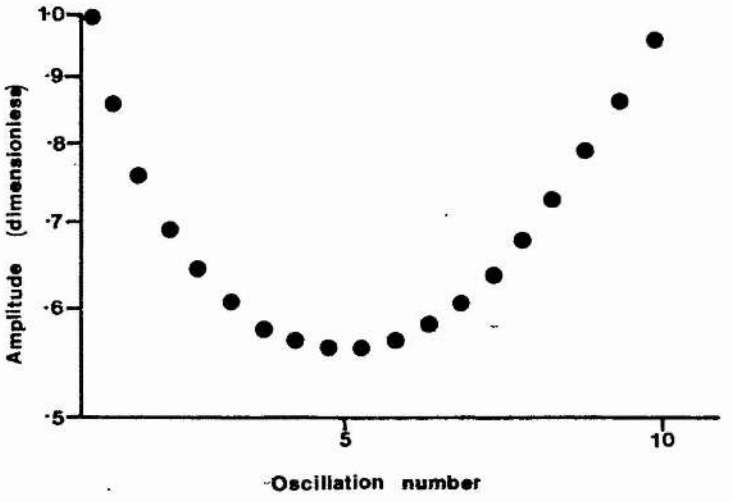

FIGURE 7.5 No = 1.5, R_a = 0.005 N^2

amplitude, as described above.

Larger values of R_{a0} tend to decrease the depth of the dip, and compress the time over which the dissipation occurs. If, however, we decrease R_{a0}, the vortices spend more time in the film before annihilating. Smaller values of N_0 thus produce similar decreases in the oscillation amplitude. There is also a change in the shape of the curves. Using a small value of N_0 means that the dissipation is small, while the low annihilation rate means that the dissipation occurs over a greater period of time. Relatively slow, shallow dips in amplitude can thus be generated, remarkably similar to type II behaviour. Figure 7.5 shows such a curve, very like the type II behaviour in R5S1.

The second expression (7.18b) for the annihilation rate gives results which are very similar to those obtained using (7.18a). There is a difference in the behaviour with very large N_0, since with (7.18b) N always eventually falls below 1 and the amplitude, having fallen to a very low level, eventually starts to rise again. Since such behaviour was never observed experimentally, this difference is of no consequence.

To summarise, we find that our vortex relaxation model reproduces the type I, type II and type IV behaviour well, at the expense of allowing the vortex annihilation rate to vary during a run. Type III behaviour (a sudden drop followed by a rise at a reduced rate) is not explained by the model as it currently stands. The results do not allow us to decide between the two postulated forms for the annihilation rate. The step-function creation rate seems to be neessary to explain the abrupt onset of dissipation. However, the critical oscillation amplitude (or film velocity) at which this occurs appears not to be a constant (as evidenced by the varying maximum amplitudes in R5S1). The

large variation in period is not explained by the theory.

Possible reasons for the remaining discrepancies between the theory and the experimental results include the previously mentioned fact that the theory is a global rather than a local one. The proportion of dissipation which takes place in the menisci may alter as N changes, thus complicating the situation. We have also ignored the conclusion drawn in section 6.3, that generation of free vortices may be a two-stage process. Incorporating the variable X from that section into our theory would introduce a third differential equation and one extra adjustable parameter, to further complicate the equations. However, such a process might explain the variation in the vortex-creation velocity. Thirdly, the rate at which the oscillation amplitude recovers after its fall in type II and type III behaviour is lower than the expected rate based on the values of γ_R and γ_F. This strongly suggests that there is still significant vorticity present in the film.

Nevertheless, major features of the experimental results are described qualitatively by the model, and hopefully further refinement of the theory will result in a better agreement with the results.

CHAPTER 8

THE SURFACE TENSION MENISCUS

8.1 Introduction

In Chapter 6, it was pointed out that any film thickness gradient would result in an effective force on the vortices due to their changing length. Such a change in thickness will occur wherever there is a surface tension meniscus. The calculations of section 6.2 show that most of the dissipation in the film may well take place in the meniscus region, and this is corroborated by recent theoretical work on dissipation in beaker film flow[107]. It is therefore important to know the shape of the meniscus where it joins onto the film, and how the shape changes at different film velocities.

The differential equation describing the shape of the meniscus, when modified to include the van der Waals force and the Kontorovich thinning term, becomes unsuitable for analytic solution. With the aid of a computer, we can calculate the film profile near the bulk surface to an accuracy of better than 0.5%, using the numerical technique of analytic continuation. This method has the advantage of being easily extended to the case of dissipative flows.

Where there are vortices perpendicular to the plane of the film, the chemical potential will be increased due to the higher mean square superfluid velocity, or equivalently due to the extra pressure exerted by the tension in the vortex lines. From section 6.1, the vortex tension is $\rho_s \kappa^2 \ln(R/a) / 4\pi$, and the extra pressure P is just this times the vortex density n. The additional term in the chemical potential due to "vortex pressure" will thus be:

$$P/\rho = (\kappa^2 n/4\pi) \ln(1/a\sqrt{n})$$

where we have used $1/\sqrt{n}$ for the cut-off radius (see section 6.1).

The magnitude of the vortex contribution to the chemical potential can be estimated from the above equation as approximately $10^{-9}.n$ g cm^{2}s^{-2}. In the meniscus region, the vortex density can be up to 10^7 cm^{-2}, as described in reference 107. Under such conditions, the vortex contribution to μ is comparable to the other terms, and the meniscus shape will be considerably modified.

When there is dissipation, the chemical potential (given by equation (8.1) below, plus the above term P/ρ) will have a gradient over the length of the film, which from equation (6.8) is equal to $\kappa n v_\perp$. This differential equation could be solved to yield the total chemical potential difference over the flow path for a given transfer rate. Some progress has been made in this complex calculation[107]; however in this chapter we shall ignore dissipation and set n=0.

Note that in this chapter, the notation does not always correspond with that in previous chapters. In particular, we use the symbol h rather than d to refer to the film thickness.

The work presented in this chapter has been published in Cryogenics, volume 22 p.527 (reference 110).

8.2 The Theoretical Model

We consider an incompressible superfluid forming a layer of thickness h on a solid vertical wall which extends out of a superfluid bath. On the surface of the film, at a height z above the horizontal bulk liquid level, the chemical potential is:

$$\mu = \frac{\rho_s}{\rho}\frac{v_s^2}{2} + gz + \Omega - \frac{\alpha}{\rho}\frac{d^2h}{dz^2}\left\{1 + \left(\frac{dh}{dz}\right)^2\right\}^{-3/2} \qquad (8.1)$$

where v_s is the superfluid velocity at that point, α is the surface tension, and Ω is the van der Waals potential:

$$\Omega = - a/h^3 \qquad (8.2)$$

When there is no dissipation, the shape of the surface is determined by the condition that the chemical potential (8.1) should always be equal to the chemical potential at the surface of the bulk liquid, which is $\mu = 0$. The problem is thus to find the appropriate solution of (8.1) for various values of the film flow rate.

The superfluid velocity on the film surface changes in magnitude and direction as we move down the film, always remaining tangential to the film surface. To solve (8.1) exactly, it should be solved simultaneously with the appropriate differential equations for v_s, which incorporate conservation of mass and momentum, and the requirement of irrotational flow. However, in section 8.3, we shall show that it is sufficient to make the approximation that v_s is constant over the thickness of the film at a given height (even in the meniscus region). Conservation of mass then requires that:

$$\rho_s v_s h = \rho \sigma \qquad (8.3)$$

where σ is the film transfer rate. This equation is certainly valid above the meniscus, where $dh/dz \ll 1$.

Using equations (8.2) & (8.3), (8.1) may be written:

$$\frac{\rho}{\rho_s}\frac{\sigma^2}{2}\frac{1}{h^2} + gz - \frac{a}{h^3} - \frac{\alpha}{\rho}\frac{d^2h}{dz^2}\{1 + (\frac{dh}{dz})^2\}^{-3/2} = 0 \qquad (8.4)$$

We now introduce a dimensionless height, $x = z/z_0$, and a dimensionless thickness $y = h/h_0$. z_0 and h_0 are given by:

$$z_0^2 = 2\alpha/\rho g$$
$$a/h_0^3 = g\, z_0 \qquad (8.5)$$

z_0 ($\sim 7 \times 10^{-2}$ cm) is the height to which the surface tension meniscus would rise in the absence of the van der Waals force. h_0 ($\sim 6 \times 10^{-6}$ cm) is the thickness of the static film at a height of z_0 cm in the absence of surface tension. The ratio of these quantities, $A = h_0/z_0$, is of order 10^{-4}.

Equation (8.4) may be rewritten in terms of these dimensionless units:

$$\frac{A}{2}\frac{d^2y}{dx^2} = \left(x + \frac{B}{y^2} - \frac{1}{y^3} \right) \left\{ 1 + \left(A\frac{dy}{dx}\right)^2 \right\}^{3/2} \qquad (8.6)$$

where B is a dimensionless flow dependent quantity given by:

$$B = \frac{\rho}{\rho_s}\frac{\sigma^2}{2h_0^2}\frac{1}{gz_0} \qquad (8.7)$$

For $\sigma = 10^{-4} cm^2 s^{-1}$, B is approximately 1.4.

For $x \gg 1$, the curvature of the film is so small that surface tension is negligible, and the ordinary (Kontorovich) equation for the film thickness is applicable:

$$x + B/y^2 - 1/y^3 = 0 \qquad (8.8)$$

Solving for y, and using (8.5), we obtain:

$$h = (a/2gz)^{1/3}\{(1+\sqrt{1+z_K/z})^{1/3} + (1-\sqrt{1+z_K/z})^{1/3}\} \qquad (8.9)$$

where the flow dependent quantity z_K is what we have called the "Kontorovich length":

$$z_K = (\rho\,\sigma^2/\rho_s)^3/54\, g\, a^2 \qquad (8.10)$$

At a flow rate of 10^{-4} $cm^2 s^{-1}$, z_K is of the order 3×10^{-2} cm.

For $z >> z_K$, the expansion of (8.9) to lowest order in the flow term is:

$$h = (a/gz)^{-1/3}\{1-(z_K/4z)^{1/3}\} \tag{8.11}$$

At small x, the film is pulled out by surface tension, y becomes large, and the terms in $1/y^2$ and $1/y^3$ in equation (8.6) become negligible. If these terms are set to zero, the resulting equation may be solved analytically[111] to give:

$$y = \frac{1}{A\sqrt{2}}\left\{\cosh^{-1}\frac{\sqrt{2}}{x} - 2\sqrt{1-\frac{x^2}{2}}\right\} + y_0 \tag{8.12}$$

where y_0 is a constant of integration. This is simply the equation of the classical meniscus in the absence of van der Waals forces, and in this case y_0 is given by:

$$y_0 = \{1 - (\cosh^{-1}\sqrt{2})/\sqrt{2}\}/A \tag{8.13}$$

Thus, for $x << 1$, the solution of (8.6) is very close to (8.12) with some value of y_0; and for $x >> 1$, it is very close to (8.8).

The only previous published work on this problem seems to be that of Arkhipov[112], where it was also studied in connection with calculations on dissipation in the flowing film. Arkhipov assumes that (8.8) is a sufficiently good solution for $x \geq 1$. He then approximates the term linear in x in equation (8.4) to 1 in the region $x \leq 1$. The resulting equation may be solved analytically, and he obtains a solution (his equation (20)) which for the static case we can write in dimensionless form as

$$x = 1 - A^{1/2}(y+1/2)^{1/2} + (A/6)^{1/2}\cosh^{-1}\{(y+2)/(y-1)\} \tag{8.14}$$

Unfortunately, this solution is unsatisfactory for the following reasons.

Equation (8.14) diverges as y tends to 1. This is the result

of the boundary condition imposed on dh/dz, which was that it should be zero at x = 1 (equation (18) in reference 112). In fact, Arkhipov's solution (8.14) does not join onto the ordinary film profile at any point, and is 25% in error at x = 1. (Figure 2 in reference 112 illustrates this, although the discontinuity is shown smaller than the calculation indicates.)

Secondly, the behaviour of (8.14) as y becomes large is also unsatisfactory. At large y, (8.14) tends towards

$$y = (x - 1)^2 / A \qquad (8.15)$$

(cf equation following equation (20) in reference 112). This is also the limit of the classical equation (8.12) for x close to 1. However, these two limits do not pertain to the same range of x, and the curves of (8.14) and (8.12) do not join.

A more basic drawback of Arkhipov's method is that it is inapplicable in the presence of dissipation. Our method of solution may be extended to cover the case of dissipative flows, as described in the previous section.

8.3 The Method of Solution

To determine the correct film profile, a solution of (8.6) is required which behaves like (8.8) at large x, and like (8.12) at small x. To solve (8.6), the technique of analytic continuation[113] was used.

If $y(x_0)$ and $y'(x_0)$ are known for some point x_0, then $y(x_0+\Delta x)$ and $y'(x_0+\Delta x)$ may be found from their Taylor series expansions:

$$y(x_0+\Delta x) = y(x_0) + \frac{\Delta x}{1!}y'(x_0) + \frac{(\Delta x)^2}{2!}y''(x_0) + \ldots \qquad (8.16)$$

$$y'(x_0+\Delta x) = y'(x_0) + \frac{\Delta x}{1!}y''(x_0) + \frac{(\Delta x)^2}{2!}y'''(x_0) + \ldots \qquad (8.17)$$

The second and higher derivatives are determined from equation (8.6) in terms of the lower derivatives which have already been calculated. Provided Δx is sufficiently small, repeating this procedure indefinitely yields a series of values of x and y(x) which lie on the required solution curve.

This method was chosen because it was found to be relatively easy to control the shape of the solution by adjusting the starting conditions, and because it was capable of being extended to the case of dissipative flows.

The boundary conditions are set by taking the slope $y'(x_0)$ from the classical meniscus and varying the thickness at that point $y(x_0)$ until a match is obtained with the van der Waals equation (8.8) higher up the film. An initial value of $x_0 = 0.9$ was chosen, since at that point the classical solution is valid, thus ensuring that the meniscus joins the bulk liquid level correctly.

The calculation was performed in Fortran on a mainframe computer. Starting at x_0, the program calculates y, y' and y'' as x is incremented up the film. If at any point y'' becomes negative (indicating the film is too thin), $y(x_0)$ is incremented by ε, and the calculation restarts. If y' becomes positive (indicating that the film is too thick), $y(x_0)$ is decreased by ε and the calculation starts again from x_0. The amount ε by which $y(x_0)$ changes is reduced by a factor of 2 each time, so that the program effectively performs a binary search to find the appropriate $y(x_0)$. When ε falls below 10^{-9}, the program prints

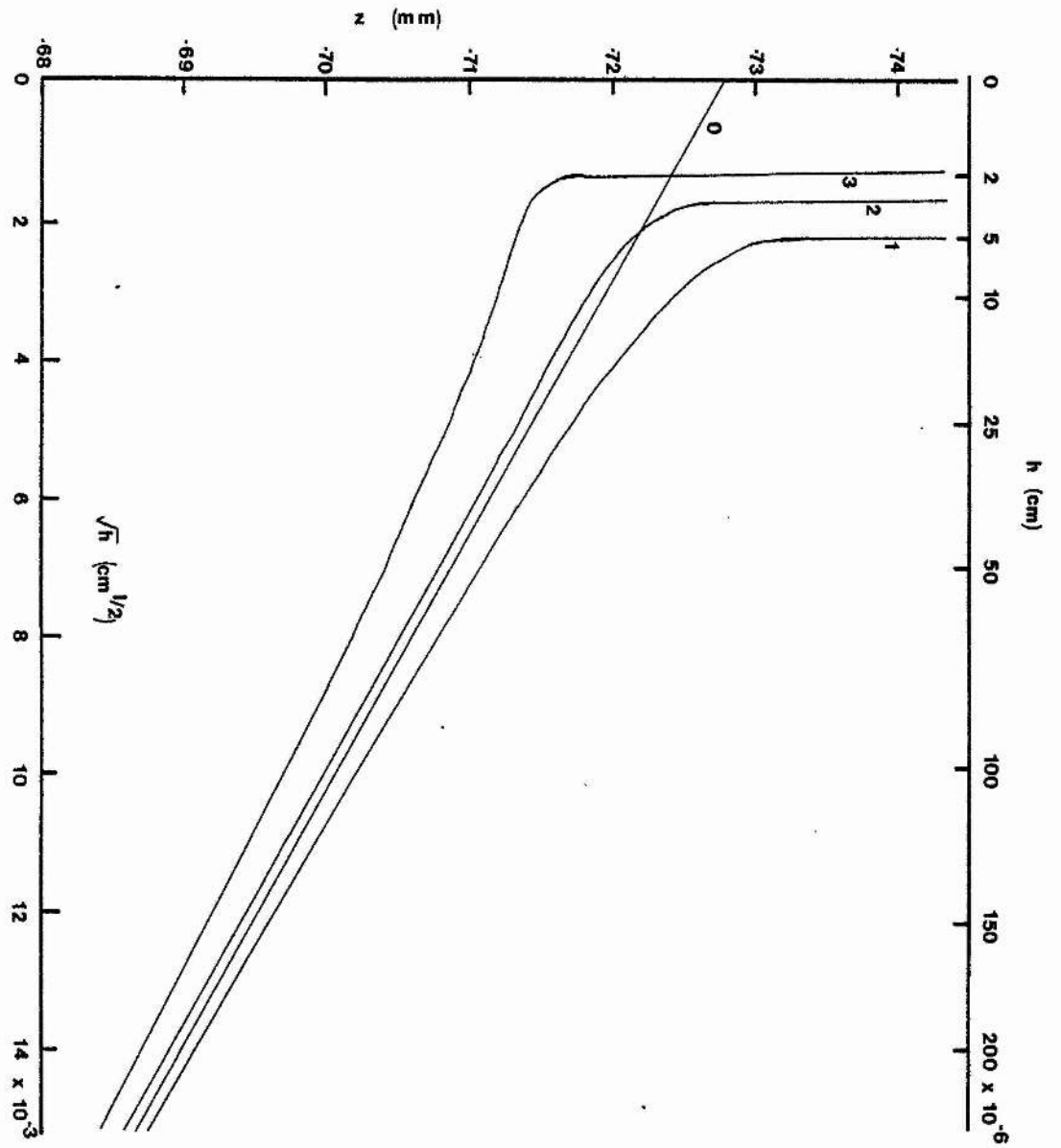

FIGURE 8.1 Height above the liquid level z film thickness h for ^{4}He. Curve 0: no van der Waals force; 1: $\sigma=0$ 2: $\sigma=8\times10^{-5}$ 3: $\sigma=12\times10^{-5}$ cm^{2}s^{-1}

out the final profile and terminates.

It should be pointed out that the curves y(x) obtained by using different values of $y(x_0)$ are all solutions of (8.6). The binary search for the correct $y(x_0)$ is merely a way of selecting the solution which satisfies the boundary condition (8.8).

A step size of $\Delta x = 5 \times 10^{-4}$ was chosen. Increasing this by a factor of 2 did not change the results by more than 0.5%, whereas decreasing it below this figure added substantially to the computing time required. The Taylor series expansions were calculated up to and including the third derivative. The fourth derivative was incorporated on a trial basis, but was found not to influence the results by more than 0.01%, while adding about 20% to the time required.

A very fine adjustment of $y(x_0)$ (to greater than one part in 10^9) resulted in a match between the computed solution and equation (8.8) of better than 0.2%, over a vertical height $1 < x < 1.04$ (for the static case) before the computed solution diverged. For the moving film, the vertical height over which the match was good was reduced.

The results are shown in figure 8.1 for ^{4}He at 0 K, for a variety of film flow rates. The square root of the film thickness is plotted in order to include a wider range of thicknesses, and to aid comparison with the classical meniscus, which from equation (8.15) appears as a straight line with intercept z_0. Note that the negative curvature of curve 3 in figure 8.1 is a result of plotting $\sqrt{h}$, and is not a real effect. The meniscus shape for ^{3}He at 0 K is shown in figure 8.2. In the calculations, instead of equation (8.2), the van der Waals potential was represented by

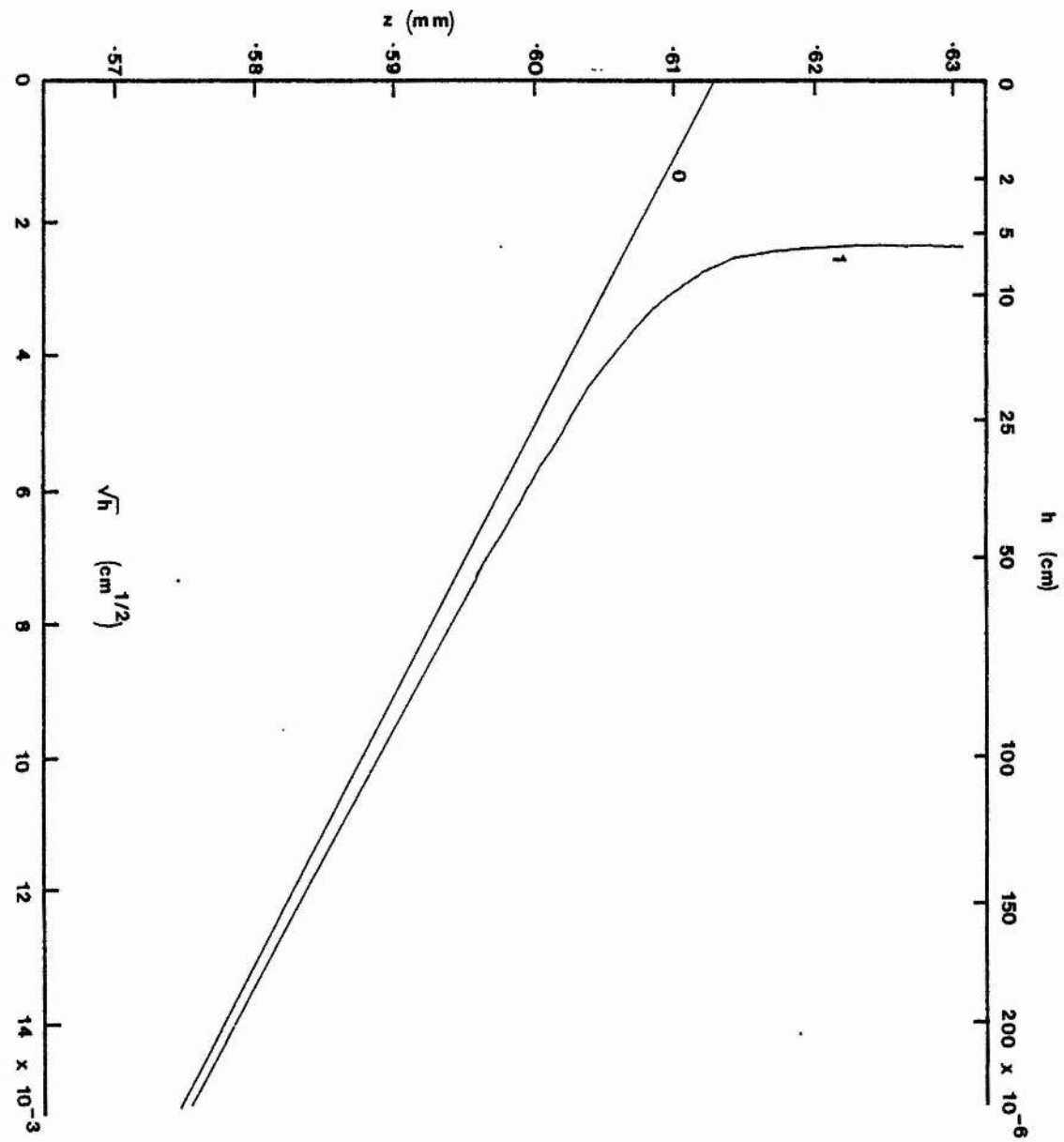

FIGURE 8.2 Height above the liquid level z film thickness h for ^{3}He. Curve 0: no van der Waals force; 1: σ=0

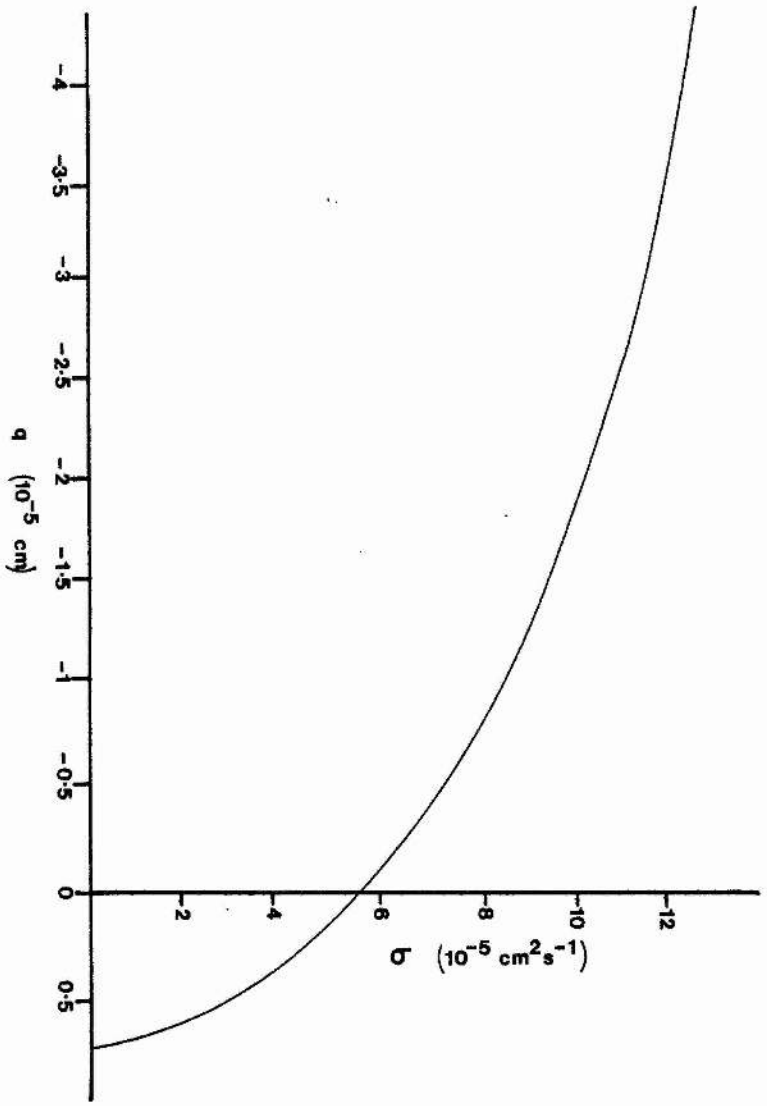

FIGURE 8.3 Meniscus offset q versus transfer rate

$$\Omega = -\frac{a}{h^3}\left(1 + \frac{h}{d'}\right)^{-1} \qquad (8.18)$$

which incorporates retardation effects.[114] For ^{4}He on a metallic substrate, $d' = 8.09 \times 10^{-6}$cm and $a = 1.76 \times 10^{-14}$ cm^{5}s^{-2}. For thicknesses $h >> d'$, Ω varies as h^{-4}. Use of (8.18) slightly complicates the equations, but the principle of solution is unchanged. For $T = 0$, we calculate $h_0 = 5.74 \times 10^{-6}$ cm and $z_0 = 7.29 \times 10^{-2}$ cm.

Temperature variation of both the superfluid fraction and the surface tension were incorporated; the only discernable difference between the calculated profiles for 0 K and 1.6 K was a difference in z_0 due to the change in surface tension.

The shape of the surface tension meniscus is found to be essentially unaltered by the van der Waals forces for $x < 0.95$. It is, however, shifted outwards a distance of 8.2×10^{-6}cm relative to the meniscus position in the absence of the van der Waals force. This offset, q, varies with flow rate, and is calculated by subtracting the y_0 determined from (8.12) and (8.13), from the final $y(x_0)$ determined from our calculated solution. q is plotted against flow rate in figure 8.3. The meniscus is pulled in rapidly as the flow rate increases.

The point at which the meniscus joins the ordinary film profile decreases by only 2% between the stationary film and a film flowing at a rate $\sigma = 1.2 \times 10^{-4}$ cm^{2}s^{-1} (see Fig. 1). Thus, the height of the surface tension meniscus is relatively insensitive to film flow rate.

We can now confirm that the approximation involved in equation (8.3) is valid. At a value of $y = 15$, the kinetic term proportional to v_s^2 in equation (8.1) is approximately 0.5% of gz

for a flow rate of 1.2×10^{-4} $cm^2 s^{-1}$. Equation (8.3) is still valid at this point. Provided that the kinetic term (v_s^2) decreases at least as fast as gz as we go further down the film, the error introduced by our approximate kinetic term B/y^2 (which decreases much faster than gz) will be kept to less than 0.5%. Now, for potential flow round a corner of radius r, the velocity is approximately proportional to 1/r. In the surface tension dominated part of the profile the radius is proportional to 1/z. The kinetic term thus decreases as z^2, and the above requirement is satisfied.

Based on these considerations, it is believed that the computed profiles are accurate to at least 0.5%. To summarise, for $x < 0.95$ the profile is just the classical meniscus (8.12), shifted horizontally by a flow dependent amount q. There is a transition region for $0.95 < x < 1.05$, while for $x > 1.05$, the usual Kontorovich profile (8.8) applies.

The method described in this chapter is not restricted to the case of a vertical wall entering a liquid helium bath. By using the appropriate boundary conditions, any experimental geometry may be modelled.

I would like to thank J G M Armitage for demonstrating how to alter $y(x_0)$ to make the solution satisfy the boundary condition (8.8), and for the idea of plotting $\sqrt{h}$ rather than h in figures 8.1 and 8.2.

CHAPTER 9

CONCLUSIONS

9.1 Summary of Results

A number of conclusions can be drawn from the experimental and theoretical results presented in the preceeding chapters. In the first place, we can summarise the lessons learned about the particular experimental techniques used.

The concept of using a sealed cell filled with helium gas at room temperature and providing a very small working volume of liquid helium has been shown to be feasible. However, the "DC" experiments (section 5.1) and the capacitor calibration (section 4.1) show that extremely careful attention to the uniformity of capacitor plate spacing and the relative heights of the capacitors is necessary to make full use of the available liquid.

The electrostatic drive mechanism is also workable, although the dielectric strength of liquid helium limits the chemical potential difference which can be achieved. Analogue programming of the driving potential has been shown to be a very useful method of controlling film flow, and the Film Drive Unit which was constructed is suitable for a variety of film flow experiments. The most important design consideration for such equipment is flexibility, and the provision of capability for expansion.

The two pulse mechanisms for the elimination of unwanted oscillations were shown to be effective, although some skill is necessary to select the correct pulse height and/or duration.

Let us now consider the film flow measurements. Because of the variations in capacitor plate spacing and the small available range over which which flow could be studied, detailed measurements of DC flow were not undertaken. However, those

results which were obtained indicate that in the critical region there are a variety of possible transfer rates for a given voltage ramp rate. It is thus not possible to "set" the transfer rate by dialling up a particular drive rate on the FDU, as had been hoped. The second point to note about DC flows in this geometry is that the transfer rates can be considerably higher than in geometries where the minimum perimeter is maintained for a longer distance.

Because the inertial oscillations occur only in a small region of the capacitor plates, variations in plate spacing do not affect them, and they were studied in detail. Measurement of the Robinson damping enabled the thermal relaxation time of the cell to be determined. Positive feedback through the differentiator in the FDU is a completely new way of studying the oscillations, and incorporating the film in a feedback loop in this manner has produced some surprising results. We particularly mention the sudden falls in oscillation amplitude, characteristic of types III and IV behaviour (section 5.4).

Both the DC and AC results indicate that the transfer rate and level difference alone are insufficient to characterise the state of the system. There must be one or more "hidden variables" which affect the dissipation.

The theoretical work presented in Chapters 6 and 7 attempts to provide a partial explanation of some of these experimental results. Based on the premise that dissipation is due to the motion of vortices oriented perpendicular to the plane of the film, we have shown in section 6.2 that the large DC transfer rates observed are probably due to dissipation occurring away from the minimum perimeter of the flow path. This particular experimental geometry, chosen in an attempt to strongly localise the dissipation region, in fact has the effect of separating the

region of dissipation and the region of maximum velocity. We have also demonstrated (equation (6.9)) that there is a minimum length of the dissipation region if such vortices are responsible for dissipation.

The experimental observations of inertial oscillations under feedback were also analysed theoretically. The onset of non-linear dissipation was found to depend on the rate of oscillation growth, and this could be interpreted as showing the existence of some form of "trapped" vorticity which becomes free and able to cause dissipation when some critical trapped vortex density is attained.

By solving an equation for the time development of the density of free vortices simultaneously with the equation of motion of the film, some of the other features of the experimental results could be reproduced. Various velocity functions for the creation and annihilation rates of vortices were tried. It was found that a "step function" creation rate gave results which were nearest to the observed oscillation behaviour. No other theoretical justification for such a creation rate currently exists. The experimental results do not permit distinction between the two functions postulated for the vortex annihilation rate.

Despite the general agreement obtained between the model postulated and the experimental results, there are several aspects of the observed behaviour which it does not explain. Possible reasons for this are given at the end of Chapter 7. Perhaps the most notable discrepancy between the model and the results is the observed variation of oscillation period with amplitude. This variation has been shown to be much larger than predicted by film thinning, and is similar to the variation found

by other workers[44]. The phenomenon remains unexplained.

The shape of the surface tension meniscus in liquid helium is derived numerically in Chapter 8. The shape is important, since vortices will be swept downstream and may become trapped in the meniscus, where they will cross streamlines, causing dissipation. The model of vortex dissipation presented in Chapter 7 is approximately independent of where in the film the dissipation actually occurs.

9.2 Suggestions for Further Work

There are a number of questions which are suggested by the work presented in the preceeding chapters. There is scope both for further experimental work and theoretical development, and we first of all consider the former.

The positive feedback technique for studying the inertial oscillations is a useful one, and much more data could be acquired. The apparent linear relationship between the onset of non-linear dissipation and growth rate (figure 5.21) requires consolidation. More data on the intermediate oscillations is also required, particularly at low values of feedback, just sufficient to cause oscillation growth. The type IV behaviour of R3S3 is remarkable, and invites further study.

The results of Chapter 5 were observed at only one temperature. It will be very interesting to see how the temperature affects the oscillation behaviour, particularly at low temperatures where Robinson damping is absent.

The experiment presented has two major differences from previous experiments: the positive feedback technique, and the radial flow geometry, with its consequent large velocity gradients. A future experiment might use a more traditional geometry to determine which of the experimental observations are

due to the geometry and which reveal themselves through the use of positive feedback.

The large observed amplitude/period variation is also worth further study: its temperature and geometry dependence have yet to be established. In this connection, it would be interesting to see whether (under positive feedback) the oscillations depart from strict sinusoidal behaviour, as observed by Campbell et al.[44]

We did not in this experiment investigate the effect of positional (rather than velocity) feedback on the oscillations. Such feedback should affect the oscillation frequency, and it might be possible to obtain a "frequency response curve" for the dissipation.

The experimental apparatus was found (for reasons discussed earlier) to be unsuitable for extended studies on DC film flow. In many ways, DC flow is simpler than AC flow, and DC measurements are a most useful way of studying the film. However, this experiment, in common with all two-reservoir and beaker flow experiments, has the disadvantage that the transport of bulk liquid through the film tends to reduce the driving chemical potential difference by altering the liquid levels in the two reservoirs. It would be more useful to be able to set up a chemical potential difference without worrying about changes in $\Delta\mu_D$ as time progressed. This might be done using the FDU in the following way. Establish a chemical potential difference $\Delta\mu_D$ using a voltage step. When the transfer rate is established, ramp the voltage at an appropriate (velocity dependent) rate to compensate for the rate at which the level difference is changing, thus maintaining a constant $\Delta\mu_D$ between the reservoirs.

However, even this method may run into difficulties. Perhaps entirely new methods of studying DC flow are more

appropriate. Galkiewicz and Hallock[115] have created a persistent current entirely in the saturated film, and the decay of such a current would provide information about the dissipation in the same way as the experiments of Eckholm and Hallock[103] have done in the unsaturated film. Unfortunately, for the saturated film, no decay was observable over a 10 hour period, and either much longer timescales or more sensitive velocity measurements are required.

Experiments on liquid helium in space are now becoming feasible. In the absence of gravity, transfer of bulk fluid through the film no longer results in the chemical potential difference between the two reservoirs changing. It would thus be possible to have two reservoirs, maintained by electric fields, and to set up a $\Delta\mu$ between them by use of a bias voltage. Film transfer would then occur at a constant $\Delta\mu$ until one reservoir was exhausted or the other full.

Let us now turn to the theoretical models discussed in Chapters 6, 7 and 8. Experiments are possible which would test aspects of these theories. In Chapter 6, an experiment is described to compare flows on the inside and outside of a cylindrical tube, which would test whether (and at what temperatures) meniscus dissipation is important. Observation of the meniscus shape and comparison with the theoretical results of Chapter 8 could detect the presence of vortices in the meniscus region.

There is scope also for further theoretical work on the model. A local version of the theory in Chapter 7 is needed, and theoretical justification of the step function creation rate needs to be looked into. The way in which the presence of dissipation alters the meniscus shape is another thorny

theoretical problem.

We conclude by mentioning that the particular geometry used in this experiment allows high superfluid velocities to be probed, for the reasons discussed in section 6.2. The velocities achieved in the hole in the Melinex disk were up to 60 cm s^{-1}. It may be possible to design an experiment where the difference between the minimum perimeter and the perimeter at which vortex dissipation occurs is so large as to permit superfluid velocities above 10^3 cm s^{-1} in the constriction. This might enable Landau creation of rotons to be observed in the saturated film.

APPENDIX A

We shall show that $D_R < D_L$ for $V>0$ by showing that the ratio $D_R/D_L<1$. From (6.17a and 6.17b) the ratio is given by:

$$\frac{D_R}{D_L} = \frac{V^{\lambda-2}}{1 - V^{\lambda-2}} \frac{\ln\{A/[1+(A-1)V^{\lambda-2}]\}}{\ln\{1+(A-1)V^{\lambda-2}\}}$$

$$= f(Ax)/Af(x)$$

where $x = [(A-1)V^{\lambda-2} + 1]/A$ and $f(x) = (x-1)/\ln x$. Now,

$$f'(x) = \lim_{\xi \to 0} \frac{f(x+\xi x) - f(x)}{\xi x}$$

$$\Rightarrow \quad xf'(x) - f(x) = \lim_{\xi \to 0} \frac{f([1+\xi]x) - (1+\xi)f(x)}{\xi}$$

But, $xf'(x) - f(x) = \{\ln x - (x-1)\}/(\ln x)^2 \leqslant 0$ for all $x>0$. The equality holds for $x=1$. Thus (except possibly at $x=1$) it is possible to choose an integer n sufficiently large that for $\xi=(\ln A)/n$,

$$\frac{f([1+\xi]x) - (1+\xi)f(x)}{\xi} < 0$$

$$\Rightarrow \quad f([1+\xi]x) < (1+\xi)f(x)$$

$$\Rightarrow \quad f([1+\xi]^n x) < (1+\xi)^n f(x)$$

Taking the limit as $n \to \infty$, and remembering that $A=\lim(1+(\ln A)/n)^n$, we have that $f(Ax) \leqslant Af(x)$. The equality sign pertains (if at all) to $x=1$. $f(1)=1$, and since $f(A) < A$ for $A > 1$, the equality sign can be dispensed with and the result is proved.

APPENDIX B

We wish to evaluate the integral:

$$I = \int_0^{2\pi m/\omega} e^{\gamma t} \, |\sin(\omega t + \phi)| \, dt$$

We do not expect that the critical amplitude for onset will depend strongly on the phase of the oscillations, and accordingly set $\phi = 0$. This is equivalent to assuming that $m \gg \phi/2\pi$, and we can be confident in our result so long as this condition holds. The integral can be written as:

$$I = \sum_{p=0}^{m-1} \left\{ \int_{pT}^{(p+1/2)T} e^{\gamma t} \sin\omega t \, dt - \int_{(p+1/2)T}^{(p+1)T} e^{\gamma t} \sin\omega t \, dt \right\}$$

The integral without the modulus can be evaluated to give:

$$\int e^{\gamma t} \sin\omega t \, dt = (\gamma \sin\omega t - \omega \cos\gamma t) e^{\gamma t}/\omega_0^2$$

and we thus have:

$$I = \sum_{p=0}^{m-1} \left\{ e^{4kp(e^{2k}+1)\omega/\omega_0^2} + e^{4k(p+1/2)(e^{2k}+1)\omega/\omega_0^2} \right\}$$

$$= (\omega/\omega_0^2)(e^{4km}-1) \coth k$$

where $k = \pi\gamma/2\omega$.

APPENDIX C

We shall calculate the thermal time constant of the cell as follows. This is closely based on Robinson's paper[46].

The equation we work from is Robinson's equation (6), a cubic in the complex parameter $\lambda = i\omega - \gamma_R$ where ω is the observed frequency: $\omega^2 = \omega_0^2 - \gamma^2$. In our case, the values of γ for the growths and decays are only about 5% of the observed frequency; the approximation $\omega = \omega_0$ is therefore very good. Equating the imaginary part of Robinson's equation (6) to zero, and discarding the solution $\omega = 0$, we obtain:

$$3\gamma_R^2 - 2\gamma_R L + \beta\omega_0^2 = 0 \qquad (C.1)$$

Here β is a dimensionless parameter (equal to Robinson's α), and depends on the temperature and the size of the reservoirs. L is the thermal conductance (ergs s^{-1} K^{-1}) between the reservoirs, divided by the thermal mass (ergs K^{-1}) of the liquid in one reservoir. The reciprocal of L is thus the thermal relaxation time between the reservoirs.

β may be determined as a function of temperature from Robinson's figure 1, where it has been calculated for a reservoir depth of 1 cm. Rather than calculate how to scale β for the cell geometry, we take this figure as a reasonable approximation in the present situation. In the temperature range of interest, $\beta \gg 1$, and thus $\beta\omega_0^2 \gg 3\gamma_R^2$. We may therefore ignore the term $3\gamma_R^2$ in equation (C.1) and write:

$$2\gamma_R L = \beta\omega_0^2 \qquad (C.2)$$

Using the centre of gravity values of the temperature T and γ_R from figure 5.20, and the mean value of ω_0 for these flows, we obtain for the thermal relaxation time 1/L = 4ms. This is

acceptably short, and is much smaller than the time-scales observable in the experiment.

From Robinson's figure 1, we can calculate $d\beta/dT$ in the temperature range 1.1 to 1.2 K. The result is $d\beta/dT = 6.8 \times 10^{3} K^{-1}$. Assuming L to be temperature independent in this range, by differentiating equation (C.2) with respect to temperature we obtain:

$$\frac{d\gamma_R}{dT} = \frac{\omega_0^2}{2L} \frac{d\beta}{dT} = 1.45\ s^{-1}K^{-1} \qquad (C.3)$$

A straight line with this gradient has been plotted through the centre of gravity of the points in figure 5.20. It corresponds with the trend in the experimental data, showing that thermal damping adequately describes the variation of γ_R.

Hallock and Flint[42], and Campbell et al.[44] have shown that Robinson's analysis is also applicable to the case of two connected reservoirs immersed in a liquid helium bath, provided that the two reservoirs have the same volumes and thermal conductances to the bath. The bath then just acts as an extra thermal path between the reservoirs.

Satisfying as this agreement between theory and experiment is, it should be pointed out that it is probably partly fortuitous. Robinson's calculation of β is strictly only valid for temperatures greater than 1.3K. Below this, the variation of entropy with temperature differs from the form he assumed. Together with the approximations already made, this leads one to expect a greater disparity with the experimental results than is actually observed.

APPENDIX D

```
C       FILE NAME   ---------   FILM.FOR   ----------
C
C       HELIUM FILM WITH VORTICES
C
C  THIS PROGRAM SOLVES TWO SIMULTANEOUS DIFFERENTIAL
C  EQUATIONS IN N AND R BY THE METHOD OF ANALYTIC CONTINUATION
C
      DOUBLE PRECISION R,THETA,Y,RADTH,A,F,NUMR,DENOM
      DOUBLE PRECISION DR,DTHETA,SUM1,T,DT,LASTT,DEG2R,N
      DOUBLE PRECISION RA0,RC0,DN,OMEGA0
C
C  INITIALISE THE PARAMETERS
C
      DATA DEG2R/0.0174532/LASTT/0.0/
      DATA R/1.0/THETA/0.0/DTHETA/-1.0/
      DATA A/-0.1090/SUM1/0.0/
      DATA T/0.0/OMEGA0/0.309/
      DATA N/0.0/RC0/0.0/RA0/0.0/K/180/
C
C  READ IN THE ADJUSTABLE PARAMETERS
C
      WRITE(4,1013)
1013  FORMAT(' HOW MANY OSCILLATIONS ?  ')
      READ(4,1008)NOSC
1008  FORMAT(I3)
      NOSC=NOSC+1
      WRITE(4,1015)
1015  FORMAT(1H ,'TYPE IN VALUE OF RA0 - ')
      READ(4,1003)RA0
1003  FORMAT(F10.0)
      WRITE(4,1016)
1016  FORMAT(1H ,'TYPE IN VALUE OF RC0 - ')
      READ(4,1003)RC0
C
C PRINT OUT THE PARAMETERS
C
      WRITE(4,1011)A,DTHETA,RA0,RC0
1011  FORMAT(' A =',G15.4,'  DTHETA =',G15.4/
     *' RA0 =',G15.4,'  RC0 =',G15.4/)
      WRITE(4,1020)
1020  FORMAT('       LOG(R)          LOG(N)
     *          TIME          TIME DIFF.')
C
C START OF MAIN LOOP
C
1     RADTH=THETA*DEG2R
      Y=R*DSIN(RADTH)
      F=Y*A*(1-N)
C NUMERATOR OF dR/dTHETA
      NUMR=F*Y
      F=F*DCOS(RADTH)
C DENOMINATOR OF dR/dTHETA
      DENOM=R+F
C TEST FOR COLLAPSE OF OSCILLATIONS
      IF(R.LE.0.0.OR.DENOM.LE.0.0)GOTO 3000
      J=IDINT(THETA)
      J=MOD(J,360)
      IF(THETA.LE.-360.0)THETA=THETA+360.0
```

```
C IF WE ARE ON THE X-AXIS, PRINT OUT THE RESULTS
      IF(MOD(J,K).EQ.0)CALL OUTPUT(J,R,N,T,LASTT)
C IF THETA IS 0, PRINT OUT THE FRACTIONAL CHANGE IN PERIOD
      IF(J.NE.0)GOTO 4
      SUM1=SUM1/360.0+1.0
      SUM1=1.0/SUM1-1.0
      WRITE(4,1012)SUM1
1012  FORMAT(' FRACTIONAL PERIOD CHANGE = ',1PD15.7)
      SUM1=0.0
      NOSC=NOSC-1
C STOP IF NOSC OSCILLATIONS COMPLETED
      IF(NOSC.EQ.0)STOP 2002
4     SUM1=SUM1+F*DTHETA/DENOM
C CALCULATE CHANGES IN R, T AND N
      DR=DTHETA*DEG2R*NUMR/DENOM
      DT=(-R*DEG2R*DTHETA)/(DENOM*OMEGA0)
      DN=0.0
      IF(DABS(Y).GT.1.0)DN=RC0
      DN=(DN-RA0*N*N)*DT
C CALCULATE NEW VALUES OF R, T AND N
      R=R+DR
      T=T+DT
      N=N+DN
      IF(N.LT.0.0)N=0.0
      THETA=THETA+DTHETA
      GOTO 1
C
C  END OF MAIN LOOP
C
C PRINT A MESSAGE IF THE OSCILLATIONS HAVE COLLAPSED
3000  WRITE(4,1001)
1001  FORMAT(' R OR DENOMINATOR BECOMES NEGATIVE AT:')
      WRITE(4,1000)J,R,N,T,LASTT
1000  FORMAT(I5,1PD15.3,1PD15.3,1PD15.3,1PD15.3)
      STOP 2001
      END
C
C  OUTPUT SUBROUTINE. CALCULATES THE TIME DIFFERENCES BETWEEN CALLS TO IT
C
      SUBROUTINE OUTPUT(J,R,N,T,LASTT)
      DOUBLE PRECISION R,N,T,LASTT,NN
      REAL A1,A2,A3,A4
      NN=N
      IF(N.LE.0)NN=1.0E-20
C CALCULATE LOG OF R AND N
      A1=DLOG10(R)
      A2=DLOG10(NN)
      A3=T
      A4=T-LASTT
      LASTT=T
      WRITE(4,1000)A1,A2,A3,A4
1000  FORMAT(4(1PE15.3))
      RETURN
      END
```

Sample Output:

```
HOW MANY OSCILLATIONS ?  3
TYPE IN VALUE OF RAO - 0.1
TYPE IN VALUE OF RCO - 1.0
A =      -.1090       DTHETA =     -1.0000
RAO =       .1000       RCO =      1.0000

      LOG(R)          LOG(N)           TIME          TIME DIFF.
    -6.027E-18      -2.000E+01       0.000E+00       0.000E+00
FRACTIONAL PERIOD CHANGE =   0.0000000D+00
     1.215E-02       2.690E-02       9.926E+00       9.926E+00
    -7.601E-03       2.278E-02       1.999E+01       1.006E+01
FRACTIONAL PERIOD CHANGE =   1.7272510D-02
     5.133E-03      -1.704E-01       3.016E+01       1.017E+01
    -3.219E-03       1.199E-02       4.018E+01       1.003E+01
FRACTIONAL PERIOD CHANGE =   6.8077875D-03
    -3.837E-03      -6.354E-02       5.030E+01       1.011E+01
    -3.831E-03      -4.847E-02       6.039E+01       1.009E+01
FRACTIONAL PERIOD CHANGE =   6.5241939D-03
STOP  2002
```

APPENDIX E

We can relate ε to Δh in the critical regime as follows. From figure 5.3, we see that:

$$\varepsilon = \Delta h - (t_1 - t_2)\,\dot{h}$$

Recalling that $\omega_0^2\,\Delta h = \alpha\,\Delta V_0$ and $\Delta V_0 = \dot{V}_0 t_1$, we obtain:

$$\begin{aligned}\varepsilon &= h\,(1 - \dot{h}\omega_0^2/\alpha\dot{V}_0) - t_2\dot{h} \\ &= A\Delta h - B\end{aligned}$$

This result is based purely on geometrical considerations in figure 5.3. The value of t_2 (as defined in figure 5.3) was measured to be 1.0 ± 0.5 s for all runs at $\dot{V}_0 = 0.31 Vs^{-1}$. Using the estimate of α/ω_0^2 from figure 5.2, the values of A and B are:

$$A = 0.74 \pm 0.05$$

$$B = 4.9 \pm 1.0\ \mu m.$$

A and B vary depending on $\dot{h}$. The figures quoted are based on the mean and standard deviation of $\dot{h}$ at $\dot{V}_0 = 0.31\ Vs^{-1}$, and they show that the changes due to $\dot{h}$ are small. If A and B are regarded as constant, then a graph of ε against Δh should be a straight line, figure 5.4. It yields values for A and B which are in close agreement with the calculated values. This agreement merely serves to confirm that the values of $\dot{V}_0$, ΔV_0 and Δh are self-consistent, and does not in itself provide any information on the dissipation in the film.

REFERENCES

1 The Properties of Liquid and Solid Helium, J Wilks, Clarendon press, Oxford (1967)

2 B Lambert, R Perzynski and D Salin, J. Low Temp. Phys. 28 359 (1977)

3 L C Jackson and L G Grimes, Phil. Mag. Supl. 7 435 (1958)

4 A C Ham and L C Jackson, Proc. Roy. Soc. A240 243 (1957)

5 L G Grimes and L C Jackson, Phil. Mag. 4 1346 (1959)

6 O T Anderson, D H Liebenberg and J R Dillinger, Phys. Rev. 117 39 (1960)

7 L Schiff, Phys Rev 59 839 (1941)

8 J Frenkel, J. Phys. Moscow 2 345 (1940)

9 G D Halsey, J. Chem. Phys. 16 931 (1948)

10 T Oestereich and H Stenschke, Phys. Rev. B 16 1996 (1977)

11 M Chester, D F Brewer, L C Yang and K A Elinger, J. Phys. C. 7 1949 (1974)

12 M Chester and L C Yang, Phys. Rev. Lett. 31 1377 (1973)

13 L Ginzburg and L P Pitaevskii, Soviet Physics JETP 7 858 (1958)

14 Superfluid Hydrodynamics, S J Putterman, North Holland, Amsterdam (1974)

15 J G Daunt and K Mendelssohn, Proc. Roy. Soc. A170 423, 439 (1939)

16 J G Daunt and K Mendelssohn, Nature 157 839 (1946)

17 K Mendelssohn and G K White, Proc. Phys. Soc. A63 1328 (1950)

18 K R Atkins, Proc. Roy. Soc. A203 240 (1950)

19 J F Allen and J G M Armitage, Phys. Lett. 22 121 (1966)

20 R Bowers and K Mendelssohn, Proc. Phys. Soc. A63 1318 (1950)

21 B Smith and H A Boorse, Phys. Rev. 99 346 (1955)

22 B N Esel'son and B G Laserev, Zh. Eksp. Teor. Fiz. 23 552 (1952)

23 J F Allen, Nature 185 831 (1960)

24 R W Selden and J R Dillinger, Phys. Rev. 138 A1371 (1965)

25 D B Crum, D O Edwards and R E Sarwinski, Phys. Rev. A9 1312 (1974)

26 L G Grimes and L C Jackson, Phil. Mag. 4 1346 (1959)

27 W M van Alphen, G J van Haasteren, R de Bruyn Ouboter and K W Taconis, Phys. Lett. 20 474 (1966)

28 R W Selden and J R Dillinger, Phys. Rev. 138 A1363 (1965)

29 D H Liebenberg, 26 744 (1971)

30 L J Campbell and D H Liebenberg, Phys. Rev. Lett. 29 1065 (1972)

31 J F Allen and C C Matheson, Proc. Roy. Soc. 290 1 (1966)

32 R F Harris-Lowe, J. Low Temp. Phys. 28 489 (1977)

33 R F Harris-Lowe, C F Mate, K I McCloud and J C Daunt, Phys. Lett. 20 126 (1966)

34 R R Turkington and M H Edwards, Phys. Rev. 168 160 (1968)

35 R F Harris-Lowe and R R Turkington, J. Low Temp. Phys. 4 525 (1971)

36 M Toft, PhD thesis, Department of Physics, St Andrews University, (July 1979)

37 K R Atkins, Proc. Roy. Soc. A203 119 (1950)

38 E van Spronsen, H J Verbeek, H van Beelen, R de Bruyn Ouboter and K W Taconis, Physica 77 570 (1974)

39 G S Picus, Phys. Rev. 94 1456 (1954)

40 F I Glick and J H Werntz, Phys. Rev. 178 214 (1969)

41 J K Hoffer, J C Fraser, E F Hammel, L J Campbell, W E Keller and R H Sherman, LT13, 253 (1974)

42 R B Hallock and E B Flint, Phys. Rev. A 10 1285 (1974)

43 "Superfluid film flow", L J Campbell, p 127 ff, in The Helium Liquids, Armitage and Farquhar (eds.), (1975) Acad. press

44 L J Campbell, E F Hammel, J K Hoffer and W E Keller, J. Low Temp. Phys. 24 527 (1976)

45 J F Allen, J G M Armitage and B L Saunders, LT13 258 (1974)

46 J E Robinson, Phys. Rev. 82 440 (1951)

47 V M Kontorovich, Soviet Physics JETP 3 770 (1956)

48 G M Graham and E Vittoratos, Phys. Rev. Lett. 33 1136 (1974)

49 D T Ekholm and R B Hallock, J. Low Temp. Phys. 42 339 (1981)

50 D T Ekholm and R B Hallock, Phys. Rev. B 19 2485 (1981)

51 E B Flint and R B Hallock, Phys. Rev. B 11 2062 (1975)

52 L Onsager, Nuovo Cimento Suppl. 6 249 (1949)

53 R P Feynman, Prog. Low Temp. Phys. 1 1 (1955)

54 W F Vinen, Proc. Roy. Soc. A260 218 (1961)

55 S C Whitmore and W Zimmermann, Phys. Rev. Lett. 15 389 (1965)

56 G W Rayfield and F Reif, Phys. Rev. 136 1194 (1964)

57 P W Anderson, Rev. Mod. Phys. 38 298 (1966)

58 H E Hall and W F Vinen, Proc. Roy. Soc. A238 (1956)

59 Y G Mamaladze, Soviet Physics JETP 12 595 (1966)

60 D S Tsakadze, Soviet Physics JETP 15 681 (1962)

61 P L Richards and P W Anderson, Phys. Rev. Lett. 14 540 (1965)

62 L D Landau, J Phys. Moscow 5 71 (1941)

63 Liquid Helium, K R Atkins, Cambridge University Press (1959)

64 W I Glaberson and R J Donnelly, Phys. Rev. 141 208 (1966)

65 R J Donnelly and P H Roberts, Phil. Trans. Roy. Soc. A271 41 (1971)

66 L J Campbell, J. Low Temp. Phys. 8 105 (1972)

67 D J Martin and K Mendelssohn, J. Low Temp. Phys. 5 211 (1971)

68 J G M Armitage, J F Allen and M Toft, LT15, Grenoble, J. de Phys. C6-302 (1978)

69 D G Blair and C C Matheson, LT13, 272 (1974)

70 W E Keller and E F Hammel, Phys. Rev. Lett. 17 998 (1966)

71 L J Campbell, E F Hammel, D M Jones and W E Keller, LT11, St Andrews (1968)

72 R R Turkington and R F Harris-Lowe, J. Low Temp. Phys. 28 513 (1977)

73 J S Langer and J D Reppy, Prog. Low Temp. Phys. 6 1 (1970)

74 S V Iordansky, Soviet Physics JETP 21 467 (1965)

75 J S Langer and M E Fisher, Phys. Rev. Lett. 19 560 (1967)

76 J S Langer, Phys. Rev. Lett. 21 973 (1968)

77 J Clow, J C Weaver, D Depatie and J D Reppy, LT9, Colombus, Ohio, 328 (1964)

78 J D Reppy, Phys. Rev. Lett. 14 733 (1965)

79 J R Clow and J D Reppy, Phys. Rev. Lett. 19 291 (1967)

80 J R Clow and J D Reppy, Phys. Rev. Lett. 16 887 (1966)

81 G Kukich, R P Henkel and J D Reppy, Phys. Rev. Lett. 21 197 (1968)

82 H A Notarys, Phys. Rev. Lett. 22 1240 (1969)

83 G B Hess, Phys. Rev. Lett. 27 977 (1971)

84 M E Banton, J. Low Temp. Phys. 16 211 (1974)

85 W E Keller and E F Hammel, LT13, 263 (1974)

86 J L McCauley, Phys. Lett. 73A 26 (1979)

87 J L McCauley, Phys. Rev. B 20 1928 (1979)

88 L Yu, Phys Rev. B 25 198 (1982)

89 D A Browne and S Doniach, Phys. Rev. B, 25 136 (1982)

90 J M Kosterlitz and D J Thouless, J. Phys. C (Letters) 5 L124 (1972)

91 J M Kosterlitz and D J Thouless, J. Phys. C 6 1181 (1973)

92 J M Kosterlitz, J. Phys. C 7 1046 (1974)

93 D R Nelson and J M Kosterlitz, Phys. Rev. Lett. 39 1201 (1977)

94 V Ambegaokar, B L Halperin, D R Nelson and E D Siggia, Phys. Rev. Lett. 40 783 (1978); and V Ambegaokar, B L Halperin, D R Nelson and E D Siggia, Phys. Rev. B 21 1806 (1980)

95 B A Huberman, R J Myerson and S Doniach, Phys. Rev. Lett. 40 780 (1978)

96 J E Berthold, D J Bishop and J D Reppy, Phys. Rev. Lett. 39 348 (1977)

97 R J Myerson, Phys. Rev. B 18 3204 (1978)

98 I Rudnick, Phys. Rev. Lett. 40 1454 (1978)

99 D J Bishop and J D Reppy, Phys. Rev. Lett. 40 1729 (1978)

100 J A Roth, G J Gelatis and J D Maynard, Phys. Rev. Lett. 44 333 (1980)

101 J G Dash, Phys. Rev. Lett. 41 1178 (1978)

102 A N Berker and D R Nelson, Phys. Rev. B 19 2488 (1979)

103 D T Eckholm and R B Hallock, Phys. Rev. Lett. 42 449 (1979)

104 J L McCauley, Phys. Rev. Lett. 45 467 (1980)

105 R K Childers and J T Tough, Phys. Rev. Lett. 31 911 (1973)

106 J F Allen, Proceedings of the International School of Physics, Course XXI - Liquid Helium, ed. Careri (Academic, New York, 1963) p305

107 J G M Armitage and C J Adie, LT16, Physica 108 B & C 215 (1981)

108 L J Campbell, J. Low Temp. Phys. 3 175 (1970)

109 W F Vinen, Prog. Low Temp. Phys. 3 1 (1961)

110 C J Adie and J G M Armitage, Cryogenics 22 527 (1982)

111 Fluid Mechanics, L D Landau, Pergamon press 1959, p 235

112 R G Arkhipov, Soviet Physics JETP 6 90 (1958)

113 Non - Linear Differential Equations, H T Davis, Dover Publications Inc. 1962, p 251 - 254

114 E S Sabisky and C H Anderson Phys. Rev. A7 790 (1973)

115 R K Galkiewicz and R B Hallock, Phys. Rev. Lett. 33 1073 (1974)